Characterization of Precipitated Calcium Carbonate (PCC) compounds on the basis of powder X-ray diffraction data

Zur Erlangung des akademischen Grades eines

DOKTORS DER NATURWISSENSCHAFTEN

an der Fakultät für Bauingenieur-, Geo- und Umweltwissenschaften

der

Universität Karlsruhe (TH)

DISSERTATION

von

KATAYOON MOHSENI

Iran-Tehran

2007

Zusammenfassung

Gefälltes Kalziumkarbonat (PCC) sowie gemahlenes Kalziumkarbonat (GCC) finden spezifische Anwendung in industriellen Produkten, speziell in der Papierindustrie. Im Verlauf der letzten Jahre sind zahlreiche kommerzielle PCC und GCC Produkte, die vielfältige physiko-chemische Eigenschaften aufweisen, auf den Markt gekommen. Diese Eigenschaften resultieren aus der unterschiedlichen Phasenzusammensetzung, der Kristallitgröße und –morphologie sowie der Bildung von Aggregaten dieser PCC und GCC. Zur Identifizierung und um einen gezielten Einsatz von PCC und GCC zu gewährleisten, ist eine effiziente Routineanalysemethode zur Bestimmung von PCC und GCC Komponenten wünschenswert. Das Ziel der vorliegenden Arbeit ist es eine Methode zu testen, mit welcher PCC wie auch GCC zuverlässig bestimmt werden können. Eine Routinemethode, wie die Röntgenpulverdiffraktometrie (XRD), wurde hierfür ausgewählt.

Im Verlauf dieser Doktorarbeit wurden folgende kommerziell erhältliche PCC und GCC Proben untersucht: Pre800, Pre320, 360V, 160V, Fb25, Pre720, Pre100, Fb230, PFS210, PRP, GCCX, GCC90, PRF120, PS, PCLS, PCCSG, PCC1, Pre600, PSU1, PSU2, PSU3 und PSU4. Alle untersuchten Proben enthielten lediglich Kalzit und Aragonit. Weder weitere Karbonatphasen wie etwa Vaterit noch Verunreinigungen anderer Art wurden innerhalb des Messfehlers der Pulverdiffraktometrie erfasst. Kalzit als auch Aragonit treten in unterschiedlichen Verhältnissen in allen Proben auf. Die Phasenzusammensetzung der untersuchten Proben teilt sich in zwei Gruppen; dies wurde mit Hilfe eines externen Standards und mittels der Rietveld Methode gezeigt. Bei der ersten Gruppe handelt es sich um Proben, die aus fast purem Kalzit (> 96%) bestehen, während in der zweiten Gruppe Aragonit die Hauptphase (> 80%) darstellt und Kalzit lediglich mit maximal 20% auftritt.

Während der industriellen Ausfällung von Kalziumkarbonat treten strukturelle Defekte wie bspw. Versatz von Kalzit-/Aragonitkristallen auf. Dieser führt dazu, dass die Kristalle definierte Strukturen aufbauen. Kohärente Diffraktometrie wird nicht für die Untersuchung des gesamten Kristalls angewandt, sondern nur für Strukturbereiche wie Kristallite. Strukturdefekte führen somit zu einer Deformation des Kristallgitters (Dehnung). Die Defektdichte hängt dabei von der eigentlichen Ausfällungsreaktion ab und kann als eine Art Fingerabdruck der PCC Proben verwendet werden (unter der Annahme, dass die Fällungsbedingungen für unterschiedliche PCC Proben verschieden sind).

Sowohl die Kristallitgröße als auch die Dehnung bestimmen die Breite der gemessenen Diffraktometriewerte. Die mittels Rietveld Methode errechnete Halbwertsbreite für Kalzit (104) liegt im Bereich von 0,198 bis 0,560, während die für Aragonit (040) mit 0,210 bis 0,606 ermittelt wurde. Die Kristallitgröße als auch die Dehnungswerte der Proben wurden mit Hilfe von Williamson-Hall Diagrammen bestimmt. Neben der Kristallitgröße enthalten die XRD Daten auch Informationen zur Kristallmorphologie, welche dann zur Unterscheidung der PCC und GCC Proben verwandt werden. Prinzipiell tendieren nicht-sphärische Partikel dazu sich bevorzugt gemäß der Morphologie zu orientieren, was zu Intensitätsunterschieden bei den d-Werten führt. Die Intensitäten für Kalzit und Aragonit sind in Bezug zu den Effekt der bevorzugten Orientierung zu sehen. Die Identifizierung der Kristallmorphologie (Form) wird durch die Berechnung des Intensitätsverhältnisses der stärksten diffraktometrisch ermittelten d-Linie des Kalzits (104) zu den Intensitäten der darauf folgenden d-Werte (116), (012), (202), (113), (018) sowie (122) durchgeführt. Es gibt einen beachtlichen Unterschied zwischen diesen Werten durch den anzeigt wird, dass eine nicht-sphärische Probe in unterschiedlicher Weise bevorzugt orientiert wird. Die gleiche Methode wurde für Aragonit herangezogen, wobei hier das Intensitätsverhältnis der stärksten (040) Linie zu den Intensitäten der (111), (202), (022), (113) und (102) Linien berücksichtigt wurde. Bei diesem Schritt ist die Methode der Probenaufbereitung sehr wichtig und sollte reproduzierbar sein. Es sollte erwähnt werden, dass diese Methode zwar keine einfache Analysetechnik darstellt, jedoch scheint der Ansatz reproduzierbare Ergebnisse zu liefern akzeptabel.

In dieser Arbeit wurde die Charakterisierung / Identifizierung bestimmter PCC und GCC Proben und die Quantifizierung und die Kristallitgröße sowie die Morphologie von Aggregaten mittels Röntgenpulverdiffraktometrie erreicht. Die erzielten Ergebnisse wurden zusätzlich durch andere Analysetechniken wie Rasterelektronenmikroskopie (SEM) sowie Fouriertransformations-Ramanspektroskopie (FT-Raman) abgesichert.

Summary

Precipitated calcium carbonate (PCC) and ground calcium carbonate (GCC) compounds are used in various industrial applications especially in paper-making industry. In recent years, numerous commercial PCC and GCC products have emerged with a variety of physical chemical properties. These properties are a consequence of the phase composition, crystal size, crystal morphology, formation of aggregates. Based on this background, an efficient analytical method is desired, to identify PCC and GCC products on a routine basis. The aim of this Ph.D. is to characterize PCC and GCC compounds on the basis of powder XRD measurements.

In this Ph.D. thesis, 22 commercially available PCC and GCC were studied: Pre800, Pre320, 360V, 160V, Fb25, Pre720, Pre100, Fb230, PFS210, PRP, GCCX, GCC90, PRF120, PS, PCLS, PCCSG, PCC1, Pre600, PSU1, PSU2, PSU3, PSU4. The studied PCC and GCC samples contain only calcite and aragonite. No additional crystalline phases such as vaterite or other impurities were identified within the limits of error of powder XRD. Also, there is no indication of an amorphous phase. Calcite and aragonite occur in various proportions. The phase quantification of the studied samples clusters into two groups, as determined by the external standard and Rietveld method. One group consists of almost pure calcite (>96%). The other group consists of aragonite as the dominant mineral (>80%) and calcite (<20%) as lesser mineral.

During industrial precipitation, structural defects such as dislocations of unit cells are introduced into calcite / aragonite crystals. As a consequence, these crystals are built up of structural domains. Coherent diffraction does not occur over the entire crystal but is limited to the domains - also called crystallites. Furthermore, structure defects result in deformation of the crystal lattice (strain). The defect density depends on the actual precipitation reaction and can be used to characterize PCC samples (assuming that precipitation conditions are different for different PCC samples).

Crystallite size as well as strain affects the width of diffraction peaks. In calcite FWHM (104) lies in the range of 0.198-0.560 and for aragonite FWHM (040) in the range of 0.210-0.606, calculated by the Rietveld method. The crystallite size and strain values were calculated by Williamson-Hall plots. In addition to the crystallite size, powder XRD data contain information about the crystal morphology, which can also be used to characterize PCC and GCC samples. In principle, non-spherical particles tend to orient preferentially according to the morphology, and result in intensity variations of diffraction peaks. The peak intensity as derived from the peak area of XRD lines (calcite and aragonite) is related to the preferred orientation effect. The description of aggregates morphology (shape) is carried out by the calculation of the intensity ratio of the strongest diffraction line of calcite (104) to the intensity of the consecutive diffraction peaks (116), (012), (202), (113), (018) and (122). There is a significant difference between these values, which indicates that the non-spherical sample orients preferentially in different ways. The same method was considered for aragonite in terms of the intensity ratio of the strongest diffraction line (040), to the intensity of (111), (202), (022), (113), (102) XRD lines. In this step, the sample preparation method is very important and should be reproducible. It should be mentioned that, this method is not a straightforward analytical technique but the approach seems to provide reproducible results.

In this Ph.D. thesis, the characterization of the certain kinds of PCC and GCC samples in terms of identification, quantification, crystallite size and strain determination and aggregates morphology description was investigated by means of powder XRD. The XRD results were verified by complimentary analytical techniques, these were SEM, FT-Raman spectrometers.

خلاصه

فازهاي رسوبي كربنات كلسيم(Precipitated Calcium Carbonate(PCC و كربنات كلسيم خردايشي Ground Calcium Carbonate (GCC) بعنوان مواد افزودني و پر كننده در صنايع كاغذسازي كاربرد وسيعي دارا هستند.اين مواد با توجه به تركيب كيفي ،كمي،اندازه بلور و نحوه تشكيل بلور،ويژگي هاي گوناگوني را به كاغذ مي دهند.با توجه به اهميت ويژگي هاي مذكور در تركيبات كربنات كلسيم،نياز به يك روش تجزيه فراگير منظور شناسائي اين تركيبات ، هدف اصلي اين رساله دكترا مي باشد. در اين پروژه تلاش بر اين مبنا نهاده شد تا اندازه گيري ويژگي هاي ساختاري با بهره گيري از دستگاه پراش پرتو ايكس XRD، انجام پذيرد.

در اين پروژه، ۲۲نمونه صنعتي PCC و GCC مورد تجزيه و بررسي قرارگرفته است.

Pre800,Pre520,360V,Fb25,Pre720,PSU1,PSU2,PSU3,,Pre100,PCCSG,Fb230,PRP,GCCX, .GCC90,PRF120,PCLS,.PSU4,160V,PFS210,PS,Pre600,PS

در مرحله شناسائي كيفي فازهاي موجود در نمونه هاي PCC,GCC،پلي مرف هاي كلسيت (calcite) و آراگونيت(aragonite) مشاهده شد.با توجه به حد تشخيص دستگاه پراش پرتو ايكس ، پلي مرف واتريت (vaterite) و ديگر ناخالصي ها، قابل ثبت و سنجش نبوده است.

فاز غيربلورين (بي شكل) در اين نمونه ها مشهود نمي باشد.تعيين مقادير فازهاي بلورين تحت عنوان سنجش كمي بر اساس دستگاه پراش پرتوايكس (XRD) و دو روش اندازه گيري استانداردخارجي(External Standard) وروش ريت ولد (Rietveld method) پايه ريزي شد.

نمونه هاي صنعتي PCCوGCC به دو گروه مجزا تقسيم بندي گرديد.

گروه اول : نمونه ها، حاوي كلسيت (calcite) نسبتا خالص مي باشد (%۹۶<) .

گروه دوم:نمونه ها حاوي فاز غالب آراگونيت (aragonite) با غلظتي بيش از %۸۰ بوده و فاز دوم را كلسيت با درصد وزني كمتر از %۲۰به خود اختصاص مي دهد.

در طي فرآيند رسوبي ، در كلسيت و آراگونيت ، ساختار بلورين دچار انحراف مي گردد. بلور متشكل از واحدهاي سازنده (Domain) مي باشد.پديده پراش در نتيجه تداخل پرتو ايكس با واحدهاي سازنده (Crystallite) مي باشد. نواقص بلورين حاصل از انحراف در پارامترهاي بلورStrain ميباشد.تراكم نواقص كريستالي بستگي به نحوه واكنش رسوبي داشته و ميتواند نقش مهمي در شناسائي تركيبات PCC داشته باشد .

لازم به ذكراست كه اندازه واحدهاي سازنده(Crystallite) و انحراف

در ساختار بلورين (Strain) ،پهن شدگي در خط طيفي پراش پرتوايكس را موجب مي گردد.
پهن شدگي خط طيفي توسط پارامتر پهناي پيك در نصف ارتفاع پيك (FWHM) سنجيده مي شود.در سري نمونه هاي صنعتي ، پهناي پيك در نصف ارتفاع پيك (FWHM) براي كلسيت و خط طيفي پراش (١٠٤) در محدوده (٠,٥٦-٠,١٩٨) و در آراگونيت FWHM مربوط به طيف پراش (٠٤٠) در دامنه (٠,٦٠٦-٠,٢١) با روش ريت ولد (The Rietveld method) اندازه گيري گرديد. پارامترهاي اندازه واحد سازنده (Crystallite size) و انحراف در ساختار بلورين (Strain) توسط روش "Williamson-Hall"سنجيده شد.
الگوي پراش پرتوايكس دربردارنده داده هاي جامعي در رابطه با شكل بلور(مرفولوژي)مي باشد.اساسا دانه هاي غيركروي تمايل به جهت گيري انتخابي با توجه به شكل بلور و ذرات دارند. اين جهت گيري انتخابي "The preferred orientation effect" به ميزان قابل ملاحظه اي برروي شدت خطوط طيفي پراش پرتوايكس تاثير مي گذارد.
شدت پراش در خطوط طيفي پرتوايكس را مي توان به روش سطح زيرپيك(Peak area) اندازه گيري نمود.قابل ذكر است كه شدت پراش در خطوط طيفي در كلسيت و آراگونيت در ارتباط و متاثر از اثر جهت گيري انتخابي مي باشد.در نتيجه شناسائي شكل بلور(مرفولوژي) (Morphology) براساس محاسبه نسبت شدت قويترين خط طيفي پراش پرتوايكس(١٠٤) ,(١١٢) ، (٠١٨) ، (١١٣) ، (٢٠٢) ، (٠١٢) ، (١١٦)در كلسيت به شدت دومين تا ششمين خطوط طيفي پرتوايكس شكل گرفته است.
با توجه به داده هاي مربوطه ،اختلاف كاملا مشهودي بين نسبت شدت هاي خطوط طيفي پراش پرتوايكس مشهود است كه تاييدكننده اثر جهت گيري انتخابي ذرات غير كروي مي باشد.
روش مشابه در آراگونيت برحسب اندازه گيري نسبت شدت قويترين خط طيفي پراش پرتوايكس (٠٤٠) به دومين تا پنجمين(١٠٢) ، (١١٣) ، (٠٢٢) ، (٢٠٢) ، (١١١) انجام گرفت و اثر جهت گيري انتخابي در آراگونيت نيز تاييد گرديد.
در اين مرحله،به منظور دستيابي به تكرارپذيري در سنجش نسبت شدت خطوط طيفي آماده سازي نمونه بسيار حائز اهميت است .
در اين رساله دكترا،شناسائي انواع مشخصي از تركيبات PCC و GCC برحسب شناسائي كيفي ،تعيين مقادير كمي،تامين اندازه واحدهاي سازنده بلور(Crystallite size) و ميزان انحراف در ساختار بلورين(Strain effect) به روش پراش پرتوايكس پايه ريزي گرديد و نتايج بدست آمده با روش هاي تجزيه مكمل شامل ,FT-Raman SEM ،به لحاظ صحت و دقت در سنجش ، مورد تاييد قرار گرفت.

Acknowledgements

I am grateful to Prof. Dr. D.Stüben, for giving me the opportunity to do this PhD study at the Institut für Mineralogie und Geochemie, Universität Karlsruhe. I am thankful to her for providing me all the necessary facilities for mineralogical investigations and her valuable time to revise my dissertation.

My special gratitude goes to PD.Dr.D.Bosbach from INE, Forschungszentrum Karlsruhe, who was completely involved in my PhD thesis. His experience in this subject, valuable guidance and suggestions were the key in improving the quality of this research project.

I express my appreciation to PD.Dr.R.Haus from Dorfner company for supporting the samples, supplementary scholarship, and accepting to be my examiner.

I would like to thank Dr U.Kramer for technical and analytical assistance during this PhD project.

This project was mainly funded by Bruker Company and supported for intensive relevant courses. Therefore, I would express my gratitude to Dr F.Rabet, Dr J.Sawatzki, Dr I.Hegedues from Bruker-Axs company in Karlsruhe.

I am thankful to Prof.Dr.D.Eberl from USGS, who gave me the permission to have access to his publications in the library of USGS.

I am grateful to all members of the Institut für Mineralgie und Geochemie for their warm and moral support along my PhD project.

All of my affections go to my mother whose prayer and blessing always strengthened my confidence and made me capable to complete the work smoothly.

Table of Contents

List of Figures

List of Tables

Abbreviations

PCC	Precipitated Calcium Carbonate
GCC	Ground Calcium Carbonate
FT-RS	Fourier Transform Raman Spectrometry
SEM	Scanning electron Microscopy
TEM	Transmission Electron Microscopy
XRD	X-Ray Diffractometer
PDF	Powder Diffraction File
JCPDS	Joint Committee on Powder Diffraction Standards
ICDD	International Center for Diffraction Data
FWHM	Full Width at Half Maximum
$<D>_{vol}$	The number-weighted average diameter of crystallites
$<L>_{vol}$	The volume-weighted average column height of crystallites

1. Introduction

Precipitated calcium carbonate (PCC) and ground calcium carbonate (GCC) are widely applied as filler in paper (Zeshan & Yulin, 2003). The paper-making industry is continuously improving the quality of papers using PCC compounds (Zeshan & Yulin, 2003). Due to the importance of PCC and GCC, industries are interested in a fast, easy and reliable technique, which is able to characterize these compounds. Therefore, the main aim of this PhD thesis is to develop a powerful technique in order to provide detailed data on PCC and GCC products in paper-making industry. Hence, it is necessary to identify the polymorphs of calcium carbonate, quantify the amount of these minerals, and determine crystallite size, strain value and morphology of aggregates by means of X-ray diffractometry.

PCC products are manufactured via a series of controlled chemical reactions. In the PCC manufacturing process calcium carbonate deposit is crushed in a crushing unit and loaded into limekiln. A calcinations process is performed at high temperature (T>850°C) so that CO_2 is exhausted and burnt lime (CaO) is produced.

During a hydration step burnt lime reacts strongly and exothermically in contact with water to manufacture $Ca(OH)_2$ in highly alkaline conditions (pH 9-11).
In a re-carbonation step CO_2 is injected into the precipitation reactor in order to make chemically precipitated $CaCO_3$, (PCC) (Fig.1.1).

$$CaCO_3 + \text{Heat} \longrightarrow CaO + 2CO_2$$
Limestone (>850C) Burnt Lime Carbon dioxide

$$CaO + H_2O \longrightarrow Ca(OH)_2 + \text{Heat}$$
Burnt lime Hydrated lime

$$Ca(OH)_2 + CO_2 \longrightarrow CaCO_3 + H_2O$$
Hydrated lime PCC

Calcium carbonate can form three different crystal structures: calcite, aragonite, and vaterite. These are specific mineral phases (polymorphs), which relate to the distinct arrangement to the calcium, carbon, and oxygen atoms in the crystal structure. (Ahn et al, 2002).

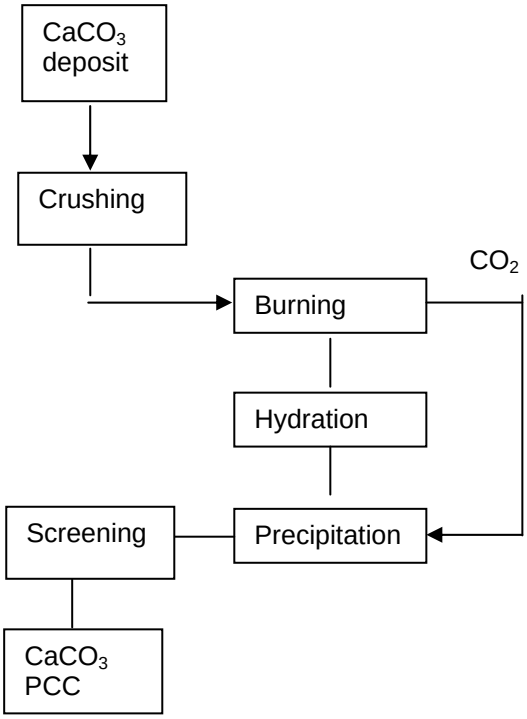

Figure 1.1. PCC production principles

The basic differences among the polymorphic phases of calcium carbonate lie in the disposition of the carbonate ion with respect to the central Ca ion in their respective unit cells (Klein & Hurlbut, 1993).

Calcite is the most thermodynamic stable phase of calcium carbonate, in hexagonal and rhombohedral systems (R3C space group). Calcite is 6-coordinated and composed of triangular carbonate ion groups (CO_3). Carbonate anion consists of a carbon at the center of the triangle and three oxygen ions at each corner (Fig.1.2) (Reeder, 1990).

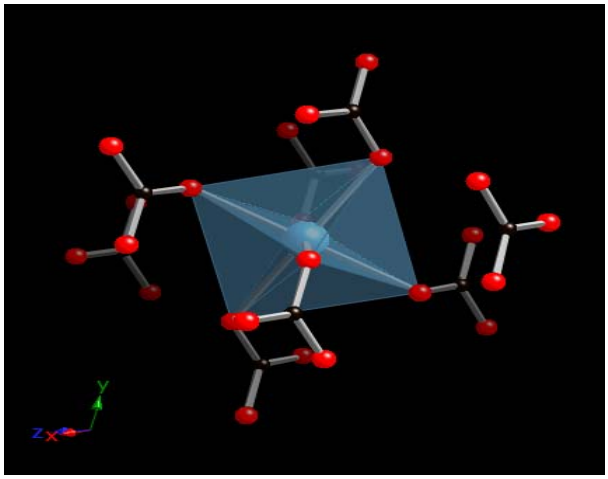

Figure 1.2. Crystal structure of calcite (Klein & Hurlbut, 1993)

Aragonite is a *polymorph* of calcium carbonate, which means that it has the same chemistry as calcite but it has a different structure, and more importantly, different symmetry and crystal shapes. Aragonite's more compact structure is composed of triangular carbonate ion groups (CO_3). Unlike in calcite, the carbonate ions do not lie in a single plane pointing in the same direction. Instead they lie in two planes that point in opposite directions, destroying the trigonal symmetry that is characteristic of calcite structure. Aragonite has an orthorhombic symmetry with Pmcn space group. In aragonite structure, Ca ions have a ninefold coordination (Fig.1.3) (Klein & Hurlbut, 1993).

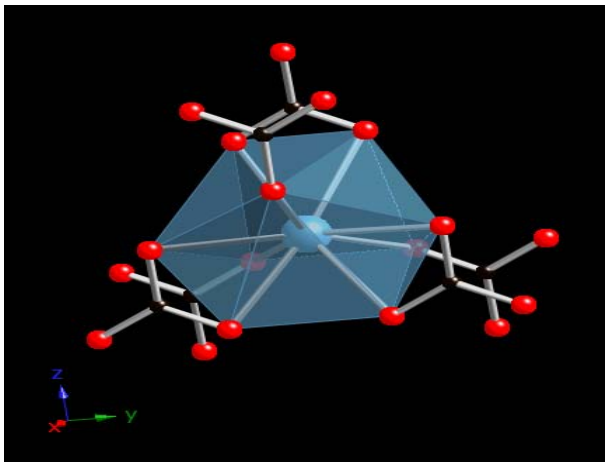

Figure 1. 3. Crystal structure of aragonite (Klein & Hurlbut, 1993).

Vaterite ($CaCO_3$) with hexagonal crystal structure with space group (P 6_3/mmc) is a mineral and polymorph of aragonite and calcite. Vaterite has a higher solubility than the other forms of calcium carbonate. Once vaterite is exposed to water, it converts to calcite (at low temperature:~40°C) or aragonite (at high temperature:~60°C) (Plummer & Busenberg, 1984). However, some impurities (metal ions or organic matter) may stabilize the vaterite and prevent its transformation into calcite or aragonite (Plummer & Busenberg, 1984, Milliman et al, 1999).

Morphology of PCC in paper sheet gives different properties to paper as final product. Plate-like calcium carbonate particles are desirable in paper-making industry, which may confer high smoothness and excellent gloss to the paper sheet since they are easily aligned in a regular way. They may confer high electric resistance and elasticity modulus to the composite (Wen et al, 2003).

Prismatic shaped of PCC are designed to give high brightness and whiteness (Wise, 1997) (Fig.1.4).

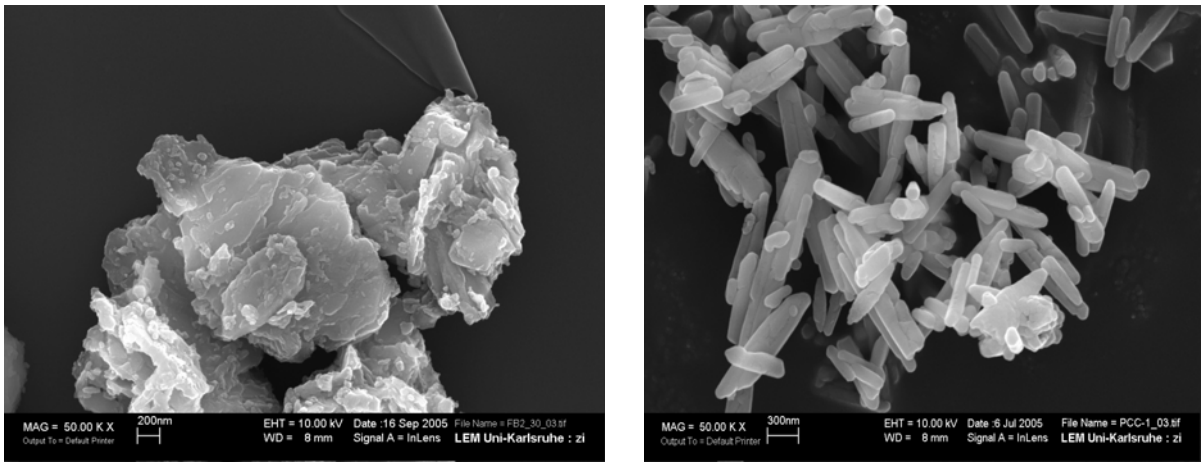

Figure 1.4. SEM images of PCC aggregates in plate shape and prismatic shape

Scalenohedral shapes of PCC are designed to supply increased paper opacity and brightness in uncoated fine papers (Klungness et al, 1998).

Recently, needle like aragonite with its high aspect ratio is desired for many applications such as reinforcing materials in the paper industry while paper quality such as printing characteristics, luster and color are greatly influenced by these polymorphs Therefore, the kind of polymorph is very important in industrial processes (Ahn et al, 2002).

It is generally known that Mg ions inhibit the growth of calcite and thus enhance relatively the formation of aragonite in the precipitation of calcium carbonate in solution. There are reports about the effects of Mg ions on the phase formation and crystal growth of calcium carbonate (Hu & Deng, 2004, Ahn et al, 2002, 2004).

The aragonite can be synthesized using these effects. The crystal can be prepared either by the reaction of solutions containing calcium ions and carbonate ions, or by the carbonation process in which CO_2 (g) is blown into $Ca(OH)_2$ slurry (Ahn et al, 2002).

It was reported that aragonite could be synthesized by blowing CO_2 gas into a mixture of $Ca(OH)_2$ slurry and $MgCl_2$ solution, with an initial value of pH 9, at a temperature of 80˚C. At the same reaction temperature, calcite is mainly formed at the pH value of 11.7 (Gen-Tao et al, 2004, Spanos & Koutsokos, 1998).

$MgCl_2$ is a product of the synthesis reaction. With the increase of Mg ion concentration, the concentration of CO3 ion will decrease because of the equation below:

$[Mg^{+2}] \times [CO_3^{-2}] = K_{sp} = 6.82 \times 10^{-6}$

Thus, the supersaturation of the synthesis reaction will decrease, which should be favorable for the formation of aragonite. Moreover, Mg ion was supposed to slow down the formation of calcite (Hu & Deng, 2004).

Temperature influences the growth rate of PCC and therefore the morphology. Solubility of CO_2 decreases with temperature increase. An optimal temperature for the formation of aragonite was investigated to be around 60˚C and above that, the fraction of calcite increased (Zeshan & Yulin, 2003, 2004).

The process of lime hydration and the quality of the product are influenced by a series of factors: size of lime particles and CaO crystals in the lime, porosity of lime, amount of water for hydration and its temperature, intensity of stirring, emitted heat from hydration, etc (Lohmus et al, 2002).

In conclusion; the different kinds of PCC can be produced under controlled synthetic conditions for different purposes in paper-making industry.

2. Methods and Materials

2.1. X-ray diffraction

X-ray diffraction is applied as major analytical technique in this PhD thesis. X-ray diffraction is a versatile, non-destructive analytical technique for identification and quantitative determination of crystalline compounds.

When monochromatic X-radiation strikes adjacent atomic planes of a crystal, the scattered rays interfere with each other as they leave the crystal. If the wavelength is approximately equal to the inter-atomic spacing. When Bragg-Brentano geometry is met, the X-rays scattered from the crystalline planes interfere constructively, producing a diffracted beam. The conditions satisfying this are defined by Bragg′s equation:

$n\lambda = 2d.\sin\theta$ (1)

where n is the diffraction order, λ is the wavelength of the incident X-ray beam, θ is the diffraction angle (the scattering angle at which an intensity peak is detected), and d is the interplaner spacing (Fig.2.1) (Guinier, 1994).

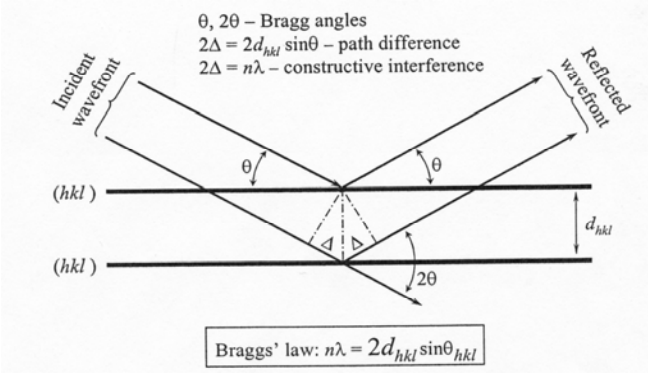

Figure 2.1. Diffraction Phenomenon concerning Bragg`s equation(Guinier, 1994)

When a monochromatic X-ray beam with wavelength λ strikes on lattice planes in a crystal at an angle θ, constructive interference occurs when the distance traveled by the rays reflected from successive planes differs by a whole number of wavelengths (Cullity & Stock , 2001).

There are different geometries but the most common type is based on Bragg-Brentano geometry (Fig.2.2) (Jenkins, 1989).

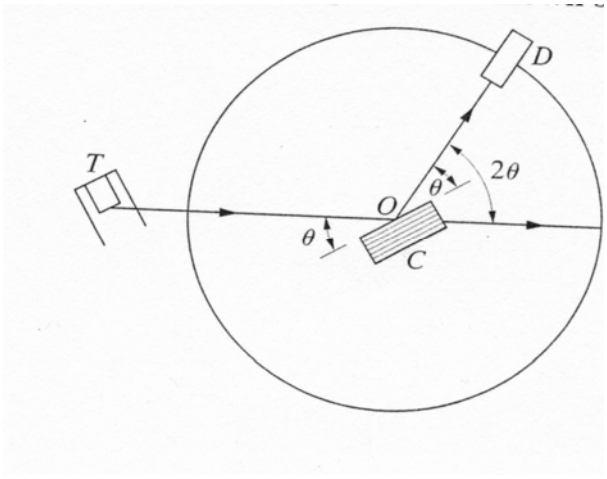

Figure 2.2. Bragg-Brentano geometry (Jenkins, 1989)

The X-rays are detected by scintillation or proportional or semi conductor counters. For $\theta/2\theta$ scans, the source, sample and receiving slit lie on the "focusing circle", which has a radius dependent on θ. Coherently scattered X-rays from a flat sample then converge on a receiving slit located in front of the detector. The detector rotates about the goniometer axis through twice the angular rotation of the sample. The purpose of the parallel-plate collimators is to limit the axial divergence of the beam and hence partially control the shape of the diffracted line profile (David et al, 2002).

The main components in the hardware of XRD are as follows:

A) X-ray tube: The source generates X-rays used in diffraction which have wavelengths lying approximately in the range of 0.5-2.5 Å, the specimen is exposed by X-rays then diffraction occurs in crystalline phase. The X-ray tube contains a source of electrons, a high accelerating voltage, and a metal target. The different kinds of X-ray tube exist in terms of the anode target but copper-manufactured is common X-ray tube, which generates Cu kα radiation.

With X-ray tube sources a high-voltage power supply is needed to provide the high voltage for the X-ray tube and to control the current through it. The optimum measurement ranges of kV and mA are usually defined by power-ratio curves supplied with the X-ray tube (Jenkins, 1989).

B) Slits: There are different kinds of slits in the optical configuration of XRD. Changing the size of the slit width affects both the width and intensity of a given line profile. In general, as the intensity increases, the resolution of the lines decreases, and vice versa (Jenkins, 1989).

C) Monochromator: this device is able to convert polychromatic beam emitted by X-ray tube to a monochromatic beam, which is needed in diffraction. The diffracted beam monochromator consists of a single crystal mounted behind the receiving slit with a detector set at the correct angle to collect the wavelength of interest diffracted by the monochromator crystal. A monochromator can be placed between the source and specimen (incident beam), or between the specimen and the detector (diffracted beam). The diffracted beam configuration is the most popular, mainly because it is very sufficient in removing specimen fluorescence (Jenkins, 1989).

D) Detectors: The function of the detector is to convert the individual X-ray photons into voltage pulses that are counted and/or integrated by the counting equipment, allowing various forms of visual indication of X-ray intensity to be obtained.

Detectors used in conventional X-ray powder diffractometers are generally one of three types, 1- gas proportional counters, 2-scintillation counters, and 3-semi conductor detector. Scintillation counter is the most commonly employed (Jenkins, 1989).

According to the available geometries, a diffractogram is plotted in terms of the intensity of diffraction lines versus the diffraction angles. A diffractogram contains different diffraction lines for minerals content in the sample.

2.1.1. Carbonate phase identification and quantification

Measurement of polymorphs (calcite, aragonite and vaterite) in PCC and GCC samples is performed using D500, Siemens (40kV, 25mA).
The identification of calcium carbonate polymorphs is performed by the comparison of d.values in the diffractogram obtained from PCC and GCC samples with an internationally recognized database such as powder diffraction database (PDF) containing reference patterns (JCPDS, 2002).

Quantitative phase analysis is the measurement of abundance of calcium carbonate polymorph phases in PCC samples. Quantitative phase analysis is performed using the external standard and Rietveld method.

The external standard method is based on plotting calibration curves of calcite and aragonite. Standards are prepared in the laboratory by means of pure calcite and aragonite. Then, the different amounts of pure calcite, aragonite are weighed and mixed as external standards (Dikinson & McGrath, 2001). In order to verify the accuracy of results, additional standard samples are prepared. The mixtures are measured using D500, Siemens (40kV, 25mA) and calibration curves are plotted based on the strongest diffraction line of calcite which appears at d.value=3.03 (104) and the strongest diffraction line of aragonite which appears at d.value=1.97 (040) respectively (Fig.2.3a, b). The accuracy of results is tested using standard samples (Table-2.1).

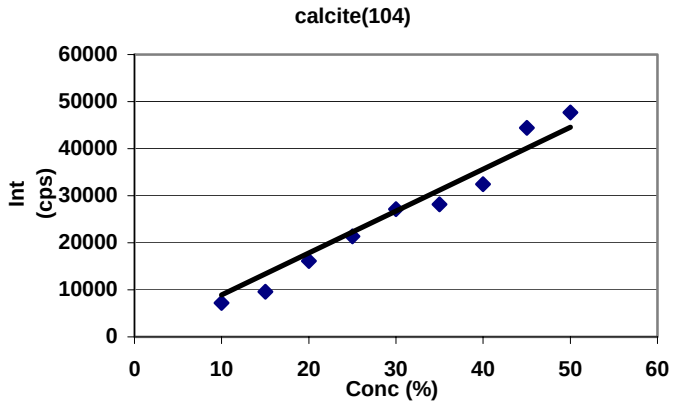

Figure 2.3a. The calibration curve of calcite based on diffraction line (d.value=3.03)(104) (R^2=0.95=correlation coefficient) line equation=y=890.98x)

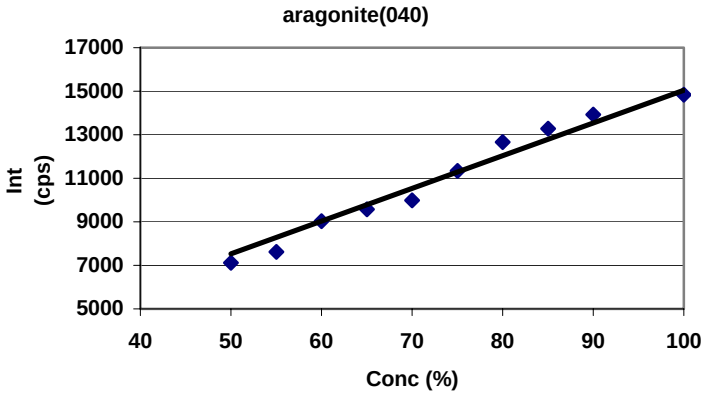

Figure 2.3b.The calibration curve of aragonite based on diffraction line (d.value=1.97)(040) (R^2=0.97=correlation coefficient)(line equation=y=150.54x)

Table-2.1. Accuracy of quantitative results, external standard method (XRD)

Standard samples	Aragonite (Meas.%) (040)	Aragonite (Known.%)	Aragonite Difference%	Calcite (Meas.%) (104)	Calcite (Known) %	Calcite Difference %
60Ar40Ca	63.6	60	±3.6	36.4	40	±3.6
70Ar30Ca	68.4	70	±1.6	31.6	30	±1.6
85Ca15Ar	14.1	15	±0.9	85.9	85	±0.9
98Ca2Ar	5	2	±3.0	95	98	±3.0

The results prove that the difference between the measured and known concentration of calcite and aragonite sets in the range of 0.9%-3.6%. These results are determined based on the strongest diffraction line of calcite (d.value=3.03(104) and aragonite (d.value=1.97(040)) in standard samples.

In order to investigate texture effect as an important error source in quantitative phase analysis, the calibration curves of calcite and aragonite based on the second strongest diffraction line of calcite (d.value=3.86 (012)) and aragonite (d.value=2.70 (121)) are plotted sequentially (Fig.2.3c,d). The accuracy of results for calcite and aragonite is tested using standard samples containing known concentration of pure calcite and aragonite (Table-2.2).

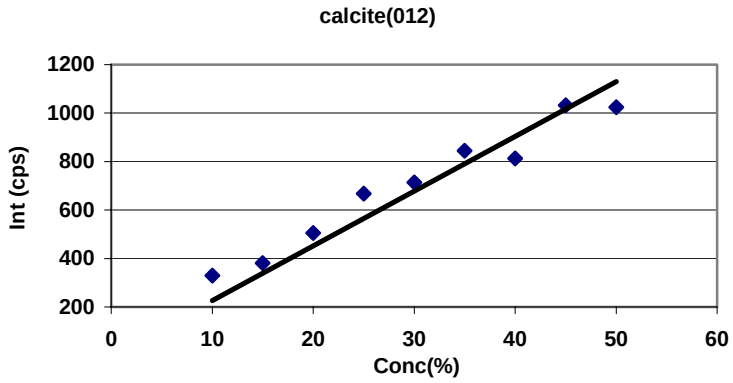

Figure 2. 3c. The calibration curve of calcite based on diffraction line (d.value=3.86)(012) (R^2=0.90=correlation coefficient) (line equation=y=22.59x)

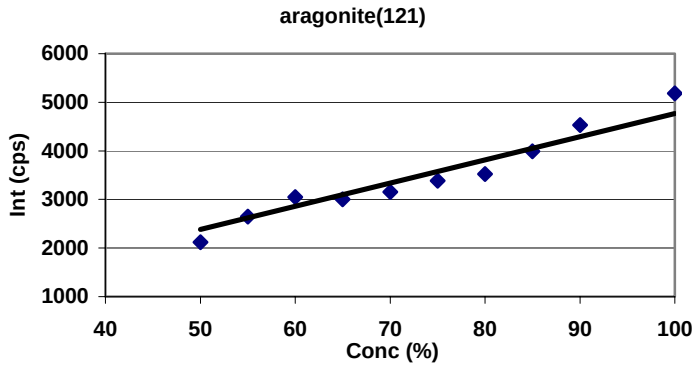

Figure 2.3d. The calibration curve of aragonite based on diffraction line (d.value=2.70)(121) (R^2=0.90=correlation coefficient) (line equation=y=48.95x)

Table-2.2. Accuracy of quantitative results, external standard method (XRD)

Standard samples	Aragonite (Meas.%) (121)	Aragonite (Known.%)	Aragonite Difference%	Calcite (Meas.%) (012)	Calcite (Known) %	Calcite Difference %
60Ar40Ca	62.3	60	±2.3	37.7	40	±2.3
70Ar30Ca	67.9	70	±2.1	32.1	30	±2.1
85Ca15Ar	13.2	15	±1.8	86.8	85	±1.8
98Ca2Ar	3.4	2	±1.4	96.6	98	±1.4

The results prove that the difference between the measured and known concentrations of calcite and aragonite sets in the range of 1.4%-2.3%. These results are determined based on the strongest diffraction lines of calcite (d.value=3.86(012)) and aragonite (d.value=2.70(121)) in standard samples.

The Rietveld method (full pattern analysis) is the second solution for quantitative phase analysis which considers the entire powder diffraction pattern using a variety of refinable parameters such as the individual intensities at each diffraction angle (2θ), interplaner spacing (d.value), full width at half maximum (FWHM) for all accessible peaks. There is more information hidden in a powder pattern. Lattice parameters and space group are deduced and refined from the peak position or the reflection; the amorphous fraction in the specimen is subtracted from the background; crystallite size, strain/stress are determined by analyzing the broadening of the peaks (FWHM). The Rietveld metod has potential to perform standardless quantitative phase analysis (Will, 2006).

The full-pattern analysis icludes: determination the materials in the specimen by the well established search-match methods, and then, assuming the crystal structures of the components are known, make a least square full pattern refinement of all components. Therefore, the crystal structure must be known, at least in principle, and this is the case in quantitative phase analysis, following as a rule in qualitative phase analysis (Will, 2006).

In the experiment, PCC and GCC samples were measured using a D500, Siemens (40kV, 25mA) system, Topas software package (Bruker), full pattern analysis.The accuracy of results is tested using standards (Table-2.3).

Table-2.3. Accuracy of quantitative results, Rietveld method (XRD).

Standard samples	Aragonite (Meas.%)	Aragonite (Known.%)	Aragonite Difference%	Calcite (Meas.%)	Calcite (Known) %	Calcite Difference %
60Ar40Ca	57.4	60	±2.6	42.6	40	±2.6
70Ar30Ca	69.7	70	±0.3	30.3	30	±0.3
85Ca15Ar	13.5	15	±1.5	86.5	85	±1.5
98Ca2Ar	1.5	2	±0.5	98.5	98	±0.5

The comparison of results (Table-2.1, 2.2, 2.3) regarding the measured concentration of calcite and aragonite in standard samples using external standard and Rietveld method prove that, Rietveld method provides less difference between the measured and known concentration of calcite and aragonite (±0.3 - ±2.6). that means more accurate and precise results.

2.1.2. Morphology description of aggregates

Aggregate morphology description is investigated by means of XRD with respect to the preferred orientation effect. In principle, non-spherical particles orient on XRD slide preferentially, which cause intensity variation on XRD lines in different crystal morphologies. Therefore, the intensity ratio of the strongest diffraction line to the intensity of the consecutive XRD lines might be the clue for morphology description. Each non-spherical grain in a polycrystalline aggregate normally has a crystallographic orientation different from that of its neighbors. Considered as a whole, the orientations of all grains may be randomly distributed in relation to some selected frame of reference, to a greater or lesser degree, about some particular orientations.

Any aggregate characterized by the latter conditions is said to have a preferred orientation, or texture, which may be defined simply as a condition in which the distribution of crystal orientation is non-random. As mentioned the preferred orientation can have a profound effect on diffracted intensities measured by diffractometer (Cullity & Stock, 2001).

Empirically, three different morphologies of aragonite were investigated by means of SEM and XRD in order to figure out the correlation of morphology determination between these two different analytical techniques (Fig.2.4).

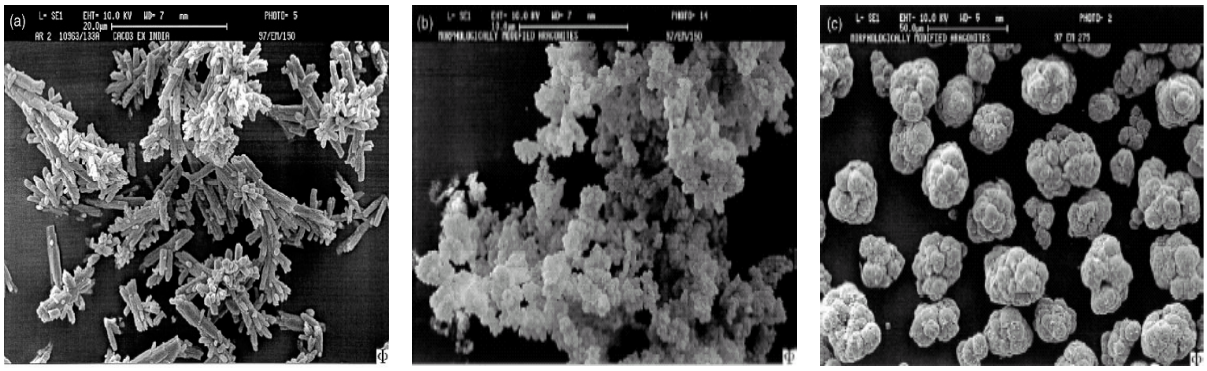

Figure 2. 4a. needle-like (i) **Figure 2. 4b.** flake-like(ii) **Figure 2. 4c.**cauliflower- like(iii)

Figure 2.4. Aggregate morphologies of aragonite (SEM) (Dobojit & Samiran, 1999)

For three kinds of aragonite quantitative powder X-ray diffraction experiments were performed in order to assess their relative degrees of crystallinity. The area under the principle XRD line at 3.39 Å (2θ = 26.3) for the flake and cauliflower-like aragonite samples was found to be 20% and 50% of that of the needle-shaped aragonite. In addition to the decrease in intensities, the peak shapes for cauliflower and flake-like aragonite were broadened. This broadening phenomenon is more pronounced in the case of the cauliflower-like aragonite than that of the flake-like aragonite, and is indicative of a lesser degree of crystallinity in these two aragonites than the needle-like aragonite sample (Dobojit & Samiran, 1999) (Fig.2.5).

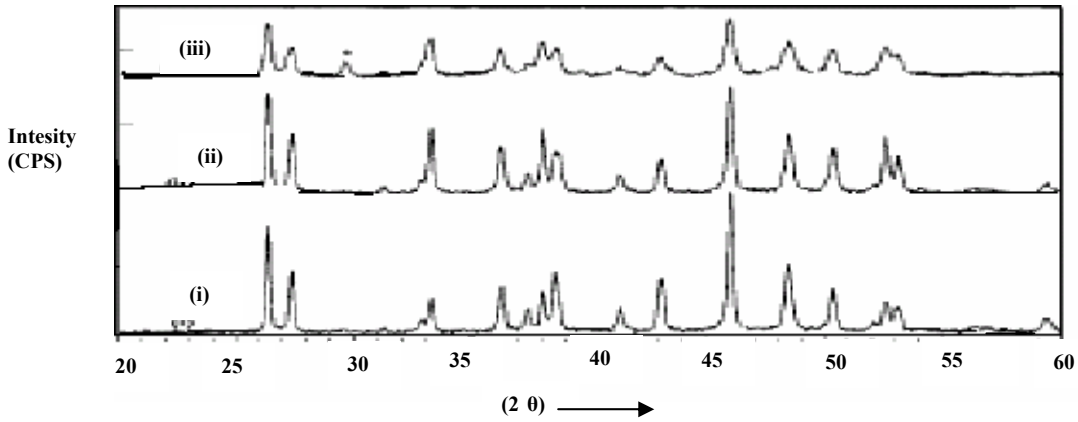

Figure 2.5. X-ray diffractograms of needle-like (i), flake-like (ii) and cauliflower-like (iii) aragonites (Dobojit & Samiran, 1999)

The XRD patterns of these morphologies of aragonite illustrate, there are no shifts in peak position but the difference is related to the intensity and the sharpness of XRD profiles at the same peak positions (Dobojit & Samiran , 1999).

In order to determine the morphology of PCC samples, the preferred orientation effect is the solution. Calcite with non-spherical particles is oriented on XRD slide preferentially, which causes intensity variation on XRD lines. In principle, one is able to distinguish different aggregate morphologies just by comparison of the intensity ratio among the strongest diffraction line of calcite and aragonite to consecutive XRD lines (Dobojit & samiran, 1999).

In the experimental section, the contribution of the preferred orientation effect in different morphologies of calcite is investigated. The method is based on the calculation of intensity ratio as the intensity of the first diffraction line of calcite (104), to the intensity of(116), (012), (202), (113), (018), and (122), diffraction lines in XRD pattern.

The same procedure is performed for aragonite in terms of the intensity ratio of strongest diffraction line (040) to consecutive lines (111), (202), (022), (113), (102).

In order to justify the reproducibility of intensity ratio (peak area, peak height) for these samples, the XRD slides were prepared and measured five times for each sample under the same measurement conditions individually. The difference among intensity ratio for calcite and aragonite is observed considerably which proves different morphologies of calcite and aragonite in PCC samples.

2.1.3 Crystallite size and strain effect measurement

The cloud of electrons around each of the atoms in a crystal can scatter an incident X-ray beam such that it retains its wavelength and frequency, i.e.; it is coherent with the incident beam. A diffracted beam, at a specific 2θ position, will result from such an interaction when the Braggs Law, is satisfied. These conditions imply that the (hkl) planes of atoms from which the diffraction occurs are all parallel, equally spaced and extend over a finite distance and for every lattice spacing there will be a unique diffraction angle. This distance may be consistent with the bounds of a particle in a powder or a grain in a metallic material. However diffraction peaks have a finite width and extend over a small 2θ range. This may in part be due to sample, i.e.; small departures from perfection in it, such as lattice bending (<1º) and the effects of low strain from internal stress or heterogeneity/solid solution effects. Such effects will not alter the size of the coherently scattering unit (Dyson, 2004).

The elasticity in a lattice will enable the material to recover its original state with respect to the certain elastic limit of each material. With increasing deformation imperfections such as dislocations and twins may be induced within a particle or grain, and sub grains will form. The limit of elasticity will vary and depend on a number of factors including the initial dislocation density in the material. Even single crystals will become polycrystalline when subjected to small amounts of plastic deformation. Particles also can develop a microstructure within their bounds. Coherent scattering will now come from smaller sample volumes. A reorientation of the sample relative to the incident X-ray beam would then be necessary to allow all

parts of a large grain or particle to contribute coherently scattered radiation to a specific 2θ position. Since particles/grains are smaller than 1000Å, which is usual, they are referred to as crystallites. The object of the analysis of line profiles is to extract information relating to the size of the component units of the microstructure of the material (Dyson, 2004).

For an ideal polycrystalline sample consisting of sufficiently large and strain free particles/grains, the breadth of the diffracted X-ray peaks will be a few seconds of arc, i.e. approach a breadth which can be attributed to effects other than size.

Contributions to the broadening of a peak profile can thus arise from the instrument as well as the sample. The sources of broadening are summarized in table-2.4.
Clearly, to be able to isolate the broadening effect from size alone, corrections of the recorded profile have to be made for the remaining effects. The quality of the result will therefore depend on the data recorded, the availability of suitable standards for correction and the method used (Dyson, 2004).

Table-2.4. The contribution of different factors on XRD profile broadening

Specimen related		Instrument related
Crystallite size	Strain effect	Beam divergence
Grain size	Dislocations	Wavelength distribution in incident beam
Sample transparency	Lattice defects	Slit system in use
Sample roughness	Micro strain	Specimen height setting

When the size of the individual crystals is less than about 0.1 μm (1000Å), the term “particle size” is usually used, but the term “crystallite size” is more precise (Cullity & Stock, 2001, Moore & Reynolds, 1997).

The contribution of crystallite size in peak broadening is calculated by Scherrer's equation as follows:

$$ß = \frac{0.9\lambda}{T \cos\theta} \qquad (2)$$

where

ß= The full width at half maximum of the diffraction profile in radians (2θ°)

T= The crystallite size.

All diffraction lines have a measurable width, even when the crystallite size exceeds 1000Å, due to such causes as strain effect of the sample and instrumental broadening (in diffractometers). The breadth (ß) in Scherrer equation refers to the broadening due to crystallite-size effect alone. In other words, ß is essentially zero when the crystallite size exceeds about 1000Å (Cullity & Stock, 2001, Moore & Reynolds, 1997).

It is also possible to determine the integral breadth of a diffraction line rather than the FWHM. The integral breadth is given by the peak area divided by the peak height. The integral breadth is contributed by all crystallites and any asymmetry in the line profile is not expressed by breadth parameters (Dyson, 2004)

The application of Scherrer's equation to loose powders is straight-forward, It is evident that the breadth of a diffraction peak will increase as the crystallite size decreases.As the crystallites decrease in size the number of them occupying the same volume increases and the range of orientations increases.

In practice, the contribution of instrumental broadening by means of pure quartz is measured and extracted from observed breadth for consecutive XRD lines.

$$ß_{observed} = ß_{crystallite\ size} + ß_{strain\ effect} + ß_{instrument\ effect} \qquad (3)$$

If the breadth of the profile, after these corrections, is caused by the effect of crystallite size alone, Scherrer equation can be used to determine the crystallite size (equation.2) (Cullity & Stock , 2001).

Williamson-Hall crystallite size-strain analysis was developed in 1953 as a method to separate the crystallite size and strain effects by their angular dependence. The W-H plot is drawn in terms of ßcosθ ($ß_{crystallite\ size+strain}$) versus sinθ. The intercept is a criterion of crystallite size and the slope of the line (tanθ) is equal to the strain value. This method is useful when many peaks in the diffraction pattern are accessible (Whitfield & Mitchell, 2004). The distribution of points in the W-H plot offers further information.

1. In a strain free material the integrated breadth is a measure of the crystallite size.
2. Strain is characterized in the W-H plot by points lying on a straight line which passes through the origin.
3. Where there is no correlation between breadth and either crystallite size or the strain effect, there will be a significant contribution from the instrumental broadening. The instrumental broadening should be measured and considered in the breadth of all consecutive XRD lines in order to minimize the mentioned miscorrelation (Dyson, 2004).

Strain in a crystal results from the displacement of a group of unit cells from their ideal position in a perfect crystal (Fig.2.6). Strain broadening represents a variation of d-spacing between the crystal planes which is related to lattice distortions arising from internal stress distributions, dislocations or deviation from ideal stoichiometry as well. A sample with isotropic strain produces peak broadening in ordered diffraction lines (Whitfield & Mitchell, 2004, Snyder et al, 1999).

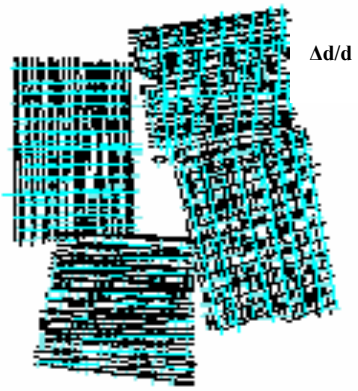

Figure 2.6. The internal lattice strain due to defects in the crystal structure (Snyder et al, 1999).

Broadening effects will become increasingly sever at high angles (David et al, 2002). Obviously at higher 2theta values the XRD peaks are broadener compared to XRD peaks at smaller 2theta values. This is simply a consequence of the sinus function in the Bragg equation. That is also the reason, why lattice constants should be determined from XRD peaks at higher 2 theta angles. The strain value in this research project is determined by the Williamson-Hall method (Cullity & Stock, 2001).

2.2. Scanning Electron Microscopy (SEM)

Scanning electron microscopy (SEM) is able to determine the number-weighted average diameter of crystals $<D>_{vol}$. XRD measures the volume-weighted average column height $<L>_{vol}$ of crystallites. Normally crystallites are smaller than crystals and for a small distribution width the difference between number weighted and volume-weighted diameters is rather small. (Goodhew & Humphreys, 1997).

The crystal shape, size and aggregates morphology of PCC are investigated using Leo 1530 Gemini, settings 100ev-30Kev, resolution 1nm(20Kev) – 3nm(1Kev). Samples are diluted by distilled water in order to select single particles. PCC samples containing pure calcite are chosen. In order to determine the crystal size 20 grains of

each sample are picked under SEM and diameter of each grain was measured and the average was taken as crystal size. SEM images illustrate a wide crystal size scattering in PCC samples depending on synthetic conditions. The morphology of aggregates in PCC samples is also determined using SEM, which proves a wide range of different aggregate morphologies in PCC samples.

2.3. Raman spectroscopy

The main spectroscopies employed to detect vibrations in molecules are based on the processes of infrared absorption and Raman scattering. They are widely used to provide information on chemical structures, to identify and quantify substances from the characteristics spectral patterns in a sample (Hendra et al, 1991, Fadini & Schnepel, 1989).

In theory, when light interacts with matter, the photons which make up the light may be absorbed or scattered, or may not interact with the material and may pass straight through it. In the scattering case there is no need for the photon to have an energy, which matches the difference between two energy levels of the molecule. The main scattering technique used for molecular identification is Raman scattering (Ferrari & Nakamoto, 1994).

The basic processes, which occur for one vibration, are shown in figure.2.7. At room temperature most molecules but not all are present in the lowest energy vibrational level. Since the virtual states are not real states of the molecule but are created when the laser interacts with the electrons and causes polarization, the energy of these states is determined by the frequency of the light source used. The Rayleigh process will be the most intense process since most photons scatter this way. It does not involve any energy change and consequently the light returns to the same energy state. The Raman scattering process from the ground vibrational state m leads to absorption of energy by the molecule and its promotion to a higher energy excited vibrational state (n). This is called Stokes scattering (Smith & Dent , 2005).

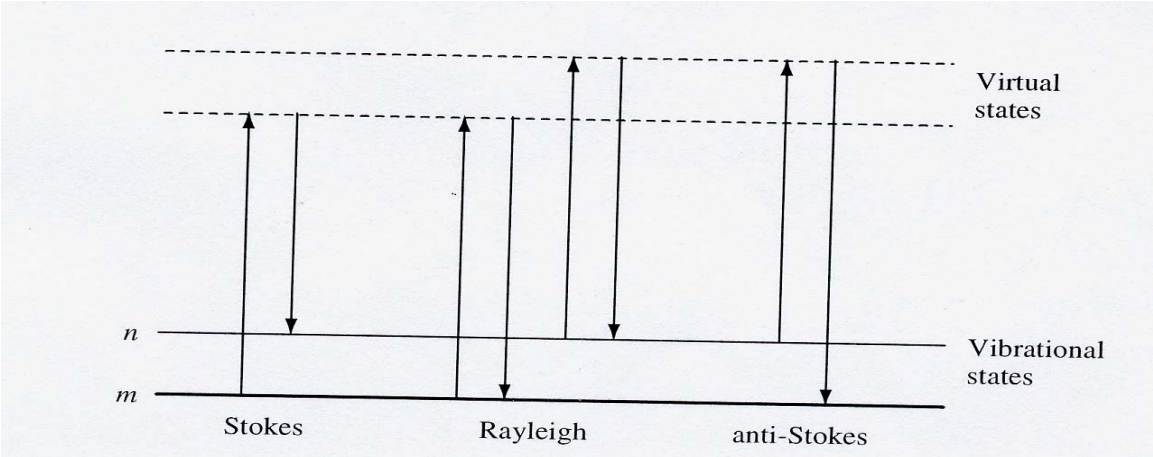

Figure 2.7. Diagram of the Rayleigh and Raman scattering processes. The lowest energy vibrational state m is shown at the foot with states of increasing energy above it. The higher energy excited vibrational state is called n. Both the low energy (upward arrows) and the scattered energy (downward arrows) have much larger energies than the energy of a vibration (Smith & Dent , 2005).

However, due to thermal energy, some molecules may be present in an excited state such as n (Fig.2.7). Scattering from these states to the ground state m is called anti-Stockes scattering and involves transfer of energy to the scattered photon.
Thus, compared to Stokes scattering, anti-stockes scattering will be weak and will become weaker as the frequency of the vibration increases. Raman scattering is recorded only on the low-energy side to give Stokes scattering but occasionally anti-Stokes scattering is preferred (Smith & Dent, 2005). In Raman spectroscopy the laser source generates some molecular vibrations. The number of peaks and their energies are linked to the overall shape of the molecule. These are called fingerprint bands, which appear in different wave number values. The pattern of these bands can help identify a specific compound in the sample.

In experiment the Raman active bands of calcite, appears at 280 cm^{-1} and the finger printing bands of aragonite are recorded at 150 cm^{-1} and 210 cm^{-1} which, are used for identification of these polymorphs in PCC samples (Fig.2.8) (He et al, 2006).

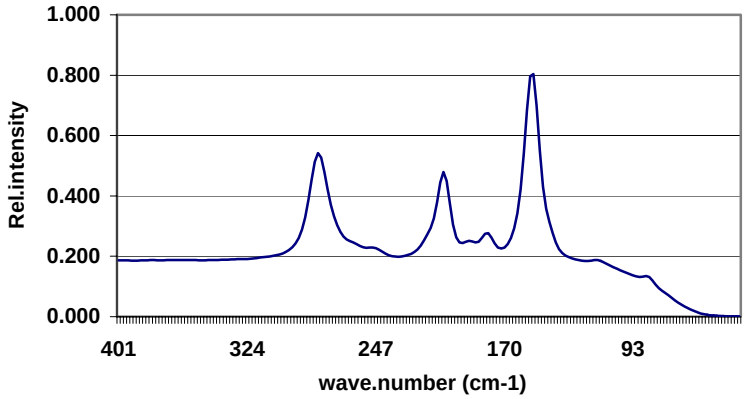

Figure 2.8. Raman spectrum of calcite and aragonite in PCC, sample (PCC-1)

In order to quantify the concentration of calcite and aragonite by Raman spectroscopy, external standard method was chosen, the different amounts of pure calcite and pure aragonite (standards) were mixed to cover a wide range of concentration for different types of PCC (Christos et al, 1999, Dandeu et al, 2006). The mixtures were measured using Raman spectrometer; RFS100/S of Bruker Company and calibration curves were plotted individually.

The measurement conditions are given as follows:

Laser source: wavelength (1064nm), power of laser radiation (250mW)

Resolution: (4 cm^{-1})

Number of scans: (200)

Sample holder: Quartz cuvettes, (diameter, 0.5 cm)

Each standard and sample are measured three times in different spots along Y axis (up to down) in order to minimize statistical error and inhomogenity.

In the quantification step Raman calibration curves for a wide range of concentrations were plotted based on the integrated peak area for aragonite (150cm^{-1}) and for calcite (280cm^{-1}) (Fig.2.9a, b) (Dandeu et al, 2006).

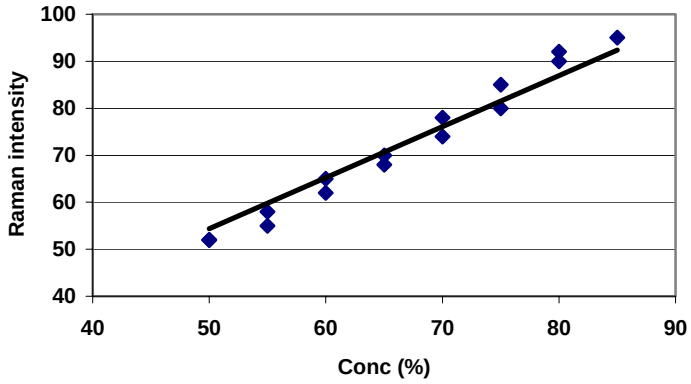

Figure 2.9a. Calibration curve of aragonite (Raman band=150cm^{-1})
(R^2=0.96=correlation coefficient (line equation=y=1.08x)

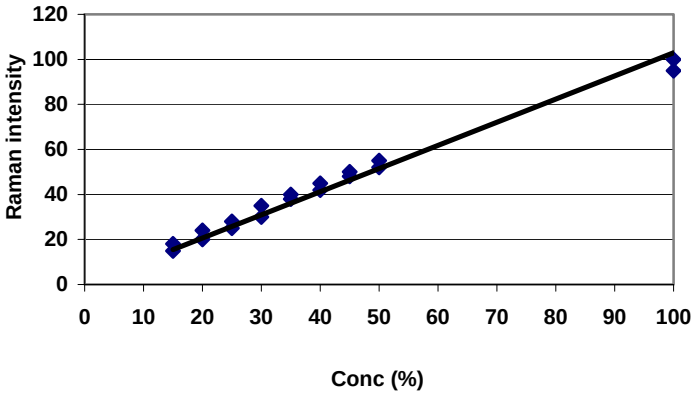

Figure 2.9b. Calibration curve of calcite (Raman band=280cm^{-1})
(R^2=0.98=correlation coefficient (line equation=y=1.02x)

The accuracy of measured concentration of calcite and aragonite was tested using standard samples (Table-2.5).

Table-2.5. Accuracy of quantitative results by Raman spectrometer

Standard samples	Aragonite (Meas.%)	Aragonite (Known.%)	Aragonite Difference%	Calcite (Meas.%)	Calcite (Known) %	Calcite Difference %
60Ar40Ca	55.4	60	±4.6	44.6	40	±4.6
70Ar30Ca	68.6	70	±1.4	31.4	30	±1.4
85Ca15Ar	12.4	15	±2.6	87.6	85	±2.6
98Ca2Ar	1.3	2	±0.7	98.7	98	±0.7

The results of Raman spectroscopy prove that the difference between the measured and calculated concentrations of calcite and aragonite sets in the range of ±0.7% - ±4.6% for standard samples.

The comparison between the measured concentration of calcite and aragonite in the series of standards samples (Tables-2.1, 2.2, 2.3, 2.5) using XRD (external standards method, Rietveld method) and Raman spectroscopy (external standard method) techniques proved that the results confirm each other. The external standard method based on the strongest diffraction lines of calcite (104) and aragonite (040) shows the difference between the measured and known concentration of calcite and aragonite in the range of ±0.9% - ±3.6%. The external standard method based on diffraction lines of calcite (012) and aragonite (121) shows the difference between the measured and known concentration of calcite and aragonite in the range of ±1.4% - ±2.3%. The Rietveld method (full pattern analysis) provides less difference between the measured and known concentration of calcite and aragonite (±0.3% - ±2.6%) in standard samples which means higher degree of accuracy.

The application of XRD pattern for PCC product characteristics is drown in figure.2.10.

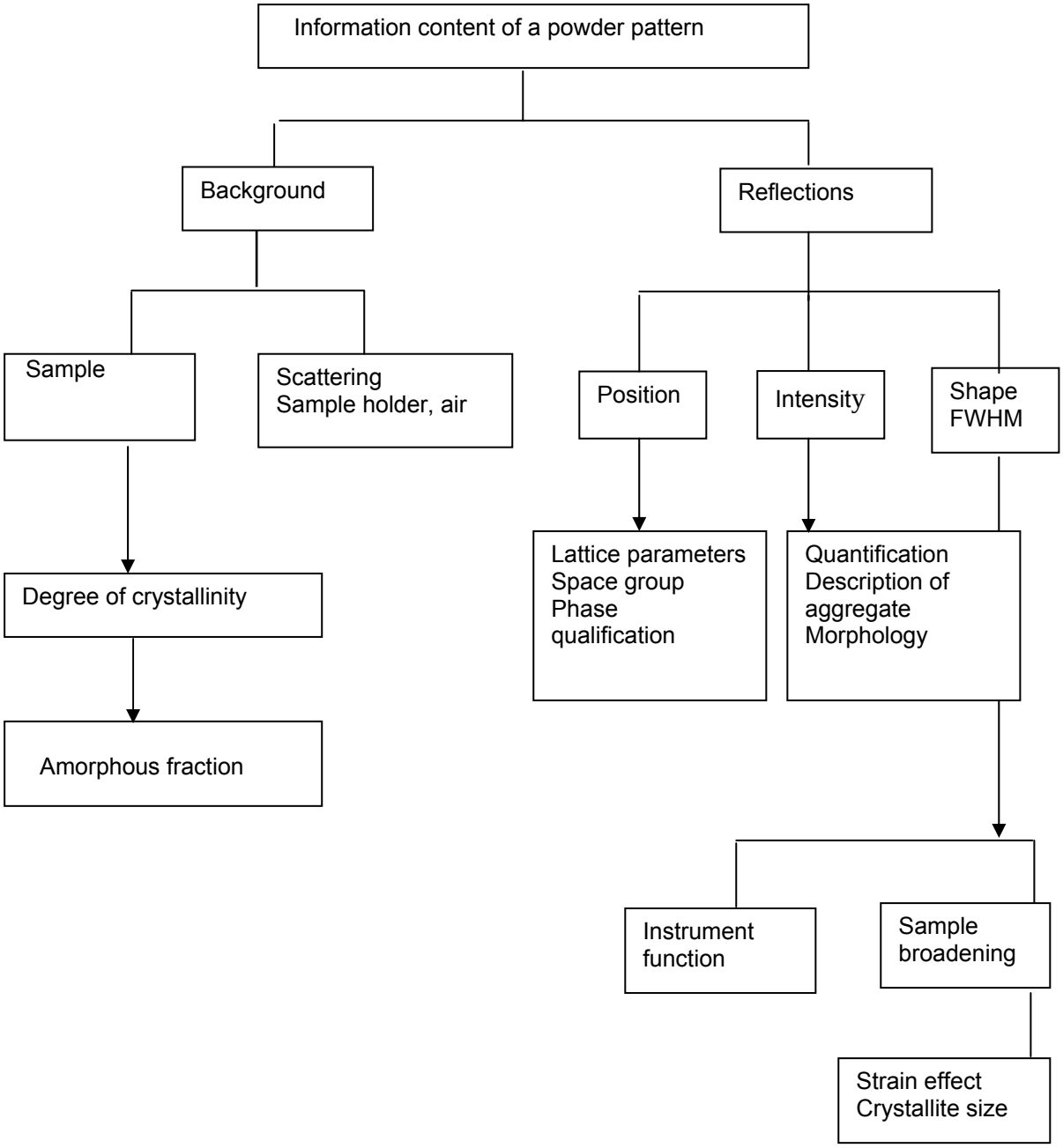

Figure 2.10. The flow sheet of XRD application

The flow sheet points out the application of different XRD variables in order to characterize PCC samples. The information content on XRD pattern is deduced from background and reflections.
Background comes from air scatterings, sample holder without any additional information on sample. Background is also deducted by sample which indicates degree of crystallinity, if the sample contains well crystallized minerals such as calcite and aragonite, therefore the intensity of background is negligible. The amorphous phase makes hump in background and the shape of background proves amorphous phase existance.

The information on reflections is deduced from peak position, peak intensity and peak shape. Peak position refers to diffraction angle and d.value (interplaner spacing) which provides basic crystallographic information on lattice parameters, Miller indices and crystalline phase identification.
Peak intensity is an important criterion to determine the abundance of calcite and aragonite, basically the intensity of XRD lines increases as the concentration of crystalline phase increases. Intensity ratio among the strongest diffraction line to consecutive XRD lines provides information on aggregates morphology description.
Peak shape is defined by Full Width at Half Maximum (FWHM) which is an important criterion in order to determine peak broadening. Peak broadening results from instrumental broadening which is measured by reference material. Peak broadening is a consequence of sample broadening as well. Sample broadening results from crystallite size and strain effect. The crystallite size of calcite and aragonite is measured by Scherrer equation and Williamson-Hall method. Strain effect results from the displacement of unit cells from their ideal position in a perfect crystal. In principle, point defects (impurities, vacancies), linear defects (dislocations) and planer defects (grain bounderies) make internal strain. Strain value is also important characteristic for PCC identification.

3. Results and Discussion

3.1. PCC and GCC characterization in powder form

3.1.1. Carbonate phase identification

Identification of calcite and aragonite is measured based on two analytical methods: XRD and Raman spectroscopy

X-ray diffraction is used for identification of polymorphs of calcium carbonates in PCC and GCC samples. The studied PCC samples in powder form and on paper sheet contain only calcite and aragonite. No additional crystalline phases such as vaterite or other impurities were identified within the limits of error of powder XRD. There is no indication of an amorphous phase (Appendix).

The Raman spectra of PCC samples are recorded and confirm the existence of calcite and aragonite without any additional crystalline phases.

3.1.2. Carbonate phase quantification

XRD and FT-RS (Raman spectroscopy) respectively, are used for quantification of PCC phases. Quantification by XRD is performed by the external standard, and the Rietveld method.

In external standard in order to plot the calibration curves of calcite and aragonite, the series of pure standards were prepared and calibration curves are drown consequently (Cullity & Stock, 2001, Dikkinson & Mc Grath, 2001).

The PCC and GCC samples were measured based on two strongest diffraction lines of calcite which appear at d.value = 3.03 (104) and d.value = 3.86 (102) and two strongest diffraction lines for aragonite which appear at d.value = 1.97 (040) and d.value = 2.70 (121) in order to investigate the texture effect in these PCC products.

The results of calcite and aragonite in the series of PCC samples based on the two strongest diffraction lines of these minerals are given in tables-3.1, 3.2.

Table-3.1. XRD results of aragonite and calcite, using external standard method.

Sample	Aragonite(%) d.value = 1.97 (040)	Aragonite(%) (standards)	Calcite(%) d.value = 3.03 (104)	Calcite(%) (standards)
PCC-1	87.3	-	12.7	-
Pre800	2.8	-	97.2	-
Pre320	5.2	-	94.8	-
360V	2.3	-	97.7	-
160G	3.1	-	96.9	-
Fb25	2.3	-	97.7	-
Pre720	3.1	-	96.9	-
Pre100	2.5	-	97.5	-
Pre600	87.1	-	12.9	-
Fb230	3.2	-	96.8	-
PFS210	2.5	-	97.5	-
PRP	2.4	-	97.6	-
GCCX	1.8	-	98.2	-
GCC90	2.1	-	97.9	-
PRF120	2.3	-	97.7	-
PS	2.2	-	97.8	-
PSU1	89.1	-	10.8	-
PSU2	81.3	-	18.7	-
PSU3	89.2	-	10.8	-
PSU4	84.9	-	15.1	-
PCLS	1.6	-	98.4	-
PCCSG	1.2	-	98.8	-
60Ar40Ca	63.6	60	36.4	40
70Ar30Ca	68.4	70	31.6	30
85Ca15Ar	14.1	15	85.9	85
98Ca2Ar	5.0	2	95.0	98

The results proved that the concentration of calcite in PCC and GCC samples based on the diffraction line (104) lays in the range of 10.8% - 98.8% and the concentration of aragonite based on diffraction line (040) sets in the range of 1.2% - 89.2%. It should be mentioned that, 60Ar40Ca, 70Ar30Ca, 85Ca15Ar, 98Ca2Ar are standards and contain the known concentrations of calcite and aragonite.

Table-3.2. XRD results of aragonite and calcite, using external standard method.

Sample	Aragonite(%) d.value=2.70 (121)	Aragonite(%) (standards)	Calcite(%) d.value=3.86 (012)	Calcite(%) (standards)
PCC-1	88.1	-	11.9	-
Pre800	4.4	-	95.6	-
Pre320	5.8	-	94.2	-
360V	3.3	-	96.7	-
160G	4.7	-	95.3	-
Fb25	3.9	-	96.1	-
Pre720	3.7	-	96.3	-
Pre100	3.6	-	96.4	-
Pre600	88.9	-	11.1	-
Fb230	4.0	-	96.0	-
PFS210	3.1	-	96.9	-
PRP	3.0	-	97.0	-
GCCX	2.4	-	97.6	-
GCC90	3.0	-	97.0	-
PRF120	2.8	-	97.2	-
PS	2.7	-	97.3	-
PSU1	90.4	-	9.6	-
PSU2	81.8	-	18.2	-
PSU3	89.8	-	10.2	-
PSU4	85.3	-	14.7	-
PCLS	2.3	-	97.7	-
PCCSG	1.1	-	98.9	-
60Ar40Ca	62.3	60	37.7	40
70Ar30Ca	67.9	70	32.1	30
85Ca15Ar	13.2	15	86.8	85
98Ca2Ar	3.4	2	96.6	98

The results show the concentration of calcite in PCC and GCC samples which refers to XRD line (012) puts in the range of 9.6% - 98.9%. Aragonite referring to XRD line (121) puts in the range of 1.1% - 90.4%.

- The measured concentrations of calcite based on crystal plane (104) sets between 31.6% - 95% and in terms of crystal plane (012) set between 32.1% - 96.6% for standard samples. The difference between the measured concentrations of calcite based on two diffraction lines results from texture effect. In order to minimize texture effect standards were reground twice.

- The measured concentration of aragonite refers to crystal plane (040) sets between 5.0% - 68.4% and crystal plane (121) sets between 3.4% - 67.9% for standard samples which proves that the results of aragonite based on two diffraction lines are affected by texture effect as well.

- The difference between the concentrations of aragonite in low concentration level refers to the detection limit of XRD for quantification. The detection limit is defined as the critical edge of measurement for each instrument; therefore, even 30-50 % error around the detection limit is acceptable.

The third possibility in order to determine the abundance of calcite and aragonite is Rietveld method (full pattern analysis). The results of PCC samples and standards are given in table-3.3.

Table-3.3. XRD results of aragonite and calcite, using Rietveld method (full pattern analysis).

Sample	Aragonite(%)	Aragonite(%) (standards)	Calcite(%)	Calcite(%) (standards)
PCC-1	84.7	-	15.3	-
Pre800	0.4	-	99.6	-
Pre320	2.8	-	97.2	-
360V	0.0	-	100	-
160G	0.0	-	100	-
Fb25	0.2	-	99.8	-
Pre720	1.1	-	98.9	-
Pre100	0.6	-	99.4	-
Pre600	84.3	-	15.7	-
Fb230	0.0	-	100	-
PFS210	0.0	-	100	-
PRP	0.0	-	100	-
GCCX	0.0	-	100	-
GCC90	0.0	-	100	-
PRF120	0.0	-	100	-
PS	0.0	-	100	-
PSU1	86.6	-	13.4	-
PSU2	80.0	-	20.0	-
PSU3	87.7	-	12.3	-
PSU4	83.1	-	16.9	-
PCLS	0.0	-	100	-
PCCSG	0.0	-	100	-
60Ar40Ca	57.4	60	42.6	40
70Ar30Ca	69.7	70	30.3	30
85Ca15Ar	13.5	15	86.5	85
98Ca2Ar	1.5	2	98.5	98

The results prove that the concentration of calcite based on Rietveld method (full pattern analysis) sets in the range of 12.3% - 100% and aragonite sets in the range of 0.2% - 87.7%. The accuracy of results by Rietveld method using standards is plotted in figure.3.1.

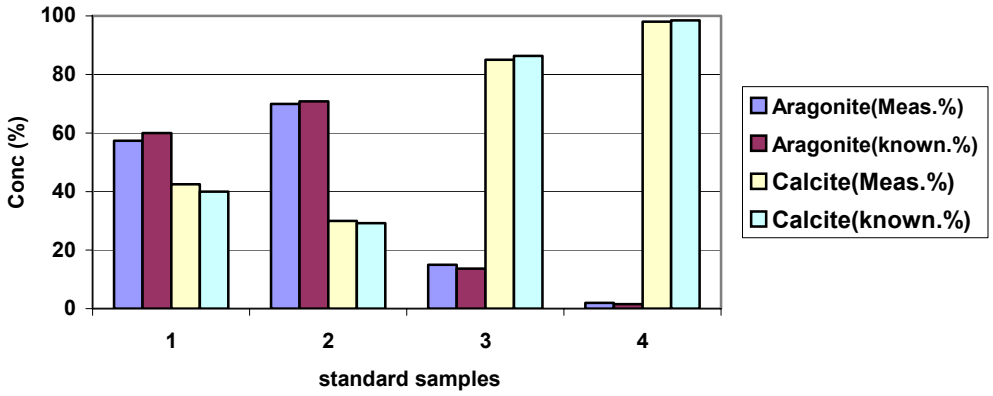

Figure 3.1. The comparison of quantitative results by Rietveld method

The advantage of Rietveld method is to fit the observed XRD profile and calculated XRD profile in terms of peak width, peak height, peak symmetry and intensity which provides the highest degree in the accuracy of results.

The accuracy of quantitative phase analysis is investigated using the standard samples, which have been calculated by different methods (external standard and Rietveld method). The comparison between the results of standard samples illustrates that the Rietveld method provides higher degree of accuracy than external standard for quantitative phase analysis. It should be pointed out that PCCs have very fine-grained size but in the external standards, it is not practical to provide the grain size of particles as fine as commercial PCCs. The over-grinding of standards destroys the crystal structure which causes hump in background and increases the background intensity as well. The background is subtracted in whole diffraction pattern by means of Rietveld method. In addition to the grain size effect, the preferred orientation effect in the external standard method is one of the major error sources.

In this method, the intensity of the strongest diffraction line is considered to minimize the statistical error. Then, the intensity of the strongest diffraction lines of calcite (104), (102) and aragonite (040), (121) versus the concentration of these minerals are plotted in the series of standards individually. The preferred orientation effect is a

dominant error source on the intensity variation and makes negative influence on the intensity of the strongest diffraction line with the highest rate of the intensity (Will, 2006).

Raman spectroscopy is the supplementary analytical instrument in order to confirm the measured concentration of calcite and aragonite by means of XRD using external standard method and Rietveld method in PCC products. The results of FT-Raman spectroscopy are given in table-3.4.

Table-3.4. FT-Raman results of aragonite and calcite, using external standard

Sample	Aragonite(%)	Aragonite(%) (standards)	Calcite(%)	Calcite(%) (standards)
PCC-1	86.8	-	13.2	-
Pre800	1.5	-	98.5	-
Pre320	3.3	-	96.7	-
360V	0.4	-	99.6	-
160G	0.4	-	99.6	-
Fb25	0.7	-	99.3	-
Pre720	2.9	-	97.1	-
Pre100	0.7	-	99.3	-
Pre600	87.2	-	12.8	-
Fb230	0.8	-	99.2	-
PFS210	0.4	-	99.6	-
PRP	0.5	-	99.5	-
GCCX	0.8	-	99.2	-
GCC90	0.7	-	99.3	-
PRF120	0.4	-	99.6	-
PS	0.5	-	99.5	-
PSU1	84.6	-	15.4	-
PSU2	82.2	-	17.8	-
PSU3	88.7	-	11.3	-
PSU4	85.1	-	14.9	-
PCLS	0.4	-	99.6	-
PCCSG	0.3	-	99.7	-
60Ar40Ca	55.4	60	44.6	40
70Ar30Ca	68.6	70	31.4	30
85Ca15Ar	12.4	15	87.6	85
98Ca2Ar	1.3	2	98.7	98

The results show the measured concentration of calcite by FT-Raman which sets in the range of 11.3% - 99.7% and aragonite in the range of 0.3% - 88.7%.

In order to compare the results of calcite and aragonite (Tables.3-1, 3-2, 3-3, 3-4), the measured concentrations of calcite and aragonite using different methods versus known concentration in standards is plotted in figure.3.2a, b.

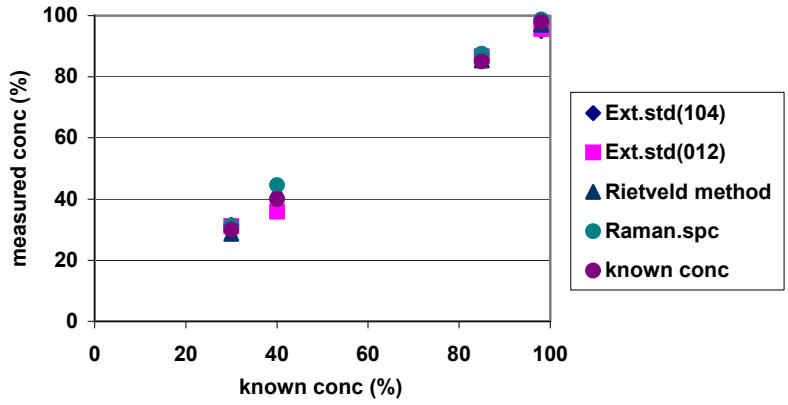

Figure 3.2a. Comparison of different methods for calcite quantification

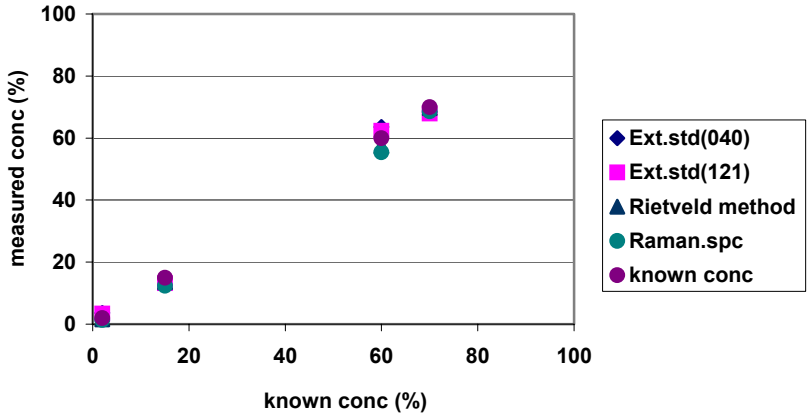

Figure 3.2b. Comparison of different methods for aragonite quantification

- According to the results of standard samples containing known concentration of pure calcite and aragonite, the results of external standard, Rietveld method and Raman spectrometer confirm each other. The Rietveld method provides the most accurate and precise data for PCC quantification (Fig.3.2a, b).

- According to the results of quantitative phase analysis by means of cluster analysis, PCC samples are classified into two main types (Fig.3.3).

  In the first type aragonite is the dominant mineral (>80%) and calcite is the minor phase (<20%) which includes samples PSU1, PSU2, PSU3, PSU4, PCC-1, Pre600.

  In the second type, the samples are almost pure calcite (>96%) consisting of samples Pre320, Pre720, Pre100, Pre800, Fb25, PCCSG, PCLS, 160G, 360V, PS, PRF120, GCC90, GCCX, PRP, PFS210, Fb230.

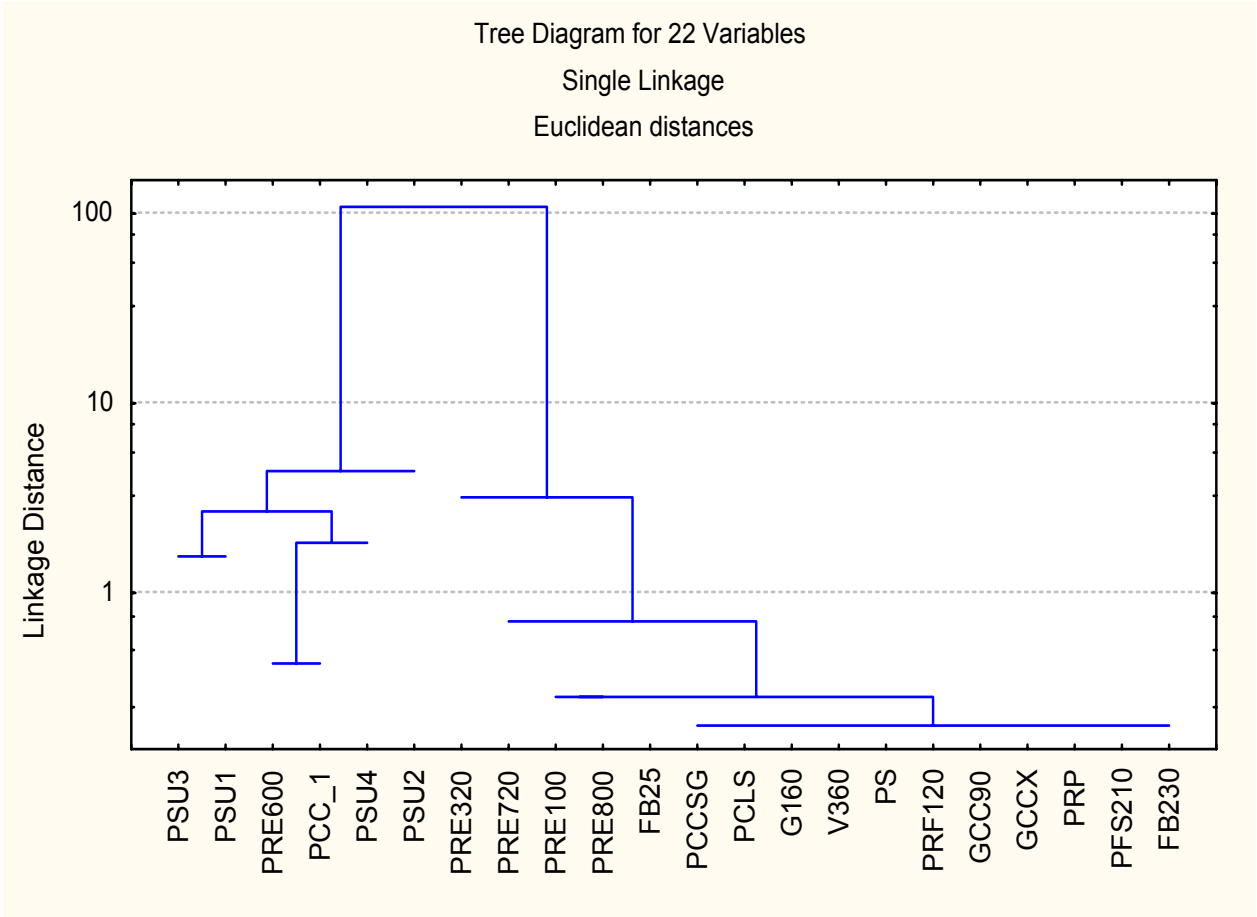

Figure 3.3. The cluster tree of PCC and GCC samples based on quantitative phase analysis

3.1.3. Morphology description

Different morphologies of calcite and aragonite in PCCs and GCCs give different properties to paper as final product.

In order to determine morphologies of single particles, aggregates and crystal size of calcite in PCC and GCC, SEM was applied and XRD was developed to determine the morphologies of aggregates (Fig.3.4). Appendix shows different morphologies in PCC and GCC samples.

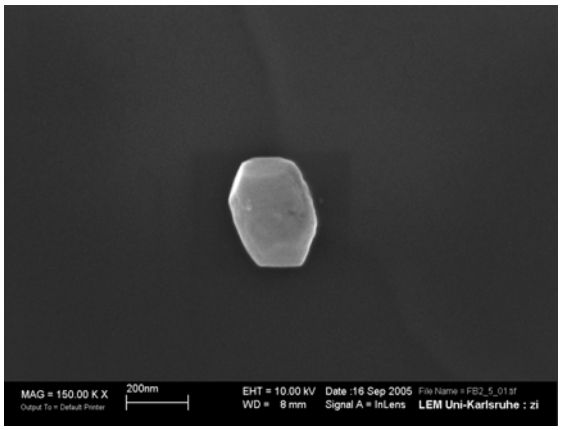

Fb25 (calcite) (PCC)
crystal size = 200nm

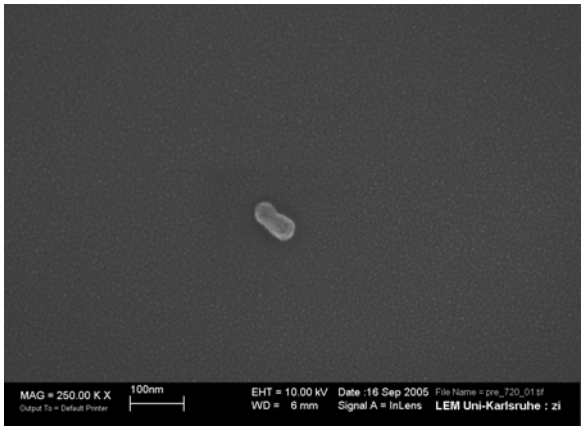

Pre720 (calcite) (PCC)
crystal size = 100nm

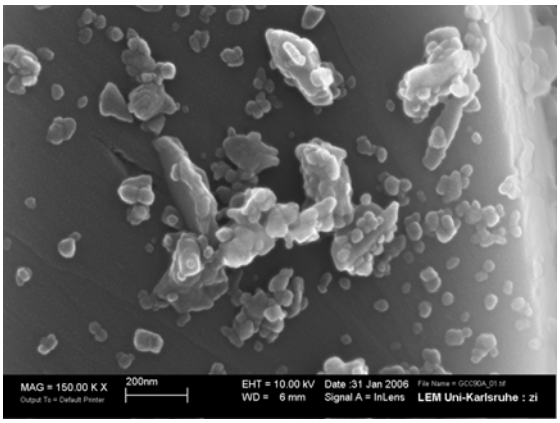

GCC90 (calcite) (GCC)
crystal size = 30nm

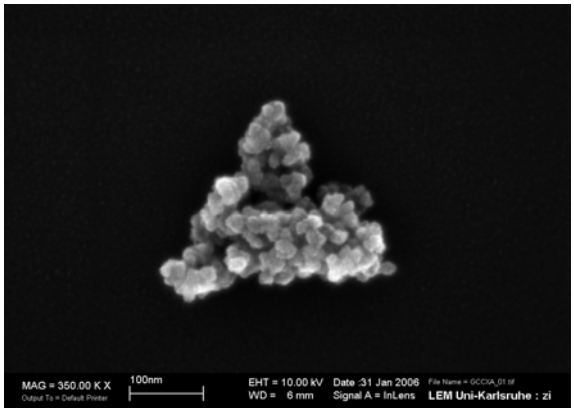

GCCX (calcite) (GCC)
crystal size = 28nm

Figure 3.4. The crystal size of single particle and shape of single crystal and aggregate description of PCC and GCC by SEM image

Different morphologies of calcite in PCC and GCC samples are shown in figure.3.4. The SEM image of sample Fb25 illustrates that the crystal has symmetrical shape (hexagonal), and the crystal size is 200±39 nm. SEM image of sample Pre720 illustrates that the crystal has asymmetrical shape, and crystal size is 100±26 nm. SEM images of GCC samples, illustrate that the crystal size of sample GCCX is 28±11 nm and of sample GCC90 is 30±14 nm. The crystal size of 16 PCC samples (calcite) is given in table-3.5. The crystal size of GCC samples is less than of PCC samples considerably, because GCC samples are highly ground in the production line. Grain sizes of polymorphs are characterized using microscope (for crystals>1 micron) or Scanning Electron Microscopy (SEM) (Eberl & Kile, 2000). In order to determine the crystal size, 20 grains of each calcite sample were picked under SEM and the diameter for each grain was measured (Table-3.5).

Table-3.5. The crystal size of calcite in PCC and GCC samples (SEM)

Sample name	crystal size (nm)
Pre320	180±18
Pre720	100±26
Fb25	200±39
Pre800	260±30
Pre100	250±41
Fb230	60±7
160G	150±34
360V	138±22
GCCX	28±11
GCC90	30±14
PCLS	100±8
PS	340±42
PFS210	265±44
PCCSG	519±37
PRP	265±58
PRF120	290±34

The wide scattering range of crystal size in calcite (28±11 - 519±37 nm) arises from the crystal growth rate which is influenced by several physical factors, such as surface tension of solution, pressure, temperature, relative crystal velocity in the solution and Reynolds number (flow pattern)(Markov, 2003).

The crystal shape and size of PCC and GCC products are affected by crystal growth mechanism. These growth mechanisms can be interpreted by analyzing crystal and crystallite size measurement and distribution (So & Choi, 2000, Isopescu et al, 1996). The significant factors of crystal growth mechanisms are relevant to the synthetic systems and crystallization conditions such as reaction temperature, initial concentration of $Ca(OH)_2$ in slurry, the blowing rate of CO_2 gas and the reaction completion time (Park & Choi, 2004).

Morphologies of aggregates are determined by XRD because particles with non-spherical shapes orient differently on XRD slide (Dobojit & Samiran, 1999).

In order to gain information on aggregates morphology, the contribution of the preferred orientation effect in different morphologies of calcite was investigated. The method is based on the calculation of intensity ratio as the intensity of the first diffraction line of calcite (104), to the intensity of the consecutive diffraction lines (116), (012), (202), (113), (018), and (122) with sensible intensity in XRD pattern. The same procedure is carried out for aragonite in terms of the intensity ratio of strongest diffraction line (040) to the subsequent lines (111), (202), (022), (113), (102) (Tables-3.6-9).

In order to justify the reproducibility of intensity ratio (peak height and peak area) for these samples, the powder of each sample was prepared as a cone shape then flattened on the XRD slides and measured five times for each sample under the same measurement conditions individually. It is evident that the preparation of the specimens is crucial for achieving reproducible results. Ideally, there should be a sufficient number of preferred oriented crystallites in the specimens to provide intensity variations for all reflections (Will, 2006).

Table-3.6. The average of intensity ratio (X) with standard deviation (δ) (peak height) for XRD lines in calcite morphologies (five times sample preparation) in PCC, GCC series

Sample	I(104)/I(116)	I(104)/(I(012)	I(104)/I(202)	I(104)/I(113)	I(104)/I(018)	I(104)/I(122)
PCC-1	1.25±0.11	5.44±0.87	1.79±0.12	4.38±0.18	4.83±0.49	7.91±0.34
Pre800	6.15±0.08	8.57±0.25	7.13±0.10	5.47±0.10	6.17±0.09	14.51±0.31
Pre320	6.34±0.12	10.17±0.06	7.35±0.16	5.75±0.09	6.38±0.11	16.16±0.28
360V	5.47±0.09	9.59±0.23	6.60±0.20	5.63±0.06	5.73±0.14	15.58±0.28
160G	5.84±0.21	8.55±0.46	6.95±0.30	5.55±0.10	6.37±0.21	15.53±0.13
Pre100	6.20±0.12	9.19±0.37	6.27±0.30	5.33±0.11	6.60±0.30	13.52±0.18
Pre600	1.14±0.05	5.58±0.19	1.68±0.09	3.34±0.08	4.87±0.14	8.68±0.20
Fb230	5.56±0.36	9.15±0.27	5.80±0.10	5.06±0.36	6.27±0.32	13.38±0.29
PFS210	6.33±0.17	8.43±0.16	6.34±0.28	5.23±0.14	6.22±0.16	14.48±0.20
PRP	5.71±0.19	7.70±0.33	5.66±0.19	5.06±0.05	6.51±0.18	12.50±0.23
PRF120	5.67±0.14	7.56±0.12	5.58±0.18	4.89±0.25	5.72±0.26	10.61±0.28
PS	5.68±0.18	7.74±0.47	5.74±0.49	4.90±0.24	6.32±0.39	12.80±1.49
PSU1	3.34±0.26	8.25±0.41	5.74±0.48	5.33±0.36	6.47±0.19	14.68±0.29
PSU2	3.14±0.12	8.25±0.43	5.32±0.37	5.43±0.45	5.42±0.18	13.06±0.41
PSU3	3.40±0.17	8.29±0.24	5.34±0.37	5.32±0.25	5.82±0.11	13.40±0.16
PSU4	3.35±0.07	8.25±0.41	5.34±0.32	5.30±0.11	5.41±0.53	13.31±1.42
PCLS	5.50±0.17	7.59±0.12	4.83±0.14	4.31±0.21	6.53±0.32	10.19±0.54
PCCSG	5.34±0.17	8.40±0.39	5.35±0.19	4.71±0.21	6.46±0.19	10.75±0.23
Fb25	5.81±0.21	8.22±0.20	5.80±0.51	5.61±0.61	6.23±0.11	11.41±0.80
Pre720	5.11±0.20	10.31±0.91	6.51±0.41	5.32±0.23	5.31±0.21	12.91±0.92
GCC90	6.71±0.40	11.50±0.51	5.51±0.21	4.80±0.31	14.81±0.21	16.30±0.71
GCCX	6.50±0.31	10.40±0.50	6.70±0.21	6.61±0.21	11.10±0.31	15.51±0.61

Table-3.7. The average of intensity ratio (X) with standard deviation (δ) (peak height) for XRD lines in aragonite morphologies (five times sample preparation) in PCC series

Sample	I(040)/I(111)	I(040)/(I(202)	I(040)/I(022)	I(040)/I(113)	I(040)/I(102)
PCC-1	0.65±0.03	1.21±0.02	2.23±0.02	1.46±0.08	1.67±0.17
Pre600	0.66±0.01	1.24±0.04	2.16±0.13	1.61±0.03	1.86±0.06
PSU1	0.55±0.02	1.13±0.05	2.03±0.06	1.13±0.04	1.56±0.11
PSU2	0.59±0.05	1.08±0.06	1.91±0.04	1.12±0.08	1.43±0.02
PSU3	0.60±0.10	1.14±0.06	2.19±0.03	1.18±0.05	1.57±0.13
PSU4	0.59±0.02	1.08±0.05	1.85±0.13	1.05±0.03	1.51±0.03

Table-3.8. The average of intensity ratio (X) with standard deviation (δ) (peak area) for XRD lines in calcite morphologies (five times sample preparation) in PCC, GCC series

Sample	I(104)/I(116)	I(104)/(I(012)	I(104)/I(202)	I(104)/I(113)	I(104)/I(018)	I(104)/I(122)
PCC-1	1.06±0.03	5.19±0.38	1.66±0.27	4.56±0.33	5.01±0.27	7.90±0.29
Pre800	6.18±0.06	8.95±0.05	7.26±0.12	5.49±0.22	6.24±0.03	14.34±0.20
Pre320	6.39±0.12	10.63±0.16	7.34±0.14	5.69±0.21	6.80±0.13	16.24±0.11
360V	5.19±0.15	9.93±0.13	6.34±0.12	5.68±0.43	6.10±0.06	15.61±0.16
160G	6.25±0.04	8.92±0.04	6.80±0.16	5.30±0.08	6.46±0.24	15.36±0.30
Pre100	6.17±0.05	9.09±0.19	6.21±0.49	5.28±0.16	6.68±0.16	13.38±0.20
Pre600	1.31±0.21	5.66±0.25	1.73±0.08	3.60±0.17	4.64±0.17	8.85±0.20
Fb230	5.41±0.26	9.19±0.20	5.67±0.16	4.61±0.09	5.70±0.26	13.66±0.12
PFS210	6.58±0.06	8.92±0.09	6.26±0.03	5.40±0.07	6.04±0.12	14.69±0.17
PRP	5.70±0.19	7.70±0.33	5.65±0.19	5.06±0.04	6.51±0.17	12.50±0.23
PRF120	5.59±0.32	7.80±0.07	5.60±0.26	4.82±0.32	5.66±0.26	10.40±0.08
PS	5.60±0.37	7.66±0.15	5.63±0.43	4.98±0.09	6.48±0.29	12.87±1.40
PSU1	3.19±0.04	7.75±0.11	5.48±0.13	5.81±0.39	6.49±0.23	14.60±0.27
PSU2	3.37±0.21	8.57±0.38	5.30±0.09	5.45±0.09	5.51±0.15	13.52±0.18
PSU3	3.26±0.13	8.27±0.25	5.26±0.39	5.33±0.18	5.66±0.13	13.42±0.21
PSU4	3.33±0.12	8.26±0.09	5.24±0.33	5.46±0.23	5.49±0.33	14.25±0.43
PCLS	5.66±0.09	7.94±0.05	4.90±0.04	4.48±0.29	6.69±0.18	10.49±0.31
PCCSG	5.55±0.06	9.33±0.22	5.52±0.12	4.89±0.26	6.83±0.12	10.59±0.27
Fb25	5.61±0.21	8.71±0.20	5.30±0.20	5.20±0.11	6.30±0.20	11.41±0.40
Pre720	5.21±0.10	10.71±0.60	6.31±0.20	5.30±0.20	5.40±0.30	13.01±0.40
GCC90	6.11±0.60	11.30±0.21	5.61±0.40	4.80±0.50	15.41±0.71	16.50±0.31
GCCX	5.90±0.11	10.30±0.20	6.70±0.30	6.81±0.11	11.80±0.21	15.30±0.21

Table-3.9. The average of intensity ratio (X) with standard deviation (δ) (peak area) for XRD lines in aragonite morphologies (five times sample preparation) in PCC series

Sample	I(040)/I(111)	I(040)/(I(202)	I(040)/I(022)	I(040)/I(113)	I(040)/I(102)
PCC-1	0.68±0.03	1.48±0.03	2.21±0.03	1.78±0.03	1.74±0.03
Pre600	0.92±0.02	1.51±0.06	2.15±0.09	2.05±0.04	1.91±0.03
PSU1	0.72±0.03	1.13±0.08	1.92±0.08	1.41±0.08	1.69±0.04
PSU2	0.78±0.05	1.32±0.04	1.94±0.10	1.46±0.11	1.23±0.17
PSU3	0.76±0.03	1.27±0.06	2.29±0.17	1.34±0.05	1.25±0.04
PSU4	0.73±0.02	1.28±0.05	1.83±0.09	1.30±0.11	1.25±0.09

Powder diffraction is based on fully random distribution of crystallites of equal size and spherical shape. Any deviation from a random distribution will affect more or less the measured intensities in the diffraction pattern. This deviations are meant “preferred orientation effect which is a clue for morphology description (Will, 2006). The morphology of aggregates is investigated by the intensity ratio of the strongest diffraction line to consecutive XRD lines. The intensity ratios based on peak height and peak area for the polymorphs of calcite and aragonite in PCCs and GCCs are reproducible. Obviously, some of these differences in intensity ratio are significant and determine the morphology of aggregates. The results given in tables-3.6, 3-7,3-8,3-9, prove these facts as follows:

- The intensity ratios based on peak area are more reproducible than the intensity ratios based on peak height, because peak width changes depending on strain/crystallite size broadening. If a peak gets broader, its height should get smaller because the peak intensity should remain constant. Peak height can change as a consequence of texture effect or as a consequence of peak broadening.

- The intensity ratios in different polymorphs are affected by texture effects. Although the preferred orientation effect causes negative influence on quantification on the other hand, it provides indirect information on the aggregates morphology description.

- The correlation between texture effect and intensity ratio for calcite and aragonite in the series of PCC and GCC samples were investigated. The fluctuation of intensity ratio proved that, texture effect has important contribution, which makes considerable differences among the intensity ratios of calcite and aragonite.

- The numerical values of intensity ratio (peak area) of calcite and aragonite were translated and converted to corresponding graphical model by means of

radar diagram as a practical solution. These graphical models are used to visualize the significant difference between intensity ratio in calcite and aragonite for description of aggregate morphologies (Fig. 3.5,3.6).

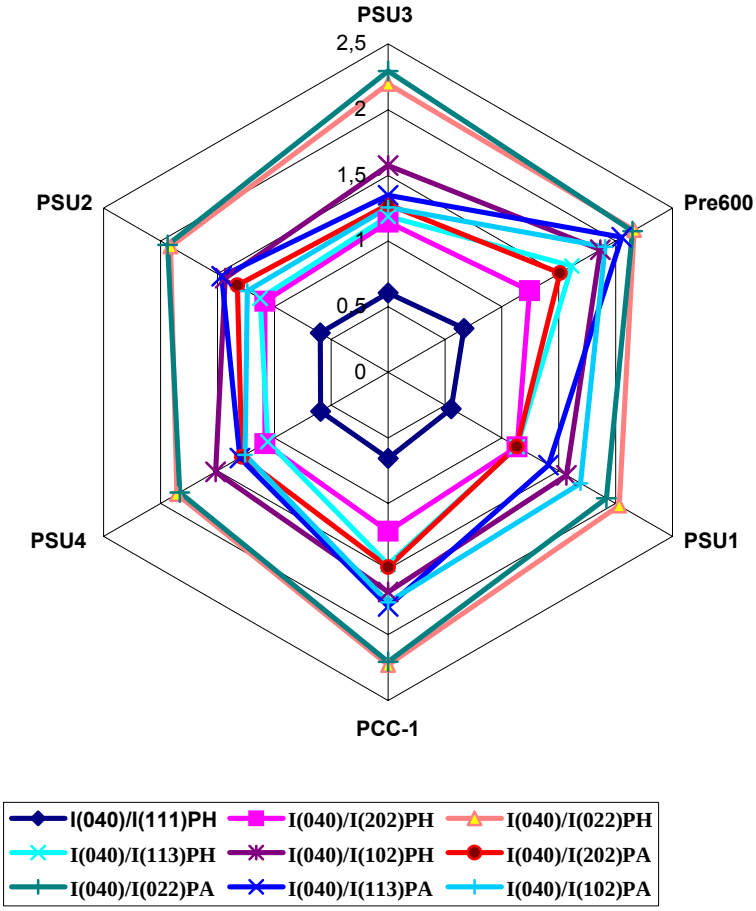

Figure 3.5. The graphical model (radar plot) of intensity ratio variation for aggregates morphology description in aragonite (PCC samples)

The graphical model based on the intensity ratio in aragonite indicates homogeneous shape relatively. That points out the intensity ratios of aragonite are not highly affected by texture effects .The particles of aragonite have moderately spherical shape with more tendency to random orientation effect. Different morphologies of aggregates in aragonite are not observed dramatically.

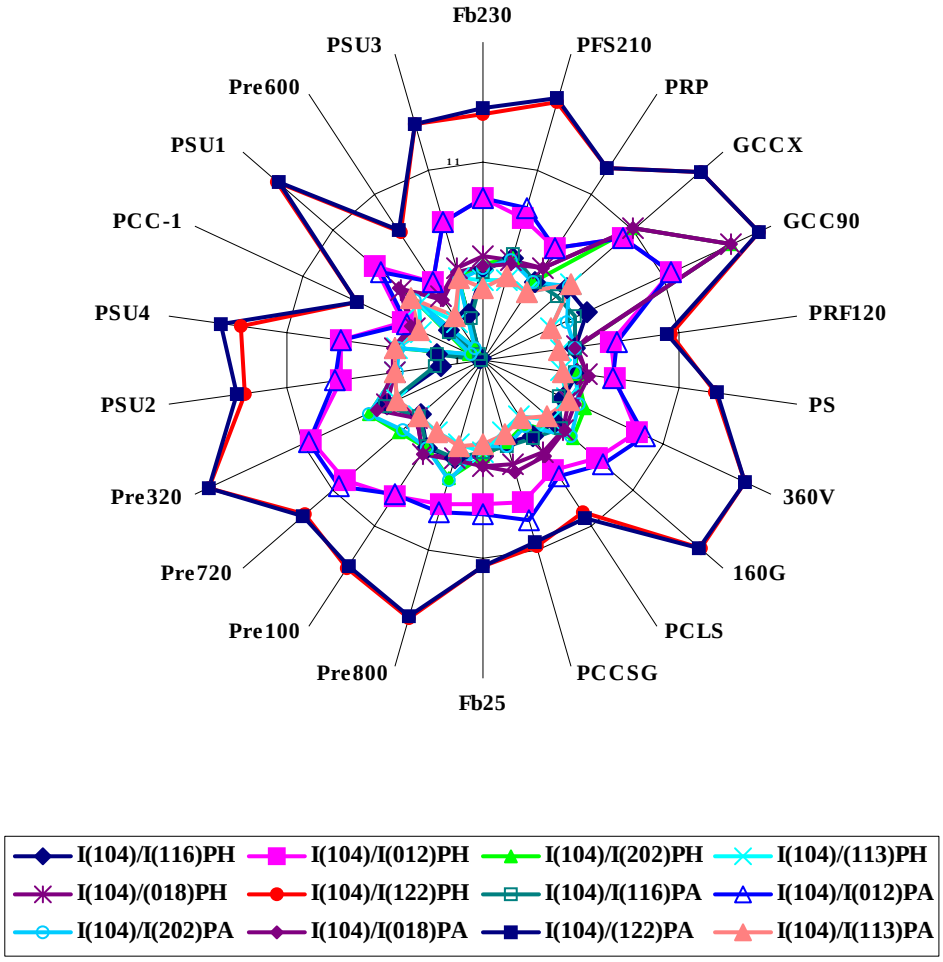

Figure 3.6. The graphical model (radar plot) of intensity ratio variation for aggregates morphology description in calcite (PCC samples)

The graphical model based on the intensity ratio in calcite illustrates inhomogeneous shape sharply. That points out the intensity ratios of calcite are highly affected by texture effect .The particles of calcite have non spherical shape dominantly with high tendency to preferred orientation effect. Different morphologies of aggregates in calcite are observed considerably. That means, calcite aggregates include a wide range of different morphologies in PCC and GCC samples.

3.1.4. Crystallite size and strain determination

Crystallite size and strain effect are determined in terms of XRD profile broadening. XRD profile broadening is a consequence of sample broadening and instrumental broadening. Therefore, the contribution of instrumental broadening has to be measured, and counted in order to determine crystallite size and strain in calcite and aragonite in the series of PCC and GCC samples. Instrumental broadening arises from the distribution of wavelengths in the incident beam, convoluted with several functions resulting from the geometry of the instrument, such as beam divergence, the finite width of source and receiving slit, specimen transparency and residual misalignment (David et al, 2002).

In the experimental section, the series of measurements were carried out for different divergence slit and receiving slit. The comparison of resolution in different receiving slit widths (0.6°, 0.3°, 0.18°) and fixed divergence slit at 1° was investigated in order to improve the resolution and minimize the contribution of instrumental broadening (Fig 3.7). The data are given for calcite, $FWHM_{obs}$ (104) and intensity of XRD profile (104) versus the slit width settings in tables 3.10, 3.11 and plotted (Fig.3.8, 3.9).

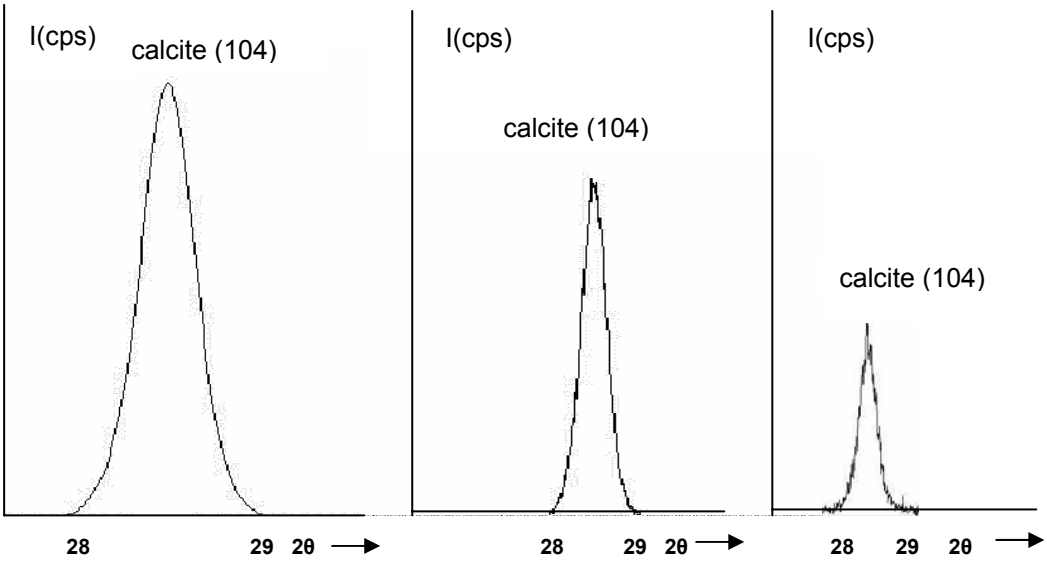

Figure 3.7. The comparison of instrumental resolution at different receiving slits (0.6°, 0.3°, 0.018°) and fixed divergence slit1°

Three different slit width settings (Fig.3.7) show the resolution of XRD profile of calcite (104) at different receiving slits (0.6°, 0.3°, 0.18°) and fixed divergence slit 1°.
At receiving slit of 0.6° XRD line (104) is identified by $FWHM_{obs}$ = 0.229°and intensity (peak area) = 1251 cps. There is no resolution in XRD profile, this peak looks quite smooth.
At receiving slit of 0.3° XRD line (104) is specified by $FWHM_{obs}$ = 0.217°and intensity (peak area) = 581 cps. There is an acceptable resolution in XRD profile, besides the XRD profile is sharper and the intensity is sensible enough for quantification and morphology description of aggregates. That provides optimum measurement conditions for PCC and GCC samples.
At receiving slit of 0.018° XRD line (104) is characterized by $FWHM_{obs}$ = 0.198°and intensity (peak area) = 43 cps. The resolution is in the best conditions, XRD profile is the sharpest one in these measurement campaigns. The point is that the main part of intensity is lost therefore the statistical errors rise up which make erroneous results in quantification and morphology description of aggregates.

Table-3.10.The correlation between divergence slit and peak broadening, receiving slit of 1°

Receiving slit	$FWHM_{obs}$ (104)	Intensity (height)	Intensity (peak area)
0.018	0.198	157	43
0.05	0.204	513	110
0.1	0.207	554	221
0.15	0.209	1689	394
0.3	0.217	1755	581
0.6	0.229	4936	1251

Table-3.11.The correlation between divergence slit and peak broadening, receiving slit of 3°

Receiving slit	$FWHM_{obs}$ (104)	Intensity (height)	Intensity (peak area)
0.018	0.204	173	46
0.05	0.208	582	131
0.1	0.211	597	245
0.15	0.214	1786	427
0.3	0.219	1803	588
0.6	0.231	5155	1314

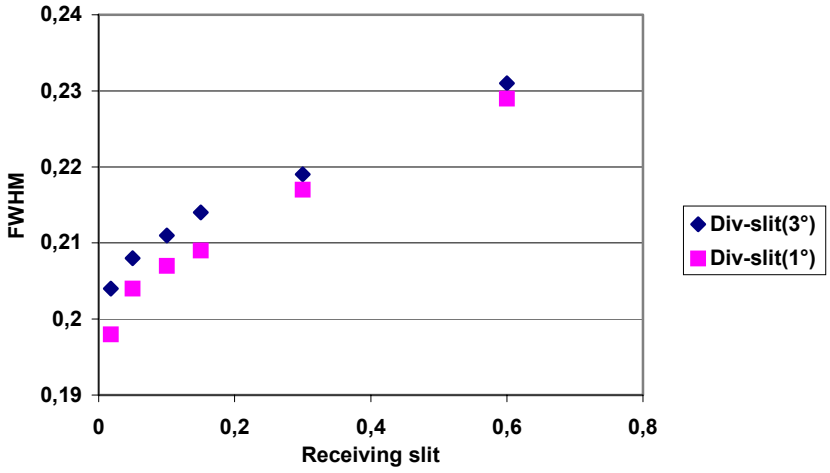

Figure 3.8. The correlation between slits and FWHM (104) in calcite

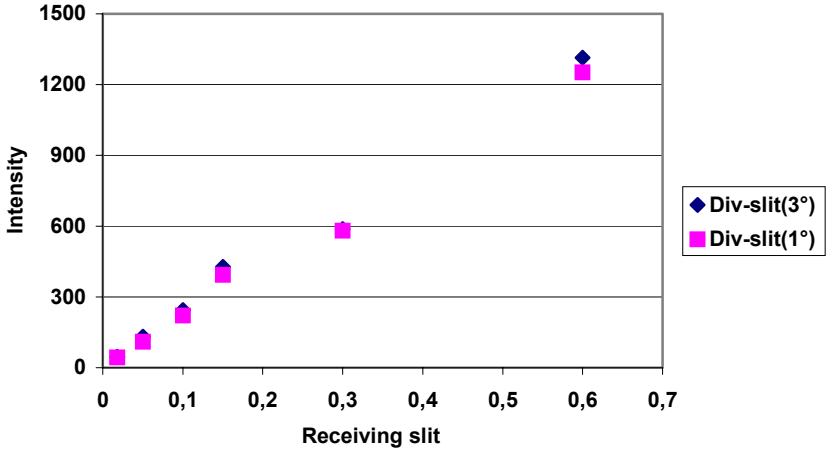

Figure 3.9. The correlation between slits and intensity in calcite (104)

The comparison of $FWHM_{obs}$ and intensity of XRD profile (104) in calcite versus slit width settings is plotted and shown in figures.3.8, 3.9. The optimum slit width settings are fixed at the divergence slit of 1° and receiving slit of 0.3°. In principle, the size of receiving and divergence slits width affect both width and intensity of a given line profile (104) in calcite.

In terms of optimum slit width settings, the contribution of instrumental broadening is calculated and considered in further calculations for crystallite size and strain effect determination.

That means $FWHM_{obs}$ is the sum of FWHM with respect to instrumental broadening ($FWHM_{Inst}$) and FWHM corresponding sample ($FWHM_{sample}$= $FWHM_{crystallite}$ +$FWHM_{strain}$). In order to determine the instrumental broadening contribution, pure quartz was measured under the optimum slit width conditions then FWHM of the strongest diffraction line of quartz was calculated and considered as a constant value for all measurements as a systematic error (David et al, 2002).

Crystallite size $<L>_{vol}$ indicates the volume weighted average column length, which is determined by the Rietveld method and the Williamson-Hall plots (Krill et al, 2000, Krill & Birringer, 1998).

The crystallite size in terms of the volume weighted average column length $<L>_{vol}$ of aragonite and calcite were measured based on Scherrer equation using Rietveld method and data are given in tables -3.12, 3.13.

Table-3.12. The crystallite size $<L>_{vol}$ in aragonite by Rietveld method ($FWHM_{instrument}$ =0.157°)

SAMPLE	Crystallite size(nm) $<L>_{vol}$Rietveld method	$FWHM(040)_{obs}$
FB25	65	0.266
Pre800	29	0.393
Pre100	27	0.445
Pre720	15	0.606
Pre320	135	0.210
PSU2	79	0.248
PSU4	82	0.245
PCC1	90	0.237
PSU1	82	0.246
Pre600	91	0.236
PSU3	74	0.256

Table-3.13. The crystallite size $<L>_{vol}$ of calcite by Rietveld method ($FWHM_{instrument}$ =0.157°)

SAMPLE	Crystallite size(nm) $<L>_{vol}$Rietveld method	$FWHM(104)_{obs}$
Fb230	47	0.291
PFS210	85	0.246
PRP	120	0.219
GCCX	21	0.560
GCC90	26	0.395
PRF120	175	0.198
PS	60	0.283
360V	62	0.281
160G	60	0.284
PCLS	101	0.236
PCCSG	143	0.210
FB25	119	0.220
Pre800	88	0.243
Pre100	90	0.246
Pre720	39	0.334
Pre320	123	0.219
PSU2	113	0.224
PSU4	109	0.226
PCC1	113	0.224
PSU1	129	0.215
Pre600	114	0.223
PSU3	148	0.206

The results (Tables-3.12, 3.13) indicate Rietveld method provides relative crystallite size of calcite (21-175 nm) and aragonite (15-135 nm) in semi quantitative sketch. Using Rietveld method whole $FWHM_{sample}$ is considered for crystallite size and replaced in Scherrer equation. That means the contribution of strain effect broadening is not subtracted in this method. In order to determine accurate crystallite size and strain effect in PCC and GCC samples Williamson-Hall method is proposed.

Williamson-Hall size-strain analysis was developed in 1953 as a method to separate size and strain effects by their angular dependence. This method gives $<L>_{vol}$ of crystallites.

In order to calculate $<L>_{vol}$, $FWHM_{sample}$ (ß) of all accessible diffraction lines of each mineral has to be determined (Whitfield & Mitchell, 2004).

$FWHM_{sample}$ $\cos\theta$(Y) is plotted versus $\sin\theta$(X) for calcite and aragonite in PCC and GCC samples individually (Fig.3.10, 3.12). The linear equation is given as follows:

$$Y=\varepsilon X+\lambda/ T$$

ε = slope =strain = ß $\cot(\theta)$

λ= wave length of X-radiation

$T=\lambda/$ ß $\cos\theta$= crystallite size (the volume weighted average column length $<L>_{vol}$)

The advantage of this method is that, one can determine the contribution of crystallite size (column length$<L>_{vol}$) extracted from the intercept and strain from the slope individually.

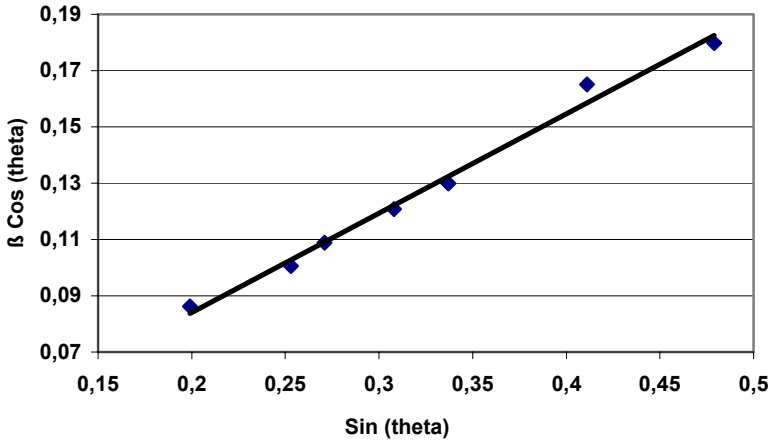

Figure 3.10. The Williamson-Hall plot in calcite, sample (Pre720)
(Y= 0.34 X + 0.0617) R^2= 0.9605

Table-3.14. The crystallite size<$L>_{vol}$ of calcite by Williamson-Hall method

Sample	Crystallite size <$L>_{vol}$ (nm) Williamson-Hall method
Fb230	46.7± 6.6
PFS210	73±10.20
PRP	118±8.40
GCCX	11.2±2.30
GCC90	20.2±3.70
PRF120	177.2±9.9
PS	58.3±5.60
360V	59.7±6.30
160G	50.8±4.10
PCLS	106.2±1.4
PCCSG	136.4±7.9
FB25	105±11.0
Pre800	77.7±8.20
Pre100	103.3±7.8
Pre720	25.0±4.40
Pre320	131.5±8.7
PSU2	110.0±9.6
PSU4	97.7±7.70
PCC1	128.1±10.8
PSU1	113.4±10.9
Pre600	127.6±11.6
PSU3	163.5±11.1

The data prove that crystallite size of calcite sets in the range of 11.2±2.30–177.2±9.9 nm . The crystallite size distribution of calcite calculated by Williamson-Hall plots for all PCC and GCC products is shown (Fig.3.11). The Williamson-Hall plots of calcite for all PCC and GCC products are given in appendix.

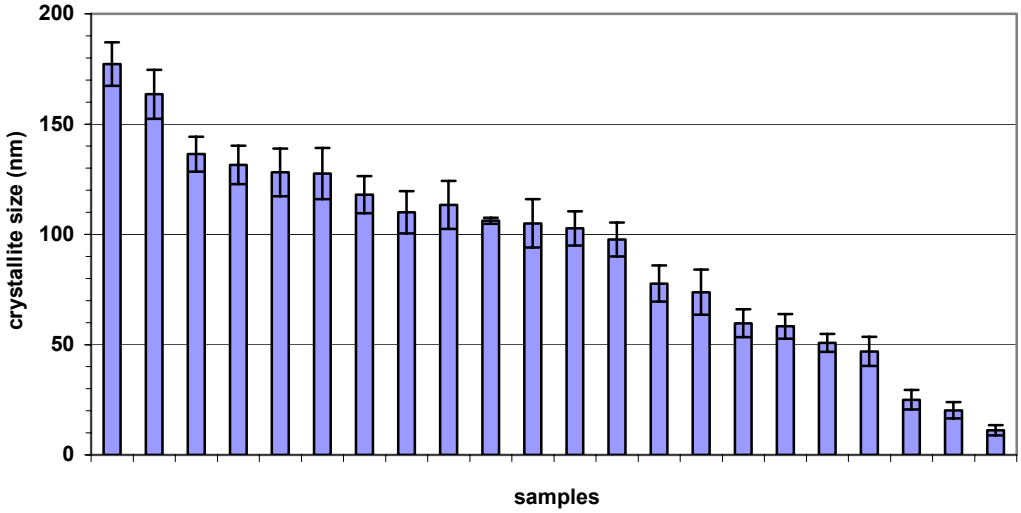

Figure 3.11. The crystallite size distribution of calcite by Williamson-Hall plot

The wide distribution range of crystallite size for calcite in PCC and GCC samples refer to synthetic conditions in terms of pressure, temperature, pH, flow rate and stirring speed in super saturation solutions. Flow rate is one important factor in crystallite size growth. In laminar conditions (Reynold's number < 2300) crystallites grow properly with larger size but in turbulent conditions (Reynold's number >2300) crystallite size becomes smaller (Markov, 2003).

The same measurement campaign was carried out in order to determine the crystallite size (column length$<L>_{vol}$) in aragonite based on Williamson-Hall method .The plot was drown in terms of the $FWHM_{sample}$(ß) cos(θ) versus sin(θ) for the presented diffraction lines of aragonite (Fig.3.12). It should be mentioned in the Williamson-Hall plot, $FWHM_{sample}$ of the accessible XRD lines are calculated in radians of 2 theta. The $<L>_{vol}$ of aragonite is calculated by the intercept of Williamson-Hall plot (Table-3.15).

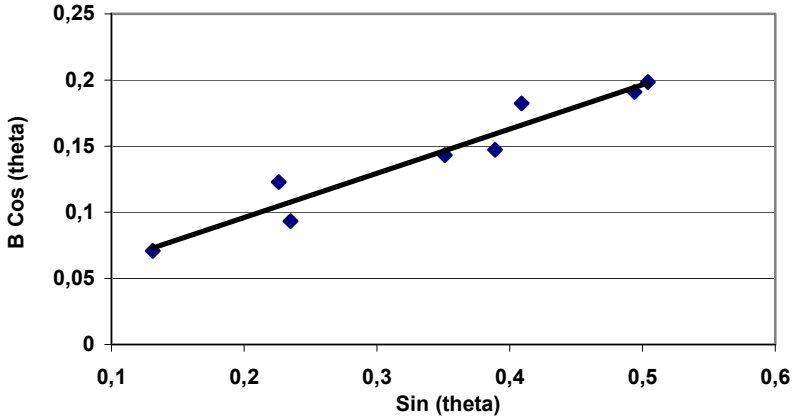

Figure 3.12. The Williamson-Hall plot in aragonite, sample (PSU2) (Y = 0.331 X + 0.020) R^2 =0.853

Table-3.15. The crystallite size $<L>_{vol}$ of aragonite by Williamson-Hall method

Sample	Crystallite size $<L>_{vol}$ (nm) Williamson-Hall method
PSU2	76.1±5.3
PSU4	84.5±6.3
PCC1	87.5±6.7
PSU1	83.2±6.7
PSU3	68.7±4.9
Pre600	87.1±6.5

Data prove that crystallite size of aragonite sets in the range of 76.1±5.3–87.5±6.7 nm. The crystallite size distribution of aragonite calculated by Williamson-Hall plots for all PCC and GCC products is shown in figure.3.13. The Williamson-Hall plots of aragonite for all PCC and GCC products are given in appendix.

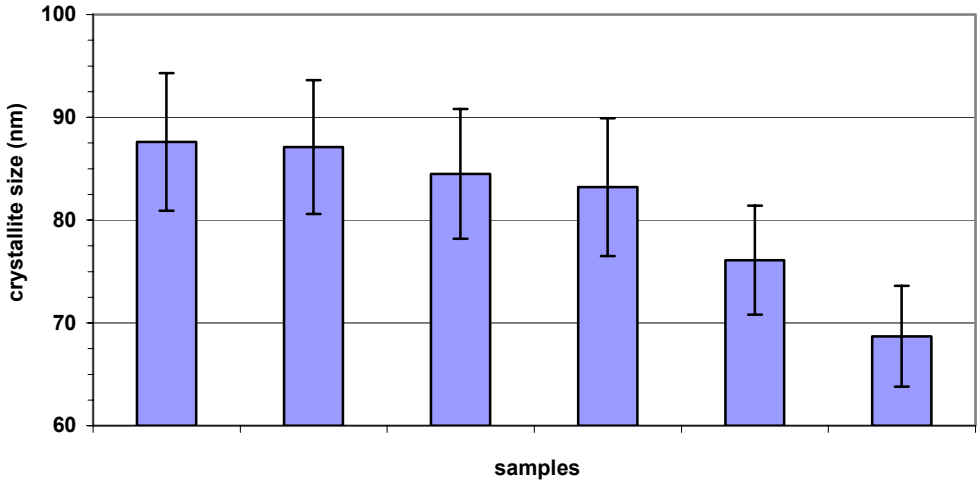

Figure 3.13. The crystallite size distribution of aragonite by Williamson-Hall plot

The scattering in crystallite size of aragonite depends on synthetic conditions of PCC samples. The comparison between the crystallite size of calcite and aragonite by Rietveld method (Tables-3.12, 3.13) and using Williamson-Hall method (Tables-3.14, 3.15), prove that Williamson-Hall method has higher degree of accuracy than the Rietveld method. The main reason is that the contribution of strain effect in XRD profile broadening is subtracted and considered to determine strain effect (Whitfield & Mitchell, 2004).

The strain effect represents displacements of unit cell from their ideal position caused any crystallographic defect (point, linear, planer), which happens during the synthetic conditions of PCC and GCC products.

Point defects arise from the vacancies and impurities. Vacancies are sites, which are usually occupied by an atom, but these are unoccupied. If a neighboring atom moves to occupy the vacant site, the vacancy moves in the opposite direction to the site, which used to be occupied by the moving atom. The stability of the surrounding crystal structure guarantees that the neighboring atoms will not simply collapse around the vacancy (Hammound, 2001).

Dislocations refer to linear defect caused by insertion of extra half plane of atoms into a perfectly layered structure. There are edge and screw dislocations which causes micro strain (Hammound, 2001).

Sample microstructure often contributes to diffraction line broadening. The contribution resulting from strain broadening is order-dependent. This means broadening effects will become increasingly severe at high diffraction angles (David et al, 2002).

The strain broadening effect was observed for aragonite in the series of crystal planes (121), (242), (102), (204). Data for aragonite are given in table-3.16. The strain broadening effect in ordered diffraction lines was also investigated in the series of crystal planes in calcite (012), (024), (113), (226) where FWHM increases at high angles. Strain broadening in ordered diffraction lines is dominant and shown in table-3.17.

Table-3.16. The effect of strain broadening in ordered diffraction lines $FWHM_{obs}$ in aragonite

Sample	d.value 2.70 2θ(33.13) (121) $FWHM_{obs}$	d.value 1.36 2θ(30.22) (242) $FWHM_{obs}$	d.value 2.49 2θ(36.12) (102) $FWHM_{obs}$	d.value 1.24 2θ(33.22) (204) $FWHM_{obs}$
PCC-1	0.302	0.224	0.339	0.318
Pre600	0.293	0.219	0.336	0.315
PSU1	0.325	0.314	0.481	0.454
PSU2	0.326	0.314	0.492	0.478
PSU3	0.318	0.302	0.478	0.455
PSU4	0.345	0.337	0.481	0.464

Table-3.17. The effect of strain broadening in ordered diffraction lines $FWHM_{obs}$ in calcite

Sample	d.value 3.85 2θ(23.05) (012) FWHM	d.value 1.92 2θ(47.08) (024) FWHM	d.value 2.28 2θ(39.38) (113) FWHM	d.value 1.14 2θ(84.85) (226) FWHM
PCC-1	0.256	0.328	0.312	0.389
Pre800	0.236	0.334	0.300	0.428
Pre320	0.257	0.339	0.324	0.415
360V	0.217	0.277	0.241	0.295
160G	0.246	0.292	0.289	0.331
Fb25	0.220	0.249	0.243	0.268
Pre720	0.363	0.438	0.427	0.493
Pre100	0.245	0.344	0.295	0.428
Pre600	0.257	0.329	0.313	0.390
Fb230	0.210	0.230	0.225	0.239
PFS210	0.269	0.361	0.302	0.391
PRP	0.240	0.270	0.262	0.286
GCCX	0.374	0.630	0.435	0.721
GCC90	0.311	0.476	0.371	0.545
PRF120	0.227	0.319	0.245	0.358
PS	0.267	0.289	0.274	0.296
PSU1	0.281	0.292	0.283	0.293
PSU2	0.254	0.291	0.265	0.365
PSU3	0.224	0.268	0.248	0.289
PSU4	0.268	0.287	0.276	0.291
PCLS	0.254	0.275	0.265	0.278
PCCSG	0.302	0.314	0.307	0.319

The FWHM data of aragonite and calcite (Table-3.16, 3.17) show the contribution of strain broadening in ordered diffraction lines particulary at higher diffraction angles in calcite and aragonite in all PCC and GCC samples. The strain broadening is a dominant factor in ordered diffraction lines rather than crystallite size broadening.

Obviously at higher 2theta values the XRD peaks are broader as compared to XRD peaks at smaller 2theta values (Whitfield & Mitchell, 2004). This is simply a consequence of the sinus function in the Bragg equation. That is also the reason, why lattice constants should be determined from XRD peaks at higher 2theta angles.

Williamson-Hall plots separate size and strain effects by their angular dependence. In these plots, strain is extracted from the slope in a quantitative manner. Strain values of calcite for PCC and GCC samples are given in table-3.18.

Table-3.18. The strain value in calcite

Sample	The strain value Williamson-Hall method
Fb230	0.147±0.018
PFS210	0.450±0.075
PRP	0.043±0.007
GCCX	0.347±0.041
GCC90	0.388±0.074
PRF120	0.088±0.011
PS	0.212±0.032
360V	0.099±0.012
160G	0.217±0.043
PCLS	0.111±0.003
PCCSG	0.123±0.094
FB25	0.153±0.017
Pre800	0.322±0.005
Pre100	0.342±0.028
Pre720	0.340±0.126
Pre320	0.292±0.052
PSU2	0.249±0.035
PSU4	0.343±0.045
PCC1	0.504±0.067
PSU1	0.312±0.054
Pre600	0.501±0.067
PSU3	0.427±0.084

Data show that strain values set in the range of 0.043 ± 0.007 - 0.504 ± 0.067.The strain value distribution of calcite calculated by Williamson-Hall plots for all PCC and GCC products is shown (Fig.3.14).

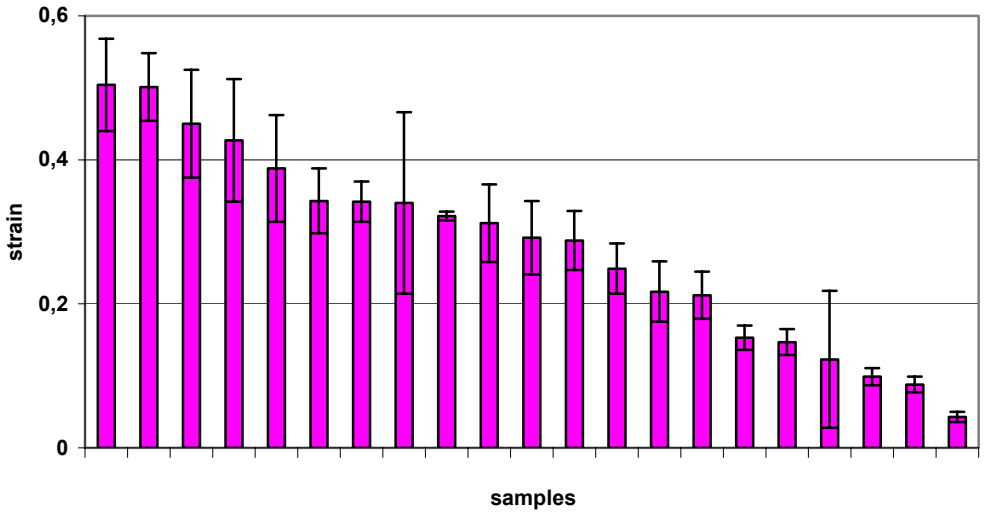

Figure 3.14. The strain value distribution of calcite by the Williamson-Hall plot

The wide distribution of strain values in calcite points out synthetic conditions by imposing pressure, temperature, grinding as external physical force, which causes external and internal strain effect in the crystal structure of calcite.

Strain values of aragonite in PCC and GCC samples are given in table-3.19. Williamson-Hall plots of aragonite for all samples are shown in appendix.

Table-3.19. The strain value in aragonite

SAMPLE	Strain value
PSU2	0.331±0.049
PSU4	0.589±0.121
PCC1	0.276±0.019
PSU1	0.316±0.018
PSU3	0.397±0.072
Pre600	0.275±0.019

Strain data of aragonite sets in the range of 0.276 ± 0.019 - 0.589 ± 0.121 for PCC and GCC samples. The strain value distribution of aragonite for PCC and GCC samples is drown (Fig.3.15).

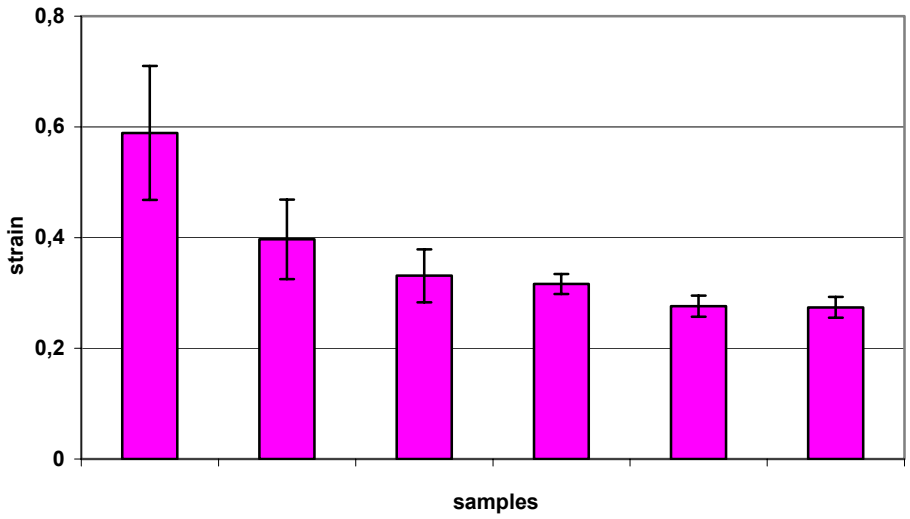

Figure 3.15. The strain value distribution of aragonite by Williamson-Hall plot

Strain distribution of aragonite in PCC is affected by internal and external strain as a consequence of imposing high temperature, grinding and synthetic conditions in super saturation solutions as well.

3.1.5. PCC & GCC characterization based on XRD data in powder form

The identification of PCC and GCC products is performed based on XRD data. The summary of important characteristics (crystallite size, strain value and intensity ratio of XRD lines) in calcite for each sample is given as follows:

Sample PRF120

Regarding crystallite size there are similar samples PRF120 177.2±9.9 and PSU3 (163.5±11.1). That means these samples can not be identified based on crystallite size, additionally characteristics such as strain value has to be compared.

By comparison strain values of PRF120 (0.088±0.011), PSU3 (0.427± 0.084), it is possible to distinguish these samples from each other.

In addition to strain values the separation of PRF120 is also verified by the peak intensity ratio.

Sample name	I (104)/I (116)	I(104)/I(122)
PRF 120	5.59±0.32	10.40±0.08
PSU3	3.26±0.13	13.42±0.21

Detailed data are available in appendix.

Sample PSU3

Regarding crystallite size there are similar samples PSU3 (163.5±11.1) and PRF120 (177.2±9.9). That means these samples can not be identified based on crystallite size, additionally characteristics such as strain value has to be compared.

By comparison strain values for PSU3 (0.427± 0.084) and PRF120 (0.088±0.011), it is possible to distinguish PSU3.

In addition to strain values, the separation of PSU3 samples is also verified by the peak intensity ratio.

Sample name	I(104)/I(116)	I(104)/I(122)
PSU3	3.26±0.13	13.42±0.21
PRF 120	5.59±0.32	10.40±0.08

Detailed data are available in appendix.

Sample PCCSG

Regarding crystallite size there are similar samples PCCSG (136±7.9), Pre320 (131.5 ± 8.7), PCC-1 (128.1± 10.8) and Pre600 (127.6±11.6). That means these samples can not be identified based on crystallite size, additionally characteristics such as strain value has to be compared.

By comparison strain values of PCCSG (0.123± 0.094) and PRP (0.043± 0.007), it is not possible to distinguish these samples.

In order to identify PCCSG, peak intensity ratio based on I (104)/I (122) is the only solution.

Sample name	I (104)/I (113)	I(104)/I(122)
PCCSG	4.89±0.26	10.59±0.27
PRP	5.06±0.04	12.5±0.23

Detailed data are available in appendix.

Sample PRP

Regarding crystallite size there are similar samples PRP (118±8.4), Pre320 (131.5 ± 8.7), PCC-1 (128.1± 10.8), Pre600 (127.6±11.6), PSU2 (110±9.6) and PSU1 (113.4±10.9).

That means these samples can not be identified based on crystallite size, additionally characteristics such as strain value has to be compared.

By comparison strain values of PRP (0.043± 0.007), PCC-1 (0.504±0.067) and Pre600 (0.501±0.067), it is possible to distinguish PRP.

In addition to strain value, the separation of PRP sample is also verified by peak intensity ratio.

Sample name	I (104)/I (113)	I(104)/I(122)
PRP	5.06±0.04	12.5±0.23
PCC-1	4.56±0.33	7.90±0.29
Pre600	3.60±0.17	8.85±0.20

Detailed data are available in appendix.

Sample Pre320

Regarding crystallite size there are similar samples Pre320 (131.5 ± 8.7), PCC-1 (128.1± 10.8), Pre600 (127.6±11.6), PSU1 (113.4±10.9), PRP (118±8.4) and PCCSG (136±7.9). That means these samples can not be identified based on crystallite size, additionally characteristics such as strain value has to be compared.

By comparison strain value of Pre320 (0.292 ± 0.052), PSU1 (0.312±0.054), it is not possible to distinguish these samples.

In order to identify Pre320, peak intensity ratio based on I (104)/I (122) is the only solution.

Sample name	I (104)/I (113)	I(104)/I(122)
Pre320	5.69±0.21	16.24±0.11
PSU1	5.81±0.39	14.60±0.27

Detailed data are available in appendix.

Sample Pre600

Regarding crystallite size there are similar samples Pre600 (127.6±11.6), PSU2 (110±9.6), PSU1 (113.4±10.9), PRP (118±8.4), PCCSG (136±7.9), Pre320 (131.5 ± 8.7) and PCC-1 (128.1± 10.8). That means these samples can not be identified based on crystallite size, additionally characteristics such as strain value has to be compared.

By comparison strain value for PCC-1 (0.504±0.067) and Pre600 (0.501±0.067) it is not possible to distinguish these samples.

In order to identify Pre600, peak intensity ratio based on I(104)/I(113), I(104)/I(122) is the only solution.

Sample name	I(104)/I(113)	I(104)/I(122)
Pre600	3.60±0.17	8.85±0.20
PCC-1	4.56±0.33	7.90±0.29

Detailed data are available in appendix.

Sample PCC-1

Regarding crystallite size there are similar samples PCC-1 (128.1± 10.8), Pre600 (127.6±11.6), PSU2 (110±9.6), PSU1 (113.4±10.9), PRP (118±8.4), PCCSG (136±7.9) and Pre320 (131.5 ± 8.7). That means these samples can not be identified based on crystallite size, additionally characteristics such as strain value has to be compared.

By comparison strain value of PCC-1 (0.504±0.067) and Pre600 (0.501±0.067), it is not possible to distinguish these samples.

In order to identify PCC-1, peak intensity ratio based on I(104)/I(122) is the only solution.

Sample name	I(104)/I(113)	I(104)/I(122)
PCC-1	4.56±0.33	7.90±0.29
Pre600	3.60±0.17	8.85±0.20

Detailed data are available in appendix.

Sample PSU1

Regarding crystallite size there are similar samples PSU1 (113.4±10.9), PRP (118±8.4), PCC-1 (128.1± 10.8), Pre600 (127.6±11.6) and PSU2 (110±9.6). That means these samples can not be identified based on crystallite size, additionally characteristics such as strain value has to be compared.

By comparison strain value of PSU1 (0.312±0.054), Pre320 (0.292 ± 0.052) and PSU2 (0.249± 0.035). It is not possible to distinguish these samples.

In order to identify PSU1, peak intensity ratio based on I(104)/I(122) is the only solution.

Sample name	I(104)/I(113)	I(104)/I(122)
PSU1	5.81±0.39	14.60±0.27
PSU2	5.45±0.09	13.52±0.18
Pre320	5.69±0.21	16.24±0.11

Detailed data are available in appendix.

Sample PSU2

Regarding crystallite size there are similar samples PSU2(110±9.6), PSU1(113.4±10.9), PRP (118±8.4), PCC-1 (128.1± 10.8) and Pre600 (127.6±11.6). That means these samples can not be identified based on crystallite size, additionally characteristic such as strain value has to be compared.

By comparison strain value of PSU2 (0.249± 0.035), PSU1 (0.312±0.054) and Pre320 (0.292 ± 0.052), it is not possible to distinguish these samples.

In order to identify PSU2, peak intensity ratio based on I(104)/I(122) is the ony solution.

Sample name	I(104)/I(113)	I(104)/I(122)
PSU2	5.45±0.09	13.52±0.18
Pre320	5.69±0.21	16.24±0.11
PSU1	5.81±0.39	14.60±0.27

Detailed data are available in appendix.

Sample PCLS

Regarding crystallite size there are similar samples PCLS (106.2± 1.4), Fb25(105± 11.0), Pre100 (102.7±7.8) and PSU4 (97.7±7.7). That means these samples can not be identified based on crystallite size then additional characteristic such as strain value has to be compared.

By comparison strain value of PCLS (0.111± 0.003), it is possible to distinguish PCLS.

In addition to strain value, the separation of PCLS is also verified by the peak intensity ratio based I(104)/I(122).

Sample name	I(104)/I(116)	I(104)/I(122)
PCLS	5.66±0.09	10.49±0.31
Fb25	5.80±0.20	11.40±0.40
Pre100	6.17±0.05	13.38±0.20
PSU4	3.33±0.12	14.25±0.43

Detailed data are available in appendix.

Sample Fb25

Regarding crystallite size there are similar samples Fb25 (105± 11.0), Pre100 (102.7±7.8), PSU4 (97.7±7.7) and PCLS (106.2± 1.4). That means these samples can not be identified based on crystallite size, additionally characteristics such as strain value has to be compared.

By comparison strain value of Fb25 (0.153± 0.017) and PCLS (0.111± 0.003), it is possible to distinguish Fb25.

In addition to strain value, sample Fb25 is also verified by the peak intensity ratio based I(104)/I(122).

Sample name	I(104)/I(116)	I(104)/I(122)
PCLS	5.66±0.09	10.49±0.31
Fb25	5.80±0.20	11.40±0.40

Detailed data are available in appendix.

Sample Pre100

Regarding crystallite size there are similar samples Pre100 (102.7±7.8), PSU4 (97.7±7.7), PCLS (106.2± 1.4) and Fb25 (105± 11.0). That means these samples can not be identified based on crystallite size, additionally characteristics such as strain value has to be compared.

By comparison with strain value for Pre100 (0.342±0.028) and PSU4 (0.343±0.045), it is not possible to distinguish these samples.

In order to identify Pre100, peak intensity ratio based on I(104)/I(116) , I(104)/I(122) is the only solution.

Sample name	I(104)/I(116)	I(104)/I(122)
Pre100	6.17±0.05	13.38±0.20
PSU4	3.33±0.12	14.25±0.43

Detailed data are available in appendix.

Sample PSU4

Regarding crystallite size there are similar samples PSU4 (97.7±7.7), PCLS (106.2± 1.4), Fb25 (105± 11.0) and Pre100 (102.7±7.8). That means these samples can not be identified based on crystallite size, additionally characteristics such as strain value has to be compared.

By comparison strain value of PSU4 (0.343±0.045) and Pre100 (0.342±0.028), it is not possible to distinguish these samples.

In order to identify PSU4, peak intensity ratio based on I(104)/(116), I(104)/I(122) is the only solution.

Sample name	I(104)/I(116)	I(104)/I(122)
Pre100	6.17±0.05	13.38±0.20
PSU4	3.33±0.12	14.25±0.43

Detailed data are available in appendix.

Sample Pre800

Regarding crystallite size there are similar samples Pre800 (77.7±8.2) and PFS210 (73.8±10.2). That means these samples can not be identified based on crystallite size, additionally characteristics such as strain value has to be compared.

By comparison strain value of Pre800 (0.322±0.005), it is possible to distinguish Pre800.

In addition to strain value, the separation of Pre800 is also verified by the peak intensity ratio.

Sample name	I(104) /I(116)	I(104)/I(202)
Pre800	6.18 ±0.06	7.26±0.12
PFS210	6.58±0.06	6.26±0.03

Detailed data are available in appendix.

Sample PFS210

Regarding crystallite size there are similar samples PFS210 (73.8±10.2) and Pre800 (77.7±8.2). That means these samples can not be identified based on crystallite size, additionally characteristics such as strain value has to be compared.

By comparison strain value of PFS210 (0.450±0.075), it is possible to distinguish PFS210.

In addition to strain value, the separation of PFS210 is also verified by the peak intensity ratio.

Sample name	I(104) /I(116)	I(104)/I(202)
PFS210	6.58±0.06	6.26±0.03
Pre800	6.18 ± 0.06	7.26±0.12

Detailed data are available in appendix.

Sample 360V

Regarding crystallite size there are similar samples 360V(59.7±6.3), PS(58.3±5.6), 160V(50.8±4.1) and Fb230(46.9±6.6). That means these samples can not be identified based on crystallite size, additionally characteristics such as strain value has to be compared.

By comparison strain value of 360V (0.099±0.012), it is possible to distinguish 360V.

In addition to strain value, the separation of 360V is also verified by the peak intensity ratio based on I(104)/I(012).

Sample name	I(104)/I(012)	I(104)/I(122)
360V	9.93±0.13	15.61±0.16
Fb230	9.19±0.20	13.66±0.12
PS	7.66±0.15	12.87±1.40
160V	8.92±0.04	15.36±0.30

Detailed data are available in appendix.

Sample PS

Regarding crystallite size there are similar samples PS(58.3±5.6), 160V(50.8±4.1), Fb230(46.9±6.6), 360V(59.7±6.3). That means these samples can not be identified based on crystallite size, additionally characteristics such as strain value has to be compared.

By comparison strain value of PS(0.212±0.032) and 160V(0.217±0.043), it is not possible to distinguish these samples.

In order to identify PS, peak intensity ratio based on I(104)/I(012) is the only solution.

Sample name	I(104)/I(012)	I(104)/I(122)
PS	7.66±0.15	12.87±1.40
160V	8.92±0.04	15.36±0.30

Detailed data are available in appendix.

Sample Fb230

Regarding crystallite size there are similar samples Fb230(46.9±6.6), 360V(59.7±6.3) PS(58.3±5.6) and 160V(50.8±4.1). That means these samples can not be identified based on crystallite size, additionally characteristic such as strain value has to be compared.

By comparison strain value of Fb230 (0.147±0.018), it is possible to distinguish Fb230.

In addition to strain value, the separation of Fb230 is also verified by the peak intensity ratio based on I(104)/I(012).

Sample name	I(104)/I(012)	I(104)/I(122)
Fb230	9.19±0.20	13.66±0.12
PS	7.66±0.15	12.87±1.40
160V	8.92±0.04	15.36±0.30
360V	9.93±0.13	15.61±0.16

Detailed data are available in appendix.

Sample160V

Regarding crystallite size there are similar samples 160V(50.8±4.1), Fb230(46.9±6.6) 360V(59.7±6.3) and PS(58.3±5.6). That means these samples can not be identified based on crystallite size, additionally characteristics such as strain value has to be compared.

By comparison strain value of 160V(0.217±0.043) and PS(0.212±0.032), it is not possible to distinguish these samples.

In order to identify 160V, peak intensity ratio based on I(104)/I(012), I(104)/I(122) is the only solution.

Sample name	I(104)/I(012)	I(104)/I(122)
160V	8.92±0.04	15.36±0.30
PS	7.66±0.15	12.87±1.40

Detailed data are available in appendix.

Sample Pre720

Regarding crystallite size there are similar samples Pre720 (25±4.4) and GCC90 (20.2±3.7).

That means these samples can not be identified based on crystallite size, additionally characteristics such as strain value has to be compared.

By comparison strain value of Pre720 (0.340±0.126) and GCC90 (0.388±0.074) , it is not possible to distinguish these samples.

In order to identify Pre720, peak intensity ratio based on I(104)/I(018), I(104)/I(122) is the only solution.

Sample name	I(104)/I(018)	I(104)/I(122)
GCC90	15.4±0.7	16.5±0.3
Pre720	5.4±0.3	13.0±0.4

Detailed data are available in appendix.

Sample GCC90

Regarding crystallite size there are similar samples GCC90 (20.2±3.7) and Pre720 (25±4.4).

That means these samples can not be identified based on crystallite size, additionally characteristics such as strain value has to be compared.

By comparison strain value of GCC90 (0.388±0.074) and Pre720 (0.340±0.126), it is not possible to distinguish these samples.

In order to identify GCC90, the peak intensity ratio based on I(104)/I(018), I(104)/I(122) is the only solution.

Sample name	I(104)/I(018)	I(104)/I(122)
GCC90	15.4±0.7	16.5±0.3
Pre720	5.4±0.3	13.0±0.4

detailed data are available in appendix.

Sample GCCX

Regarding crystallite size there is only GCCX

GCCX (11.2±2.3)

This sample can be identified by crystallite size without comparing any additional characteristics.

3.2. PCC and GCC characterization of paper sheet

Dorfner Company provided paper sheet samples in order to determine the characteristics of PCC and GCC coated on paper sheet directly. This section is considered to achieve the mentioned goal in paper sheet.

The mineral content was measured by XRD and proved the existence of calcite and cellulose. Aragonite and additional crystalline phases were not determined (Table-3.20).

Table-3.20. The minerals content in paper sheet samples

Sample	Minerals content
R1V0MP1	Cellulose tripropionate+ Native cellulose+ cellulose+ calcite
R1V0MP2	Cellulose tripropionate+ Native cellulose+ cellulose+ calcite
R1V0MP4	Cellulose tripropionate+ Native cellulose+ cellulose+ calcite
R1V1MP1	Cellulose tripropionate+ Native cellulose+ cellulose+ calcite
R1V1MP2	Cellulose tripropionate+ Native cellulose+ cellulose+ calcite
R1V1MP3	Cellulose tripropionate+ Native cellulose+ cellulose+ calcite
R1V1MP4	Cellulose tripropionate+ Native cellulose+ cellulose+ calcite
1bef16Ash	Native cellulose+ calcite
13133bef16Ash	Native cellulose+ calcite
2v3a20.3Ash	Native cellulose+ calcite
2votf1320a	Native cellulose+ calcite

Identification of different types of cellulose and calcite as filler was determined by Rietveld method.

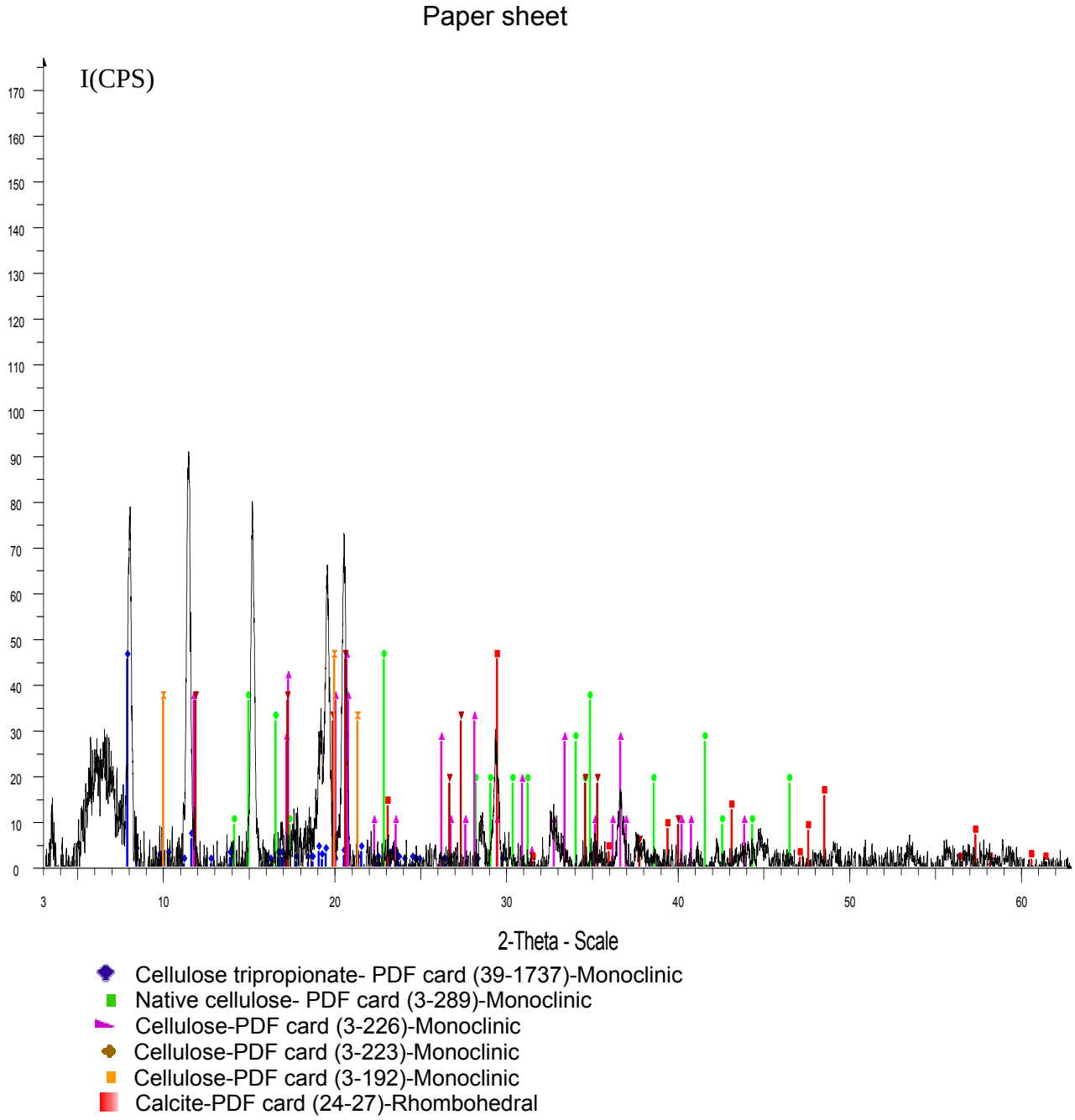

Figure 3.16. The XRD pattern of paper sheet by the Rietveld method, sample (R1V1MP3).

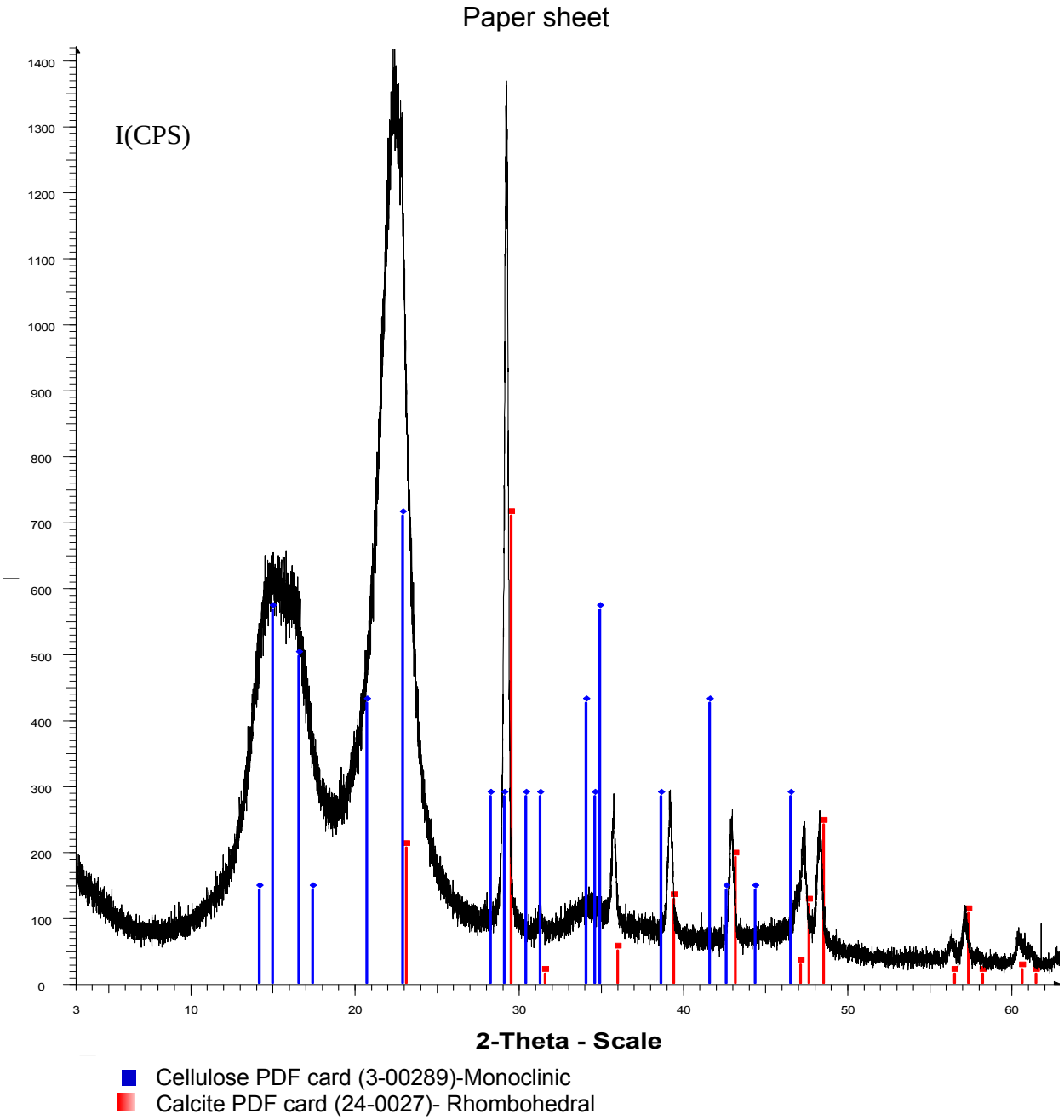

Figure 3.17. The XRD pattern of paper sheet by the Rietveld method, sample (1bef16Ash).

XRD patterns illustrate two different types of paper sheet in terms of the variety of cellulose phases. Figure.3.16 illustrates mineral content including cellulose tripropionate (PDF card: 39-1737), native cellulose (PDF card: 3-289), cellulose (PDF cards: 3-226, 3-223, 3-192) and calcite (PDF card: 24-27). Figure.3.17 illustrates mineral content consisting cellulose (PDF card: 3-289) and calcite (PDF card: 24-27).

Quantification of cellulose and calcite in paper sheet is determined by Rietveld method (Table-3.21).

Table-3.21. Quantitative phase analysis in paper sheet samples by Rietveld method

Sample	Cellulose (error)	Calcite(error)
R1V0MP1	94.7±1.2	5.3±0.61
R1V0MP2	92.8±1.6	7.2±0.71
R1V0MP4	93.1±1.4	6.9±0.50
R1V1MP1	96.3±1.3	3.7±0.43
R1V1MP2	93.9±1.4	6.1±0.54
R1V1MP3	95.9±1.3	4.1±0.45
R1V1MP4	92.8±1.2	7.2±0.54
1bef16Ash	91.4±1.1	8.6±0.52
13133bef16Ash	93.1±1.5	6.9±0.38
2v3a20.3Ash	93.5±1.5	6.5±0.36
2votf1320a	95.0±1.7	5.0±0.32

The results indicate the concentration of calcite sets in the range of 3.7%±0.43 - 8.6%±0.52 and cellulose sets in the range of 91.4%±1.1 - 96.3%±1.3.

The crystallite size $<L>_{vol}$ of cellulose and calcite was measured by Rietveld method (Table-3.22).

Table-3.22.The crystallite size $<L>_{vol}$ measurement in paper sheet samples by Rietveld

Sample	$FWHM_{sample}$(223) cellulose(2θ°)	Crystallite size nm(cellulose)	$FWHM_{sample}$(104) calcite(2θ°)	Crystallite size nm (calcite)
R1V0MP1	0.288	26.3	0.344	22.0
R1V0MP2	0.288	26.3	0.357	21.3
R1V0MP4	0.254	29.9	0.295	25.7
R1V1MP1	0.234	32.4	0.292	25.9
R1V1MP2	0.330	23.0	0.354	21.4
R1V1MP3	0.237	32.0	0.349	21.8
R1V1MP4	3.040	2.6	0.231	32.9
1bef16Ash	3.120	2.4	0.241	31.5
1313bef16Ash	3.295	2.3	0.225	33.7
2v3a20.3Ash	4.031	1.9	0.204	37.2
2votf1320a	3.155	2.4	0.221	34.4

The results (Table-3.22) show the crystallite size of cellulose puts in the range of 1.9-32.4 nm and of calcite in the range of 21.3-37.2 nm.

There is an inverse correlation between FWHM (104) and crystallite size based on Rietveld method using Scherrer equation, which is shown in figure.3.18.

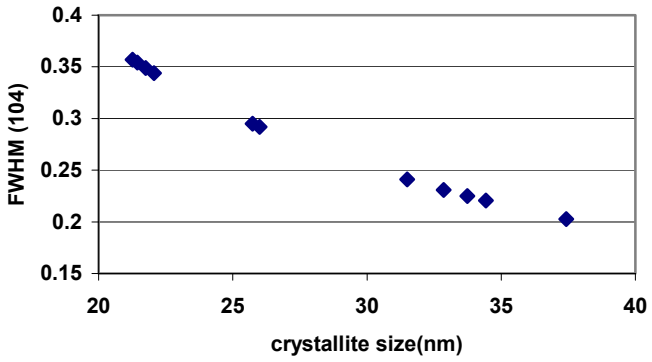

Figure 3.18. The correlation between crystallite size$<L>_{vol}$ and $FWHM_{obs}$ (104) in calcite of paper sheet

Williamson-Hall method is the second possibility in order to determine crystallite size and strain value in calcite. This method requires all accessible diffraction lines of calcite (Fig.3.19).

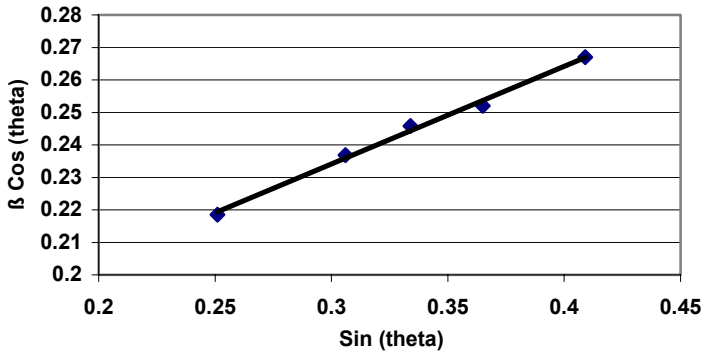

Figure 3.19- The Williamson-Hall plot in calcite in paper sheet, (sample 1313bef16Ash) (Y=0.301x+0.039, R^2=0.995)

The Williamson-Hall method could not be applied in the paper sheet including different cellulose phases because of the overlapping of XRD lines of different types of cellulose and calcite (Fig.3.16).

The Williamson-Hall data were achieved in the paper sheet including only one phase of cellulose without overlapping with XRD lines of calcite (Fig.3.17, Table-3.23).

Table-3.23. The crystallite size and strain in calcite by Williamson-Hall plot

Sample	Strain value calcite	Crystallite size nm (calcite)
1bef16Ash	0.214±0.038	34.3±6.8
1313bef16Ash	0.301±0.012	35.1±3.2
2v3a20.3Ash	0.454±0.078	37.9±6.1
2votf1320a	0.312±0.056	34.4±5.6

Data prove that strain value of calcite sets in the range of 0.214±0.038 - 0.454±0.078 and crystallite size of calcite sets in the range of 34.3±6.8 - 37.9±6.1.

Morphologies of PCCs in paper sheet were determined using SEM (Fig.3.20).

PCC is fixed and coated on paper sheet, therefore preferred orientation effect on intensity ratio of XRD lines in calcite could not be investigated.

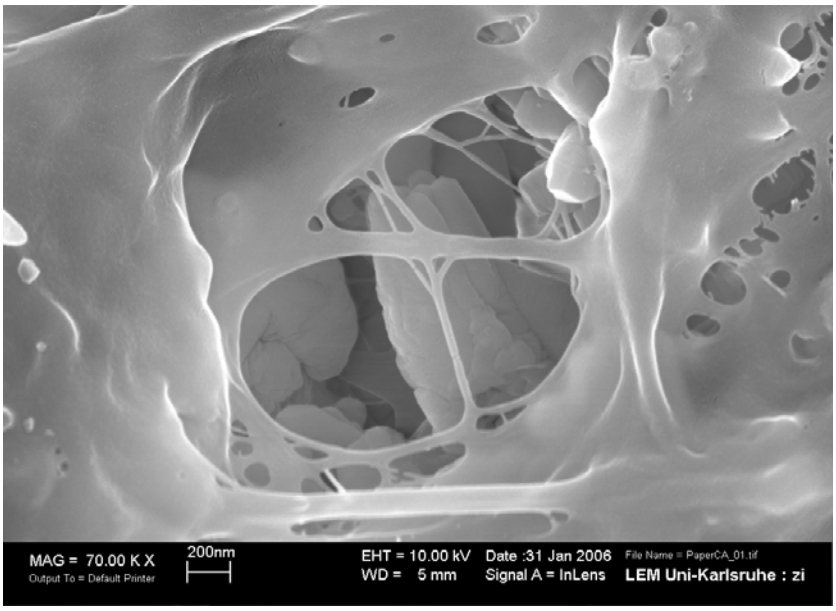

Figure.3.20. The crystals of PCC in paper sheet

Ahn, J.W., Kim, H.S., Yoon, S.H., Kim, J.S., Sung, G.W., 2002. Manufacturing of aragonite precipitated calcium carbonate by a carbonation process using dusts from a stainless steel refining sludge plant in POSCO. Ceramic processing research 3-2, 62-65.

Ahn, J.W., Choi, K.S., Yoon,S.H., Kim, H., 2004. Synthesis of aragonite by the carbonation process. American ceramic society 87-2, 286-288.

Christos, G., Kontoyannis, C.G., Vagenas, V., 1999. Calcium carbonate phase analysis using XRD and FT-Raman spectroscopy. The analyst 125, 251-255.

Cullity, B.D., Stock, S.R., 2001. Elements of X-ray diffraction, third edition, prentice Hall publication, 622-623.

Dandeu, A., Humbert, B., Carteret, C., 2006. Raman spectroscopy - A powerful tool for the quantitative determination of the composition of polymorph mixtures: Application to CaCO3 polymorph mixtures. Chemical engineering & technology 29-2, 221-225.

David, W.I.F., Shankland, K., McCusker,L.B., Baerlocher, Ch., 2002. Determination from powder diffraction data, 2nd edition, Oxford science publication, 29-34.

Dickinson, S.R., Mc Grath, K.M., 2001. Quantitative determination of binary and tertiary calcium carbonate mixture using powder X-ray diffraction. The analyst 121, 1118-1121.

Dobojit, C., Samiran, M., 1999. Aragonite crystal with unconvential morphologies. Materials chemistry 9, 2953-2957.

Dyson,D.J., 2004 . X-Ray and electron diffraction studies in materials science, First edition, Maney publication, 235-248.

Eberl,D., Kile,D.E., 2000. An assessment of calcite crystal growth mechanisms based on crystal size distribution. Geochemica et cosmochimica acta 64-17, 2937-2950.

Fadini,A., Schnepel,F.M., 1989. Vibrational spectroscopy: Methods and applications, Ellis Horwood Ltd, Chichester, 25-38.

Ferrari,J.R.,Nakamoto,K., 1994. Introductory Raman spectroscopy, first edition, Academic press, 267-294.

Gen-Tao., Zhou.H., jimmy.C., 2004. Sonochemical synthesis of aragonite- type calcium carbonate with different morphologies, New journal of chemistry 28, 1027-1031.

Goodhew, P.J., Humphreys, F.J.,1997. Electron microscopy and analysis, second edition. Tayler & Francis publication, 1-19.

Guinier, A., 1994. X-ray diffraction in crystals, imperfect crystals and amorphous bodies, first edition. Dover publications, 1-25.

Hammound,C., 2001. The basic of crystallography and diffraction, Second edition. International union of crystallography. Oxford science publications, 1-26.

Hendra,P., Jones,C., Warens,G., 1991. FT Raman spectroscopy, Ellis Horwood Ltd, Chichester. 32-41.

He,P., Bilta,S., Bousfield,D., Tripp,P., 2002. Raman spectroscopic analysis of paper coatings. Applied spectroscopy 56-9, 1115-1121.

Hu, Z., Deng,Y., 2004. Synthesis of needle-like aragonite from calcium chloride and sparingly soluble magnesium carbonate. Powder technology 140, 10-16.

Isopescu, R., Zahanaggiu, F., Filipescue, L.,1996. Growth rate models and kinetics estimation for $CaCO_3$ precipitated in continuous crystallizers. Journal of crystal growth 167, 260-264.

JCPDS-International center for diffraction data., 2002. Journal of advanced X-ray analysis, 42, 387-396.

Jenkins, R., 1989. Measurement of X-ray powder pattern-instrumentation. Reviews in mineralogy. Mineralogical society of America, Washington, 20, 19-30.

Klungness, J., Stroika, M., Sykes, M., Tan,F., Abubakr, S., 1998. In proceedings of 1998 AIChE symposium series (in cooperation with TAPPI pulping conference), "Lightweight, high-opacity paper: Process costs and energy use reduction".

Klein,C., Hurlbut,C., 1993. Manual of Mineralogy, 21st edition, John Wiley & sons publication. 167-169, 404-415.

Krill,C.E., Birringer,R.,1998. Estimating grain-size distributions in nanocrystalline materials from X-ray diffraction profile. Philosophy magazine.77, 621-642.

Krill,C.E., Haberkorn.R., Briringer.R.,2000. Specification of microstructure and characterization by scattering techniques. Handbook of nanostructured materials and nanotechnology 2, 165-170.

Lohmus,H., Räni. A., Kallavus.U., Reiska.R., 2002. A trend to the production of calcium hydroxide and precipitated calcium carbonate with defined properties. The canadian journal of chemical engineering 80, 911-919.

Markov, V.M., 2003. Crystal growth for beginners: Fundamentals of nucleation, crystal growth, and epitaxy, world scientific publisher, 77-85.

Milliman,J.D., Troy,P.J., Balch,W.M., Adams,A.K., Li,Y.-H., Mackanzie, F.T.,1999. Biologically mediate dissolution of calcium carbonate above the chemical lysocline? Deep-sea research 1 46,1653-1669.

Moore,M., Reynolds,R., 1997. X-ray diffraction and the identification and analysis of clay minerals, Oxford university press, 86-88.

Plummer,N.L., Busenberg,E., 1984. The solubility's of calcite, aragonite and vaterite in CO_2-H_2O solutions between 0 and 90°C, and an evaluation of the aqueous model for the system $CaCO_3$-CO_2-H_2O. Geochimica et cosmochimica acta. 46, 6, 1011-1040.

Park,S., Choi,W.S., 2004. Effects of operating factors on the particle size distribution and particle shape of synthesized precipitated $CaCO_3$. Advanced powder technology 15-1, 1-12.

Reeder,R.J., 1990. Carbonates: Mineralogy and chemistry, reviews in mineralogy, Minelaogical society of America,11,1-22.

Smith,W.E., Dent,G., 2005. Modern Raman spectroscopy-A practical approach.John Wiley & sons publication, 1-21.

Snyder,R.L., Fiala,J., Bunge,H.J.,1999. Defect and microstructure analysis by diffraction. Oxford university press, 63-75.

So, T.S., Choi,W.S., 2000. Effect of operating factors on the particle size distribution and particle shape of precipitated calcium carbonate synthesized, effect of initial conditions of calcium hydroxide. Society of powder technology. Japan 37, 644-657.

Spanos, N., Koutsokos, P.G.,1998. Kinetics of precipitation of calcium carbonate in alkaline pH at constant supersaturation. Spontaneous and seeded growth. Physical chemistry.B,102, 6679-6684.

Whitfield, P., Mitchell, L., 2004. X-ray diffraction analysis of nanoparticles, recent development, potential problems and some solutions 3-6, 757-763.

Will, G., 2006. Powder diffraction: The Rietveld method and the two-stage method. Springer publisher, 45-65.

Wen,Y., Xiang,L., Jin,Y., 2003. Synthesis of plate-like calcium carbonate via carbonate route. Materials letter 57, 2565-2571.

Whitfield, P., Mitchell, L., 2004. X-ray diffraction analysis of nanoparticles, recent development, potential problems and some solutions 3-6, 757-763.

Wise, K.J., 1997. Precipitated calcium carbonate particles from basic calcium carbonate. US. Patent 5, 643, 415.

Zeshan,H., Yulin,D., 2003. Supersaturation control in aragonite synthesis using sparingly soluble calcium sulfate as reactants. Colloid and interface science 266, 359-365.

Zeshan,H., Yulin,D., 2004. Synthesis of needle-like aragonite from calcium chloride and sparingly soluble magnesium carbonate. Powder technology 140, 10-16.

Sample Name	Pre carb-600
Abbreviation	PCC-1

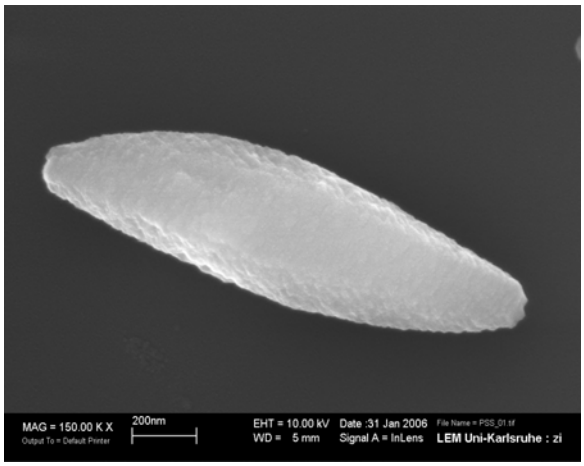

Figure 1.1. The SEM image (PCC-1)

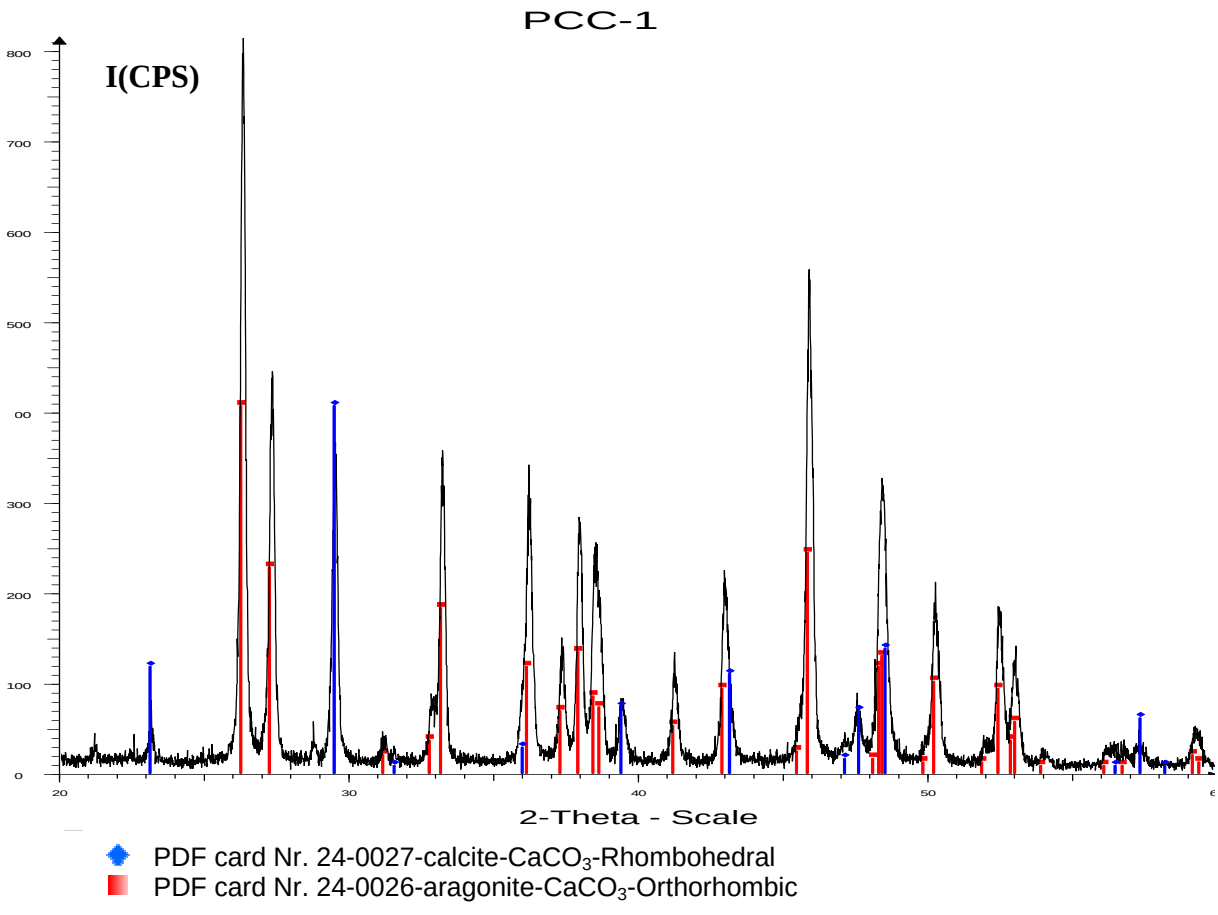

Figure 1.2. The diffractogram (PCC-1)

Table- 1.1. The peak list (PCC-1)($FWHM_{instrumental}$(0.157°)

Angle 2-Theta °	d value Angstrom	Intensity Count	Intensity %	$FWHM_{obs}$ 2-Theta °
23.115	3.84476	81	9.9	0.256
26.304	3.38538	816	70.9	0.256
27.316	3.26226	446	54.7	0.259
29.497	3.02578	367	45	0.224
31.224	2.86228	39	4.8	0.179
32.863	2.72317	80	9.8	0.224
33.229	2.69398	358	43.9	0.313
36.237	2.47697	342	41.9	0.318
37.378	2.40395	137	16.8	0.253
37.984	2.36695	284	34.8	0.318
38.534	2.33448	247	30.3	0.225
39.463	2.28161	81	9.9	0.312
41.292	2.18466	134	16.4	0.283
43.022	2.10073	225	27.6	0.239
45.955	1.97325	548	67.2	0.237
47.61	1.90845	89	10.9	0.328
48.494	1.87572	327	40.1	0.362
50.323	1.81176	212	26	0.330
52.049	1.75564	37	4.5	0.228
52.547	1.74018	184	22.5	0.235
53.082	1.7239	118	14.5	0.274
54.05	1.69528	28	3.4	0.230
57.381	1.60453	48	5.9	0.272
59.361	1.55565	52	6.4	0.434

Table-1.2. Concentration, crystallite size and strain data (PCC-1)

Method	Characteristic	Calcite	Aragonite
Rietveld method (XRD)	Concentration%	15.3±0.71	84.7±1.30
Rietveld method (XRD)	Crystallite size $<L>_{vol}$ (nm)	113	90.0
Williamson-Hall (XRD)	Crystallite size $<L>_{vol}$ (nm)	128.1±10.8	87.5±6.7
Williamson-Hall (XRD)	Strain value	0.504±0.067	0.276±0.02

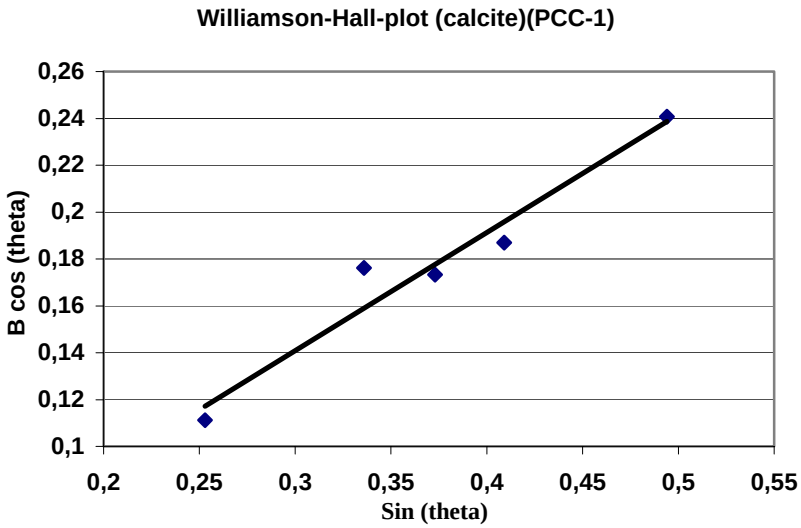

Figure 1.3a. The Williamson-Hall plot in calcite (PCC-1) (Y=0.504X-0.012) R^2=0.949

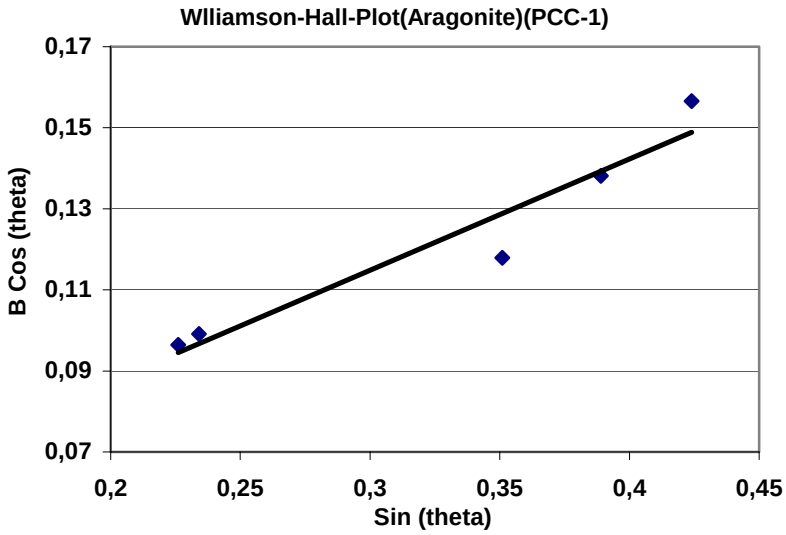

Figure 1.3b. The Williamson-Hall plot in aragonite (PCC-1) (Y=0.274X-0.0176) R^2=0.928

Table –1.3. Morphology description based on intensity ratio data (PCC-1)

Method	Characteristic	Calcite	Aragonite
Intensity Ratio peak area (XRD)	Morphology Description	I(104)/I(116) 1.06±0.03	I(040)/I(111) 0.68±0.03
Intensity Ratio peak area (XRD)	Morphology Description	I(104)/I(012) 5.19±0.38	I(040)/I(202) 1.48±0.03
Intensity Ratio peak area (XRD)	Morphology Description	I(104)/I(202) 1.66±0.27	I(040)/I(022) 2.21±0.03
Intensity Ratio peak area (XRD)	Morphology Description	I(104)/I(113) 4.56±0.33	I(040)/I(113) 1.78±0.03
Intensity Ratio peak area (XRD)	Morphology Description	I(104)/I(018) 5.01±0.27	I(040)/I(102) 1.74±0.03
Intensity Ratio peak area (XRD)	Morphology Description	I(104)/I(122) 7.90±0.29	-
Intensity Ratio peak height (XRD)	Morphology Description	I(104)/I(116) 1.25±0.11	I(040)/I(111) 0.65±0.03
Intensity Ratio peak height (XRD)	Morphology Description	I(104)/I(012) 5.44±0.87	I(040)/I(202) 1.21±0.02
Intensity Ratio peak height (XRD)	Morphology Description	I(104)/I(202) 1.79±0.12	I(040)/I(022) 2.23±0.02
Intensity Ratio peak height (XRD)	Morphology Description	I(104)/I(113) 4.38±0.18	I(040)/I(113) 1.46±0.08
Intensity Ratio peak height (XRD)	Morphology Description	I(104)/I(018) 4.83±0.49	I(040)/I(102) 1.67±0.17
Intensity Ratio peak height (XRD)	Morphology Description	I(104)/I(122) 7.91±0.34	-

Sample Name Pre carb-800 Abbreviation Pre800

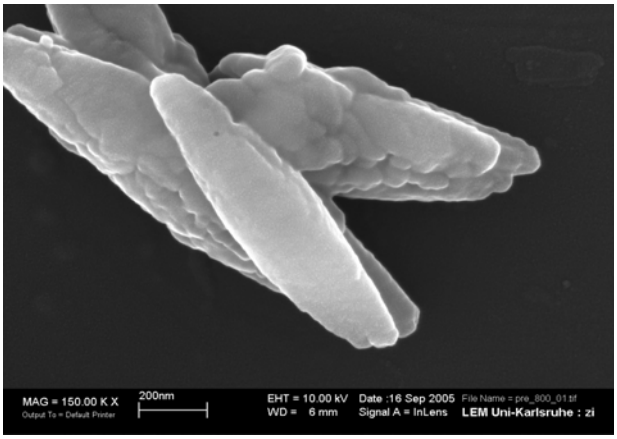

Figure 2.1. The SEM image (Pre-800)

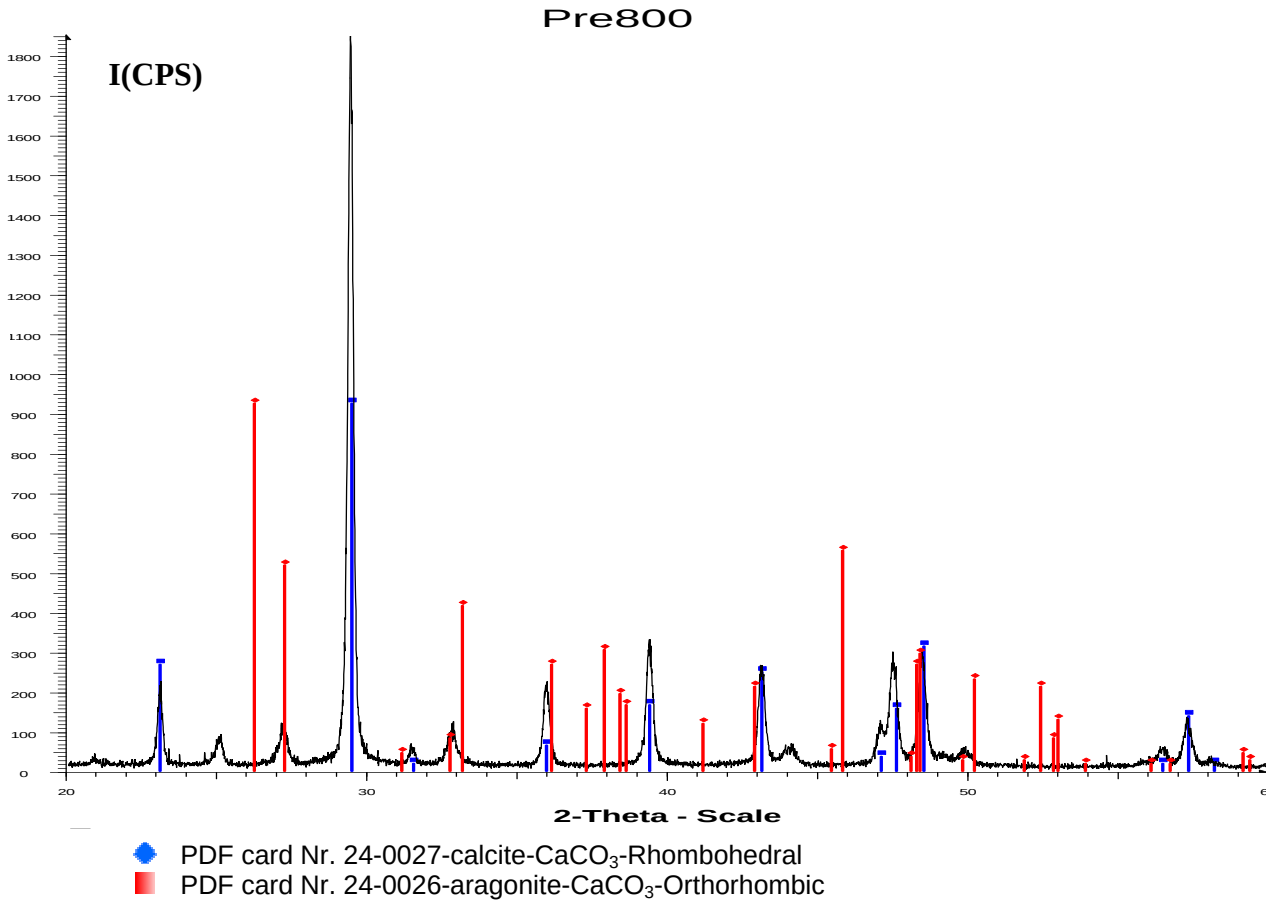

Figure 2.2. The diffractogram (Pre-800)

Table- 2.1. The peak list (Pre-800) ($FWHM_{instrumental}$ = 0.157)

Angle 2-Theta °	d value Angstrom	Intensity Count	Intensity %	$FWHM_{obs}$
23.063	3.85325	207	12.7	0.236
27.214	3.27418	117	7.2	0.369
29.459	3.02959	1631	100	0.243
31.537	2.8346	53	3.2	0.243
32.748	2.73249	97	5.9	0.433
35.973	2.49452	214	13.1	0.283
39.412	2.28444	331	20.3	0.300
42.911	2.10591	54	3.3	0.273
43.166	2.09407	262	16.1	0.273
45.493	1.99222	23	1.4	0.393
47.157	1.92572	115	7.1	0.334
48.454	1.87718	265	16.2	0.317
50.256	1.81399	22	1.3	0.417
56.162	1.63644	19	1.2	0.382
56.553	1.62604	55	3.4	0.263
57.411	1.60376	133	8.2	0.353

Table- 2.2. Concentration, crystallite size, strain and crystal size (Pre-800)

Method	Characteristic	Calcite	Aragonite
Rietveld method (XRD)	Concentration%	99.6±1.23	0.4±0.04
Rietveld method (XRD)	Crystallite size $<L>_{vol}$(nm)	88	29
Williamson-Hall (XRD)	Crystallite size $<L>_{vol}$ (nm)	77.7±8.2	-
Williamson-Hall (XRD)	Strain value	0.322±0.006	-
(SEM)	Crystal size (nm)	260±30	-

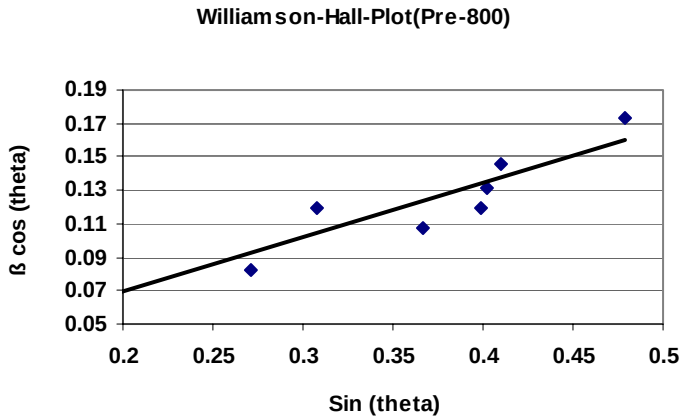

Figure 3.3. The Williamson-Hall plot in calcite (Pre-800) (Y=0.322X+0.0198, R^2=0.842)

Table–2.3. Morphology description based on intensity ratio data (Pre-800)

Method	Characteristic	Calcite	Aragonite
Intensity Ratio peak area (XRD)	Morphology Description	I(104)/I(116) 6.18±0.06	-
Intensity Ratio peak area (XRD)	Morphology Description	I(104)/I(012) 8.95±0.05	-
Intensity Ratio peak area (XRD)	Morphology Description	I(104)/I(202) 7.26±0.12	-
Intensity Ratio peak area (XRD)	Morphology Description	I(104)/I(113) 5.49±0.22	-
Intensity Ratio peak area (XRD)	Morphology Description	I(104)/I(018) 6.24±0.03	-
Intensity Ratio peak area (XRD)	Morphology Description	I(104)/I(122) 14.34±0.20	-
Intensity Ratio peak height (XRD)	Morphology Description	I(104)/I(116) 6.15±0.08	-
Intensity Ratio peak height (XRD)	Morphology Description	I(104)/I(012) 8.57±0.25	-
Intensity Ratio peak height (XRD)	Morphology Description	I(104)/I(202) 7.13±0.10	-
Intensity Ratio peak height (XRD)	Morphology Description	I(104)/I(113) 5.47±0.10	-
Intensity Ratio peak height (XRD)	Morphology Description	I(104)/I(018) 6.17±0.09	-
Intensity Ratio peak height (XRD)	Morphology Description	I(104)/I(122) 14.51±0.31	-

Sample Name Pre carb-320 Abbreviation Pre320

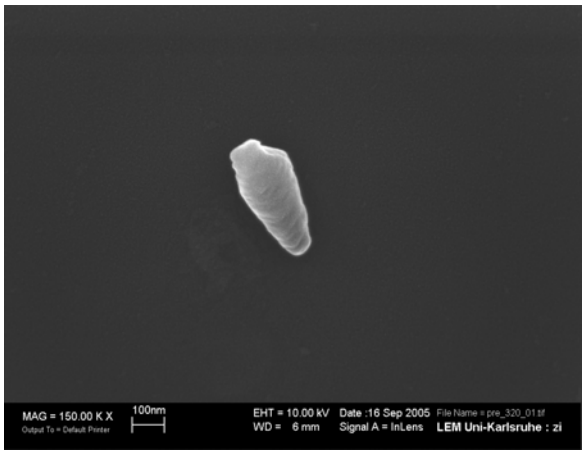

Figure 3.1. The SEM image (Pre320)

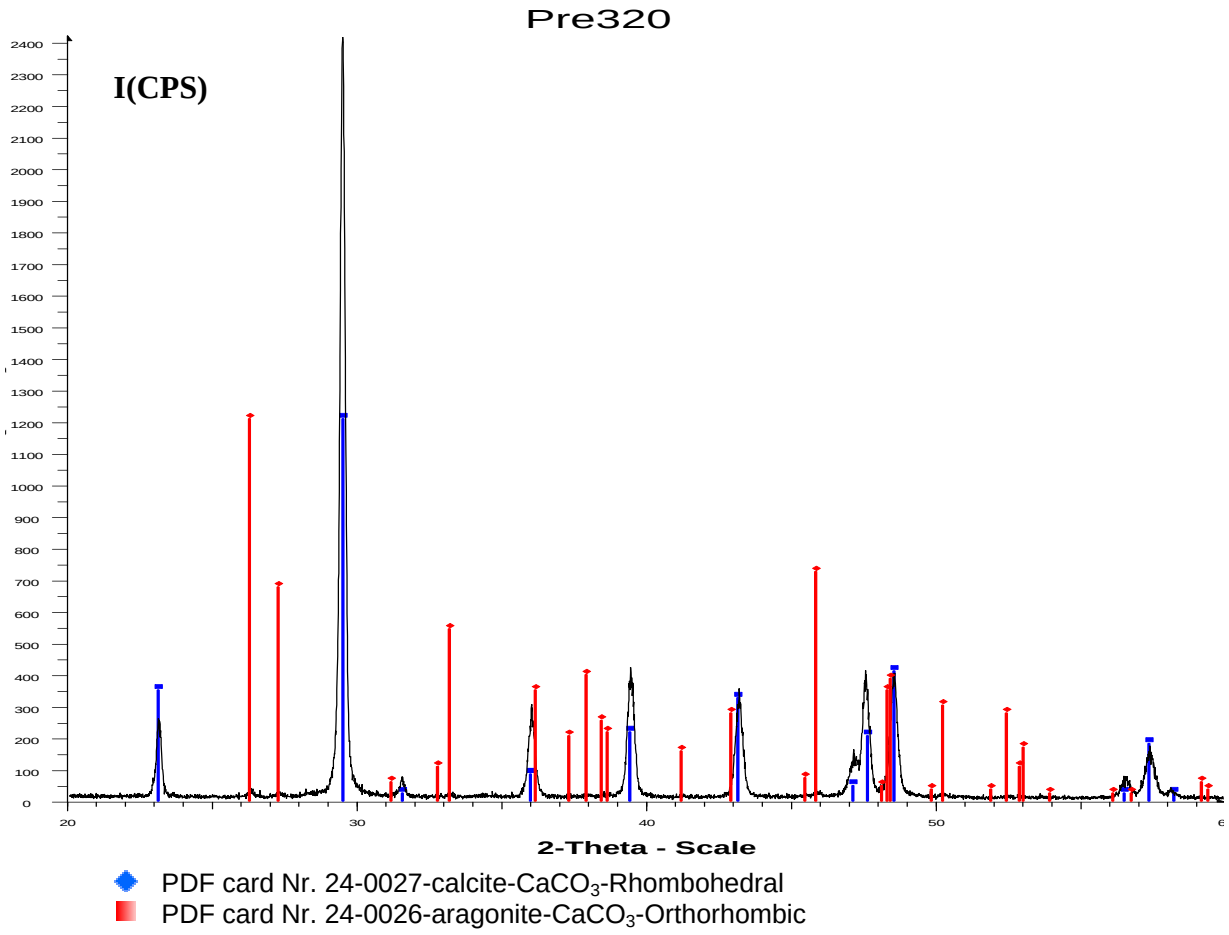

Figure 3.2. The diffractogram (Pre320)

Table- 3.1. The peak list of Pre 320($FWHM_{instrumental}$=0.157°)

Angle 2-Theta °	d value Angstrom	Intensity Count	Intensity %	$FWHM_{obs}$
23.063	3.85325	176	9.3	0.257
26.218	3.39635	26	1.4	0.181
27.214	3.27418	12	0.6	0.116
29.459	3.02959	1883	100	0.219
31.537	2.8346	65	3.5	0.282
35.973	2.49452	239	12.7	0.321
39.412	2.28444	312	16.6	0.324
43.166	2.09407	254	13.5	0.325
45.867	1.97683	19	1	0.210
47.651	1.90689	273	14.5	0.339
48.572	1.87289	311	16.5	0.315
56.553	1.62604	46	2.4	0.358
57.411	1.60376	102	5.4	0.321
58.273	1.58208	25	1.3	0.253
60.68	1.52494	55	2.9	0.595
61.531	1.50588	39	2.1	0.283

Table-3.2. Concentration, crystallite size, strain and crystal size (Pre320)

Method	Characteristic	Calcite	Aragonite
Rietveld method (XRD)	Concentration%	97.2±1.3	2.8±0.10
Rietveld method (XRD)	Crystallite size$<L>_{vol}$ (nm)	123	135
Williamson-Hall (XRD)	Crystallite size $<L>_{vol}$ (nm)	131.5±8.7	-
Williamson-Hall (XRD)	Strain value	0.292±0.051	-
SEM	Crystal size (nm)	180±18	-

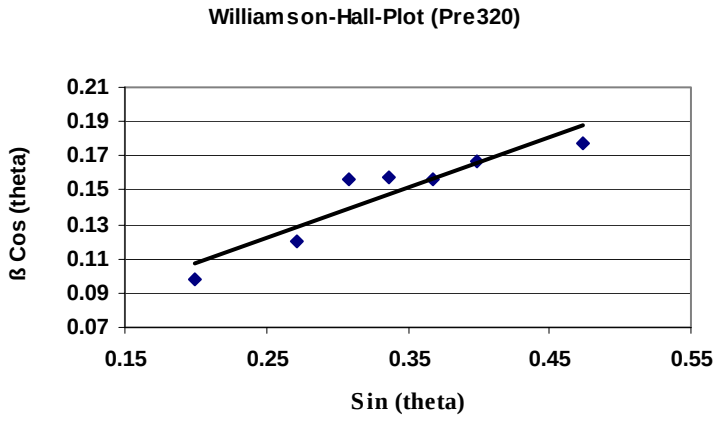

Figure 3.3. The Williamson-Hall plot in calcite (Pre320)
(Y= 0.292X+0.0117, R^2= 0.8648)

Table- 3.3. Morphology description based on intensity ratio data (Pre320)

Method	Characteristic	Calcite	Aragonite
Intensity Ratio peak area (XRD)	Morphology Description	I(104)/I(116) 6.39±0.12	-
Intensity Ratio peak area (XRD)	Morphology Description	I(104)/I(012) 10.63±0.16	-
Intensity Ratio peak area (XRD)	Morphology Description	I(104)/I(202) 7.34±0.14	-
Intensity Ratio peak area (XRD)	Morphology Description	I(104)/I(113) 5.69±0.21	-
Intensity Ratio peak area (XRD)	Morphology Description	I(104)/I(018) 6.80±0.13	-
Intensity Ratio peak area (XRD)	Morphology Description	I(104)/I(122) 16.24±0.11	-
Intensity Ratio peak height (XRD)	Morphology Description	I(104)/I(116) 6.34±0.12	-
Intensity Ratio peak height (XRD)	Morphology Description	I(104)/I(012) 10.17±0.06	-
Intensity Ratio peak height (XRD)	Morphology Description	I(104)/I(202) 7.35±0.16	-
Intensity Ratio peak height (XRD)	Morphology Description	I(104)/I(113) 5.75±0.09	-
Intensity Ratio peak height (XRD)	Morphology Description	I(104)/I(018) 6.38±0.11	-
Intensity Ratio peak height (XRD)	Morphology Description	I(104)/I(122) 16.16±0.28	-

Sample Name	Pre carb-360Versuchsmuster
Abbreviation	360V

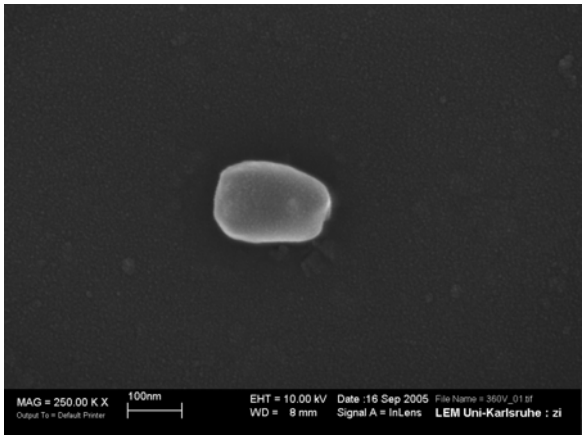

Figure 4.1. The SEM image (360V)

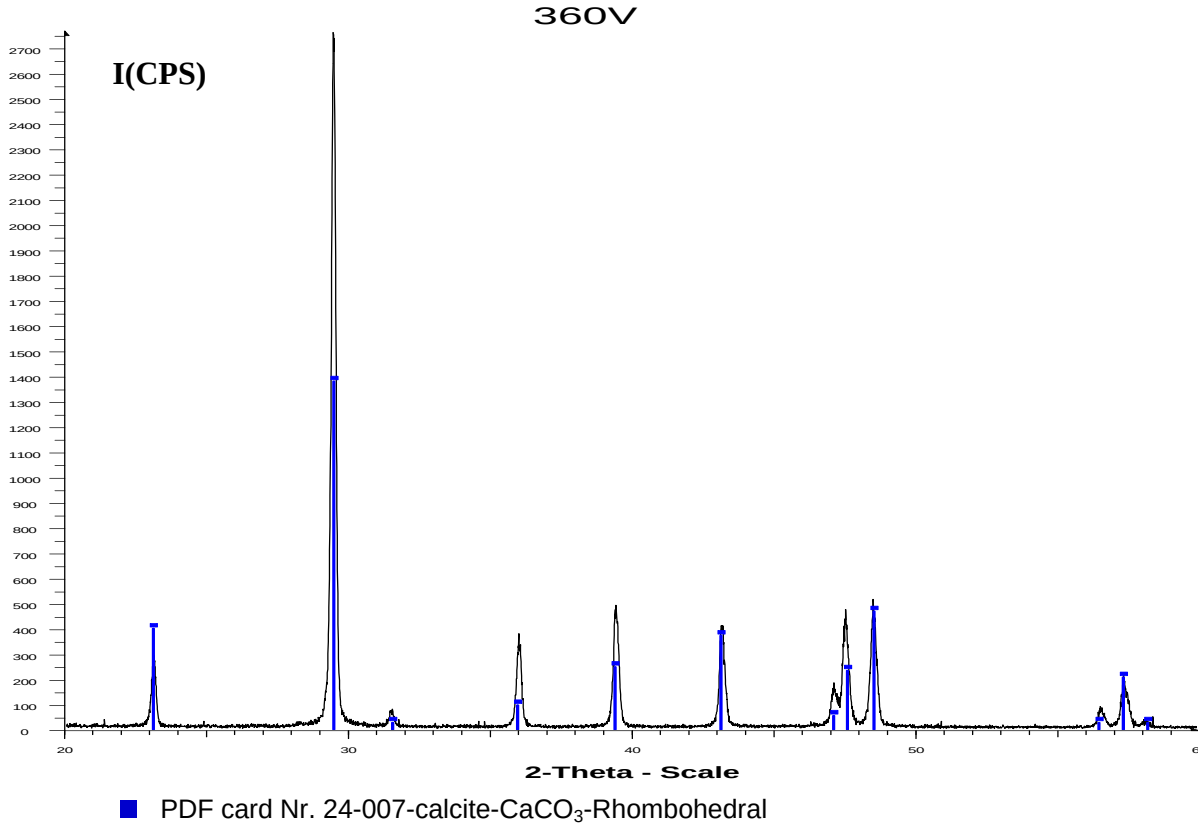

Figure 4.2. The diffractogram (360V)

Table- 4.1. The peak list of 360V ($FWHM_{instrumental}$=0.157)

Angle 2-Theta °	d value Angstrom	Intensity Count	Intensity %	$FWHM_{obs}$
23.063	3.85325	250	9.1	0.217
29.459	3.02959	2759	100	0.281
31.537	2.8346	70	2.5	0.228
35.973	2.49452	281	10.2	0.223
39.412	2.28444	435	15.8	0.241
43.166	2.09407	391	14.2	0.240
47.157	1.92572	165	6	0.277
48.572	1.87289	517	18.7	0.267
56.553	1.62604	63	2.3	0.253
57.411	1.60376	198	7.2	0.278
58.273	1.58208	29	1.1	0.256

Table- 4.2. Concentration, crystallite size, strain and crystal size (360V)

Method	Characteristic	Calcite	Aragonite
Rietveld method (XRD)	Concentration%	100±1.11	-
Rietveld method (XRD)	Crystallite size $<L>_{vol}$ (nm)	62	-
Williamson-Hall (XRD)	Crystallite size $<L>_{vol}$ (nm)	59.7±6.3	-
Williamson-Hall (XRD)	Strain value	0.099±0.012	-
(SEM)	Crystal size (nm)	138±22	-

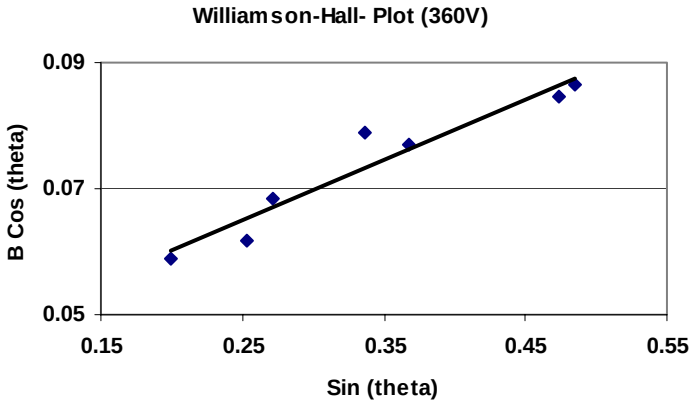

Figure 4.3. The Williamson-Hall plot in calcite(360V)
(Y= 0.0992X+0.026, R^2=0.8697)

Table-4.3. Morphology description based on intensity ratio data (360V)

Method	Characteristic	Calcite
Intensity Ratio peak area (XRD)	Morphology Description	I(104)/I(116) 5.19±0.15
Intensity Ratio peak area (XRD)	Morphology Description	I(104)/I(012) 9.93±0.13
Intensity Ratio peak area (XRD)	Morphology Description	I(104)/I(202) 6.34±0.12
Intensity Ratio peak area (XRD)	Morphology Description	I(104)/I(113) 5.68±0.43
Intensity Ratio peak area (XRD)	Morphology Description	I(104)/I(018) 6.10±0.06
Intensity Ratio peak area (XRD)	Morphology Description	I(104)/I(122) 15.61±0.16
Intensity Ratio peak height (XRD)	Morphology Description	I(104)/I(116) 5.47±0.09
Intensity Ratio peak height (XRD)	Morphology Description	I(104)/I(012) 9.59±0.23
Intensity Ratio peak height (XRD)	Morphology Description	I(104)/I(202) 6.60±0.20
Intensity Ratio peak height (XRD)	Morphology Description	I(104)/I(113) 5.63±0.06
Intensity Ratio peak height (XRD)	Morphology Description	I(104)/I(018) 5.73±0.14
Intensity Ratio peak height (XRD)	Morphology Description	I(104)/I(122) 15.58±0.28

Sample Name Pre carb-160G Abbreviation 160G

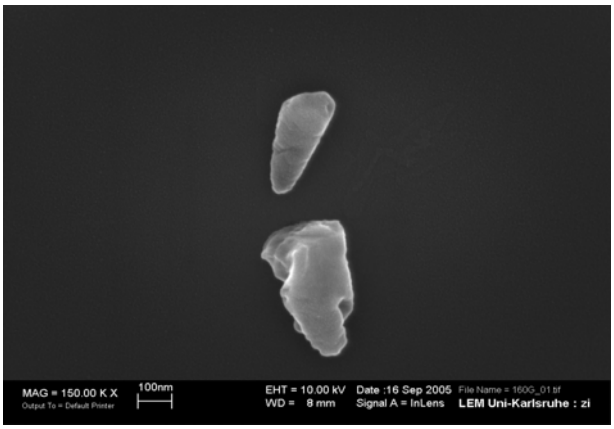

Figure 5.1. The SEM image (160G)

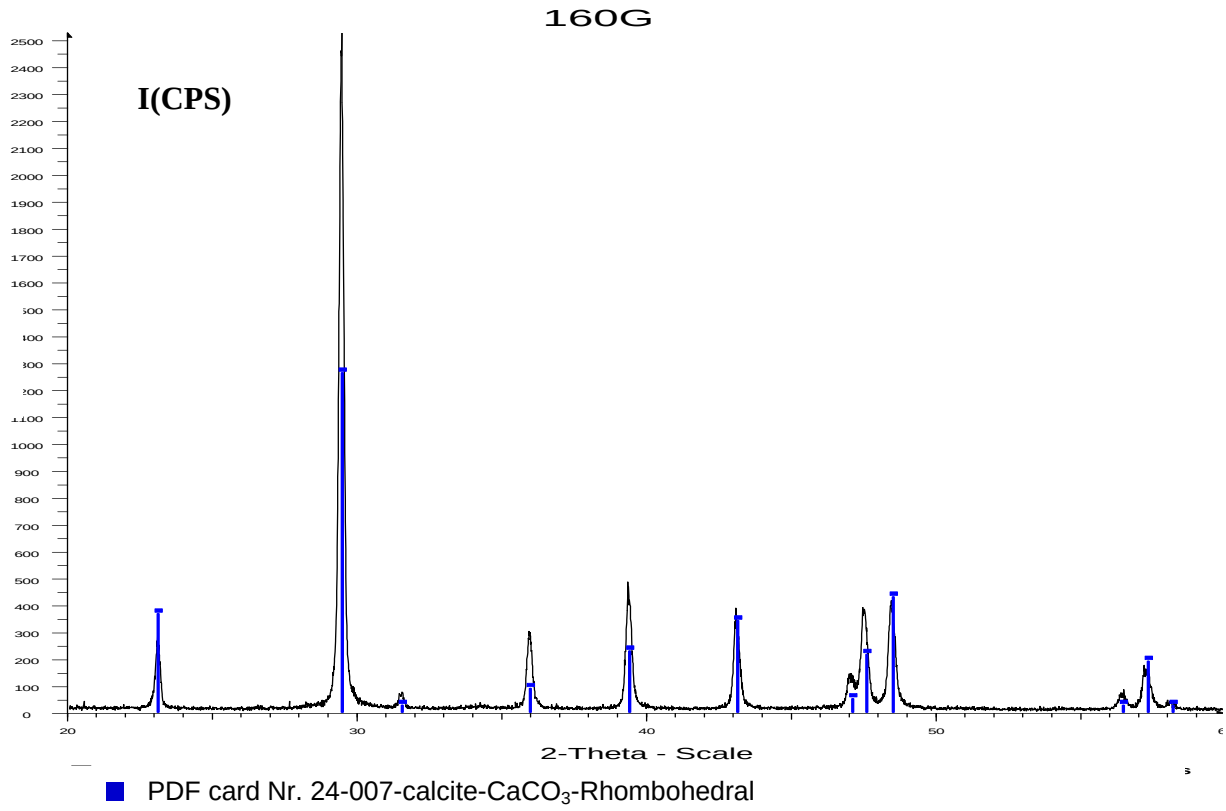

Figure 5.2. The diffractogram (160G)

Table-5.1. The peak list (160G)

Angle 2-Theta °	d value Angstrom	Intensity Count	Intensity %	$FWHM_{obs}$
23.063	3.85325	300	13.2	0.246
29.459	3.02959	2271	100	0.284
31.537	2.8346	74	3.3	0.168
35.973	2.49452	297	13.1	0.248
39.412	2.28444	411	18.1	0.289
43.166	2.09407	322	14.2	0.266
47.651	1.90689	313	13.8	0.292
48.572	1.87289	331	14.6	0.294
56.553	1.62604	69	3	0.312
57.411	1.60376	136	6	0.278
58.273	1.58208	22	1	0.398

Table- 5.2. Concentration, crystallite size, strain and crystal size (160V)

Method	Characteristic	Calcite	Aragonite
Rietveld method (XRD)	Concentration%	100±1.11	-
Rietveld method (XRD)	Crystallite size $<L>_{vol}$ (nm)	60	-
Williamson-Hall (XRD)	Crystallite size $<L>_{vol}$ (nm)	50.8±4.1	-
Williamson-Hall (XRD)	Strain value	0.217±0.043	-
(SEM)	Crystal size (nm)	150±34	-

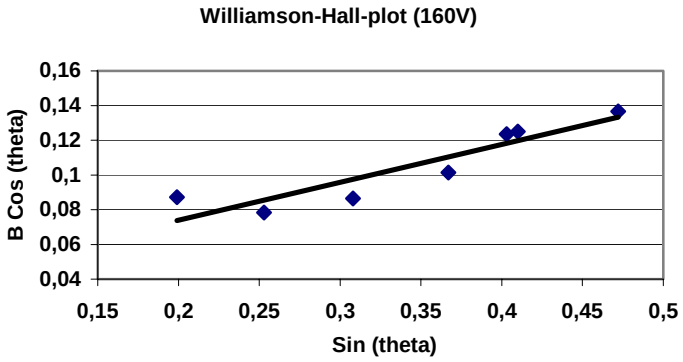

Figure 5.3. The Williamson-Hall plot in calcite(160G)
(Y= 0. 217X+0.0303, R^2=0.8403)

Table-5.3. Morphology description based on intensity ratio (160V)

Method	Characteristic	Calcite	Aragonite
Intensity Ratio peak area (XRD)	Morphology Description	I(104)/I(116) 6.25±0.04	-
Intensity Ratio peak area (XRD)	Morphology Description	I(104)/I(012) 8.92±0.04	-
Intensity Ratio peak area (XRD)	Morphology Description	I(104)/I(202) 6.80±0.16	-
Intensity Ratio peak area (XRD)	Morphology Description	I(104)/I(113) 5.30±0.08	-
Intensity Ratio peak area (XRD)	Morphology Description	I(104)/I(018) 6.46±0.24	-
Intensity Ratio peak area (XRD)	Morphology Description	I(104)/I(122) 15.36±0.30	-
Intensity Ratio peak height (XRD)	Morphology Description	I(104)/I(116) 5.84±0.21	-
Intensity Ratio peak height (XRD)	Morphology Description	I(104)/I(012) 8.55±0.46	-
Intensity Ratio peak height (XRD)	Morphology Description	I(104)/I(202) 6.95±0.30	-
Intensity Ratio peak height (XRD)	Morphology Description	I(104)/I(113) 5.55±0.10	-
Intensity Ratio height (XRD)	Morphology Description	I(104)/I(018) 6.37±0.21	-
Intensity Ratio peak height (XRD)	Morphology Description	I(104)/I(122) 15.53±0.13	-

Sample Name Pre carb-360GR,Versuchsmuster IFb25 Abbreviation Fb25

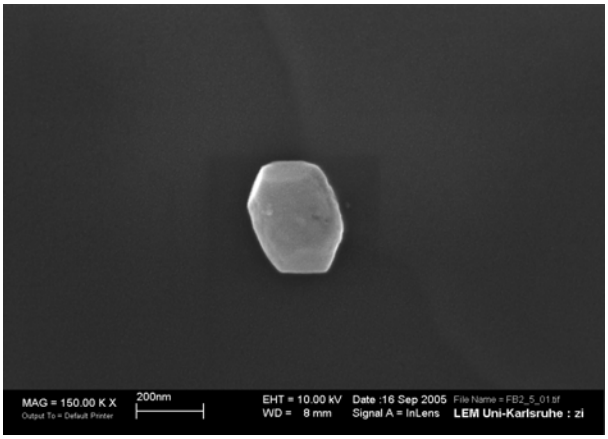

Figure 6.1. The SEM image (Fb25)

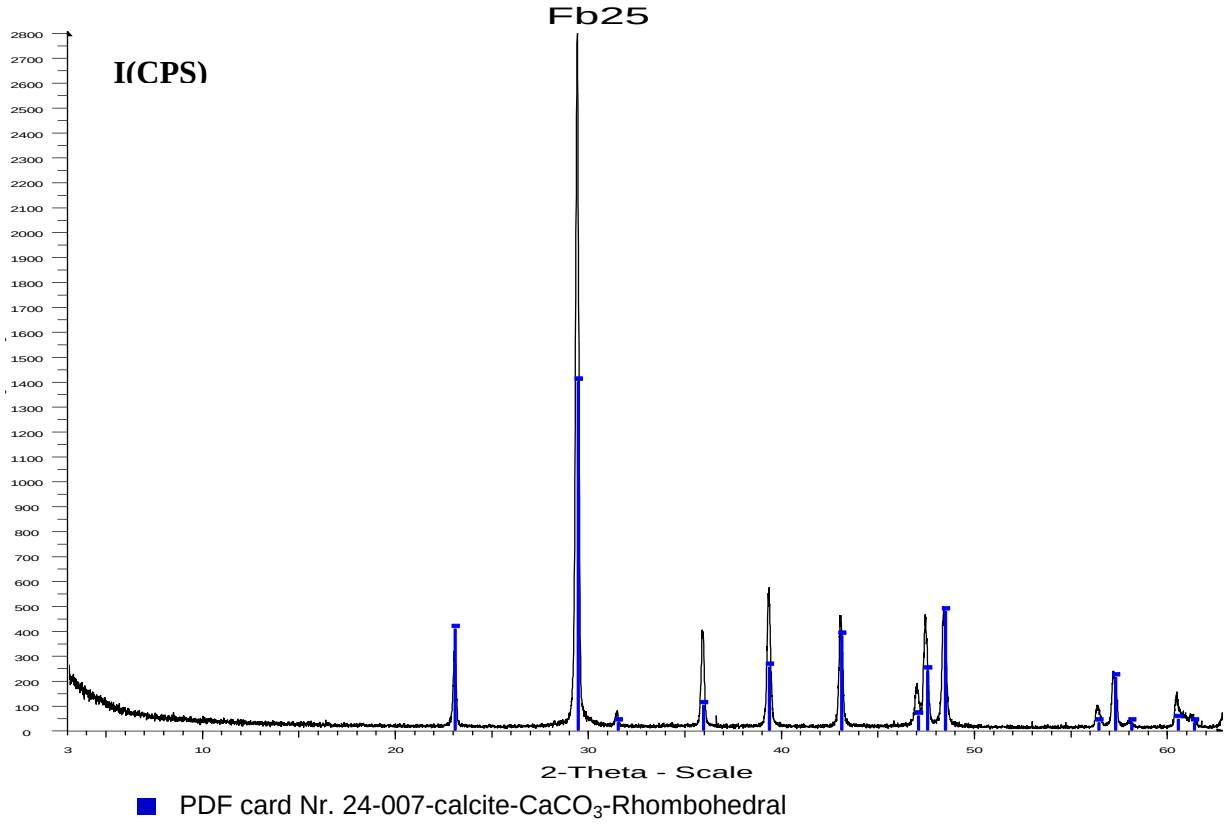

Figure 6.2. The diffractogram (Fb25)

Table- 6.1. The peak list of Fb25 ($FWHM_{instrumental}$=0.157)

Angle 2-Theta °	d value Angstrom	Intensity Count	Intensity %	$FWHM_{obs}$
23.063	3.85325	319	12.7	0.220
29.459	3.02959	2506	100	0.220
31.537	2.8346	61	2.4	0.214
35.973	2.49452	374	14.9	0.218
39.412	2.28444	573	22.9	0.243
43.166	2.09407	419	16.7	0.244
47.157	1.92572	147	5.9	0.249
48.572	1.87289	365	14.6	0.258
56.553	1.62604	82	3.3	0.257
57.411	1.60376	172	6.9	0.257
58.273	1.58208	18	0.7	0.284
60.68	1.52494	102	4.1	0.287

Table-6.2. Concentration, crystallite size, strain and crystal size (Fb25)

Method	Characteristic	Calcite	Aragonite
Rietveld method (XRD)	Concentration%	99.8±1.22	0.2±0.03
Rietveld method (XRD)	Crystallite size $<L>_{vol}$ (nm)	119	-
Williamson-Hall (XRD)	Crystallite size <L>vol (nm)	105±11	-
Williamson-Hall (XRD)	Strain value	0.153±0.017	-
(SEM)	Crystal size(nm)	200±39	-

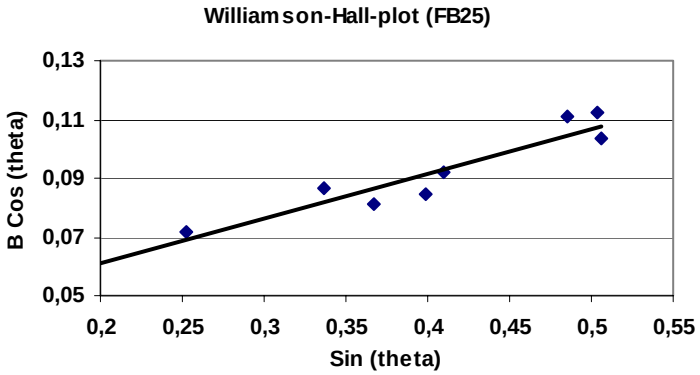

Figure 6.3. The Williamson-Hall plot (Fb25)
(Y= 0. 153X+0.0146, R^2=0.8703)

Table- 6.3. Morphology description based on intensity ratio data (Fb25)

Method	Characteristic	Calcite	Aragonite
Intensity Ratio peak area (XRD)	Morphology Description	I(104)/I(116) 5.56±0.26	-
Intensity Ratio peak area (XRD)	Morphology Description	I(104)/I(012) 8.70±0.15	-
Intensity Ratio peak area (XRD)	Morphology Description	I(104)/I(202) 5.32±0.22	-
Intensity Ratio peak area (XRD)	Morphology Description	I(104)/I(113) 5.22±0.09	-
Intensity Ratio peak area (XRD)	Morphology Description	I(104)/I(018) 6.28±0.18	-
Intensity Ratio peak area (XRD)	Morphology Description	I(104)/I(122) 11.34±0.34	-
Intensity Ratio peak height (XRD)	Morphology Description	I(104)/I(116) 5.80±0.20	-
Intensity Ratio peak area (XRD)	Morphology Description	I(104)/I(012) 8.20±0.20	-
Intensity Ratio peak area (XRD)	Morphology Description	I(104)/I(202) 5.80±0.50	-
Intensity Ratio peak area (XRD)	Morphology Description	I(104)/I(113) 5.60±0.60	-
Intensity Ratio peak area (XRD)	Morphology Description	I(104)/I(018) 6.20±0.10	-
Intensity Ratio peak area (XRD)	Morphology Description	I(104)/I(122) 11.40±0.80	-

Sample Name	Pre carb-720
Abbreviation	Pre720

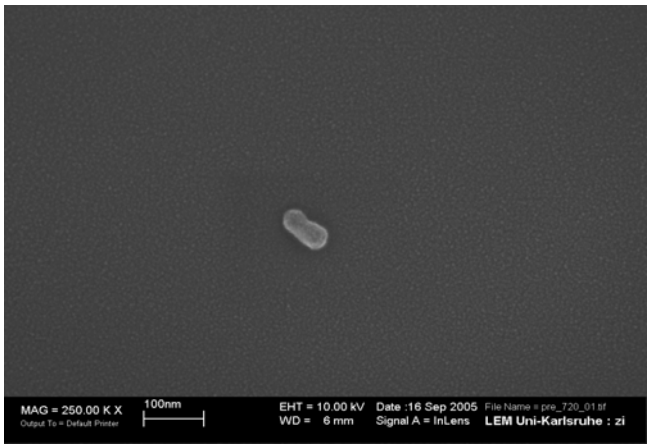

Figure 7.1. The SEM image (Pre720)

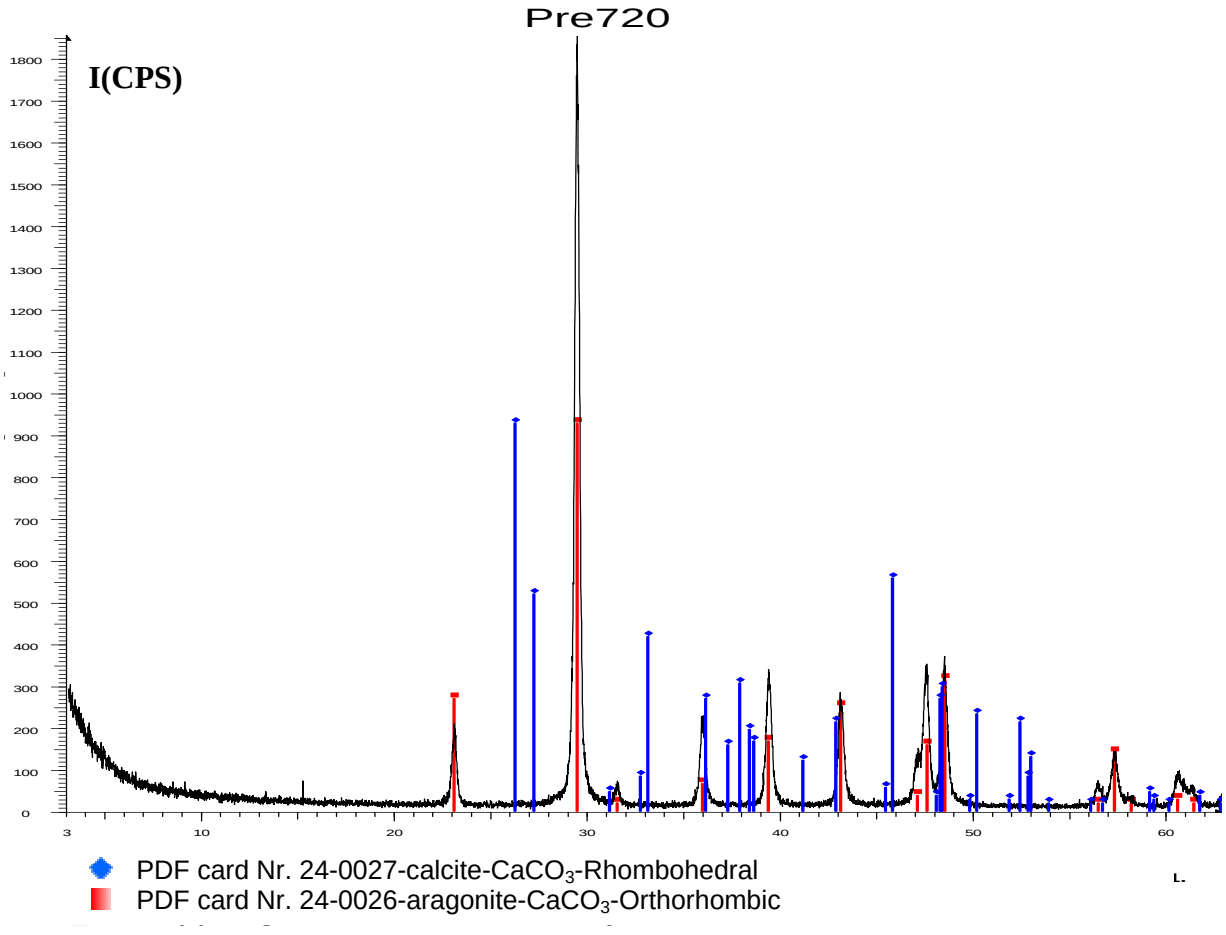

Figure 7.2. The diffractogram (Pre720)

Table-7.1. The peak list (Pre720)

Angle 2-Theta °	d value Angstrom	Intensity Count	Intensity %	$FWHM_{obs}$
23.063	3.85325	178	9.7	0.363
29.459	3.02959	1835	100	0.334
35.973	2.49452	193	10.5	0.420
39.412	2.28444	317	17.3	0.427
43.166	2.09407	252	13.7	0.414
45.867	1.97683	120	6.5	0.606
47.157	1.92572	332	18.1	0.438
48.454	1.87718	340	18.5	0.394
56.553	1.62604	35	1.9	0.322
58.273	1.58208	9	0.5	0.234
60.68	1.52494	51	2.8	0.429

Table- 7.2. Concentration, crystallite size, strain and crystal size (Pre720)

Method	Characteristic	Calcite	Aragonite
Rietveld method (XRD)	Concentration%	98.9±1.21	1.1±0.05
Rietveld method (XRD)	Crystallite size $<L>_{vol}$ (nm)	39	15
Williamson-Hall (XRD)	Crystallite size $<L>_{vol}$ (nm)	25±4.4	-
Williamson-Hall (XRD)	Strain value	0.340±0.126	-
(SEM)	Crystal size (nm)	100±26	-

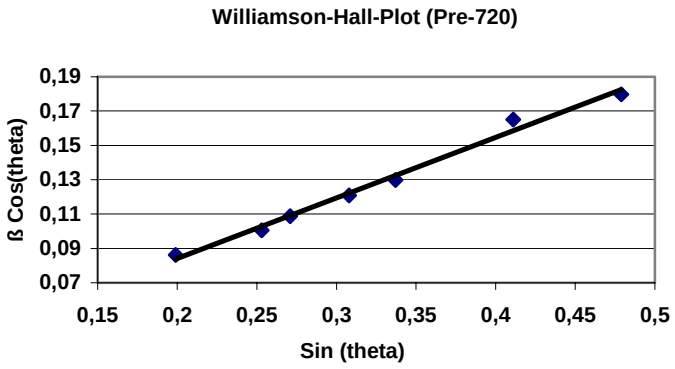

Figure 7-3. The Williamson-Hall plot (Pre720) (Y=0.34X+ 0.0617, R^2=0.9605)

Table-7.3. Morphology description based on intensity ratio (Pre720)

Method	Characteristic	Calcite	Aragonite
Intensity Ratio peak area (XRD)	Morphology Description	I(104)/I(116) 5.18±0.11	-
Intensity Ratio peak area (XRD)	Morphology Description	I(104)/I(012) 10.68±0.31	-
Intensity Ratio peak area (XRD)	Morphology Description	I(104)/I(202) 6.28±0.23	-
Intensity Ratio peak area (XRD)	Morphology Description	I(104)/I(113) 5.30±0.20	-
Intensity Ratio peak area (XRD)	Morphology Description	I(104)/I(018) 5.36±0.28	-
Intensity Ratio peak area (XRD)	Morphology Description	I(104)/I(122) 13.0±0.40	-
Intensity Ratio peak height (XRD)	Morphology Description	I(104)/I(116) 5.10±0.20	-
Intensity Ratio peak height (XRD)	Morphology Description	I(104)/I(012) 10.30±0.90	-
Intensity Ratio peak height (XRD)	Morphology Description	I(104)/I(202) 6.50±0.40	-
Intensity Ratio peak height (XRD)	Morphology Description	I(104)/I(113) 5.30±0.20	-
Intensity Ratio peak height (XRD)	Morphology Description	I(104)/I(018) 5.30±0.20	-
Intensity Ratio peak height (XRD)	Morphology Description	I(104)/I(122) 12.9±0.90	-

Sample Name	Pre carb-100
Abbreviation	Pre100

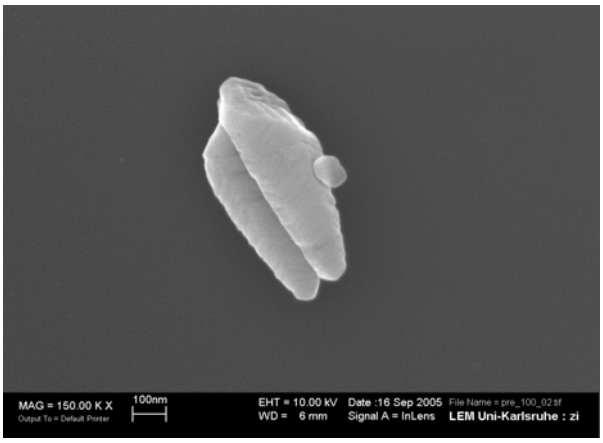

Figure 8.1. The SEM image (Pre100)

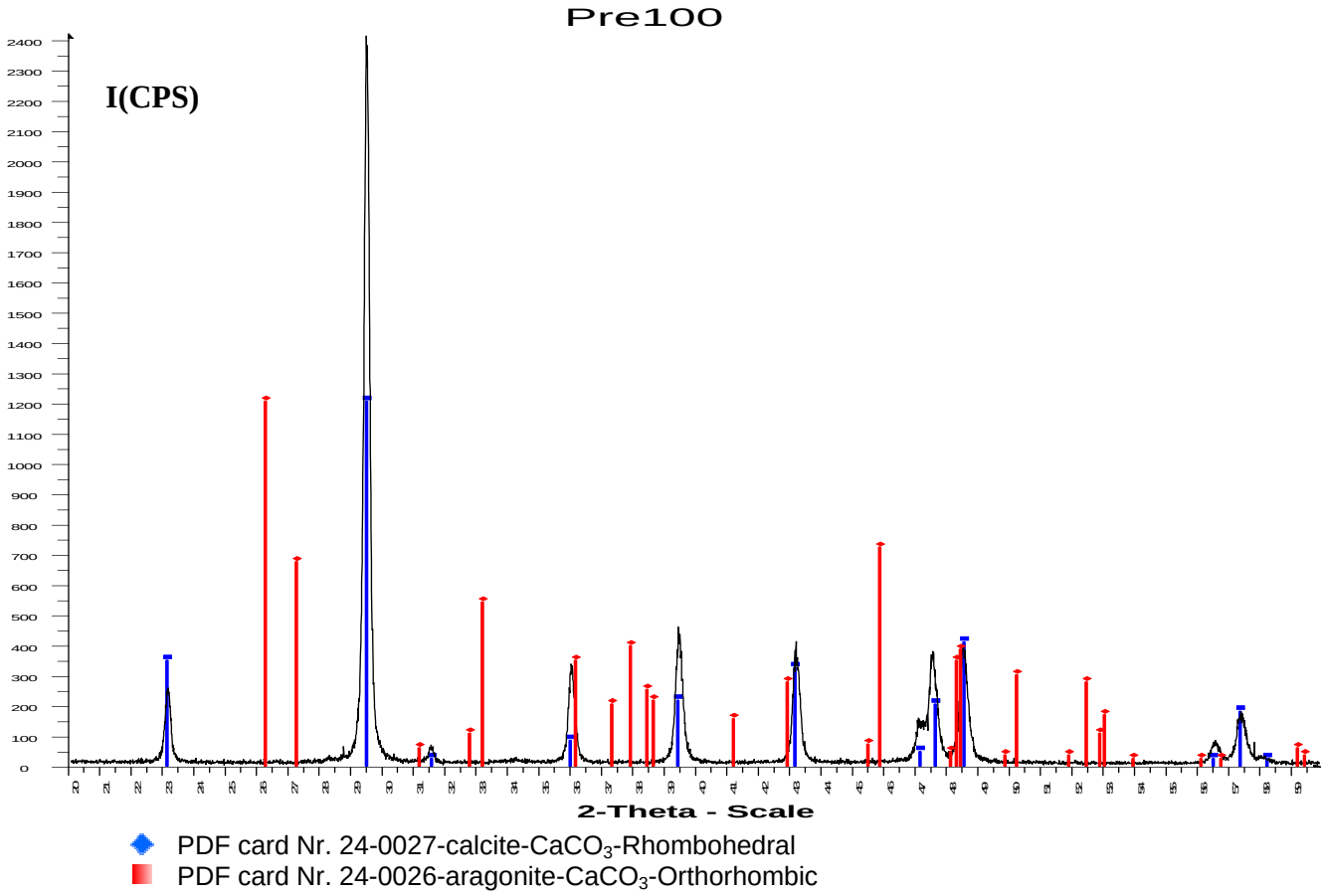

Figure 8.2. The diffractogram (Pre100)

Table- 8.1. The peak list (Pre100)

Angle 2-Theta °	d value Angstrom	Intensity Count	Intensity %	$FWHM_{obs}$
23.063	3.85325	210	8.7	0.245
29.459	3.02959	2422	100	0.246
31.537	2.8346	54	2.2	0.270
35.973	2.49452	297	12.3	0.284
39.412	2.28444	387	16	0.295
43.166	2.09407	383	15.8	0.294
47.157	1.92572	137	5.7	0.344
48.572	1.87289	389	16.1	0.338
56.553	1.62604	69	2.8	0.392
57.411	1.60376	160	6.6	0.362
58.273	1.58208	21	0.9	0.328

Table-8.2. Concentration, crystallite size, strain and crystal size (Pre100)

Method	Characteristic	Calcite	Aragonite
Rietveld method (XRD)	Concentration%	99.4±1.23	0.6±0.06
Rietveld method (XRD)	Crystallite size $<L>_{vol}$ (nm)	90	27
Williamson-Hall (XRD)	Crystallite size $<L>_{vol}$ (nm)	103.3±7.8	-
Williamson-Hall (XRD)	Strain value	0.342±0.028	-
(SEM)	Crystal size (nm)	250±41	-

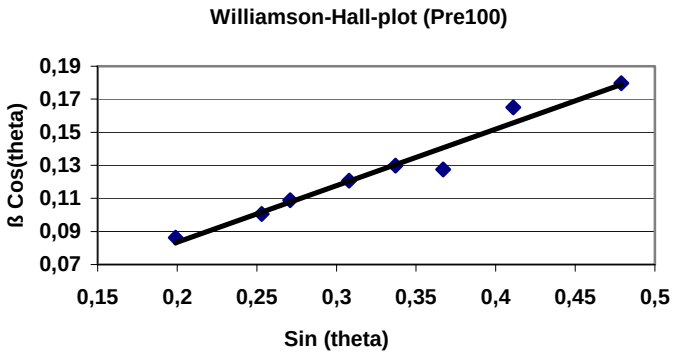

Figure 8.3. The Williamson-Hall plot (Pre100)
(Y= 0.342X + 0.0149, R^2=0.9605)

Table- 8.3 . Morphology description based on intensity ratio data (Pre100)

Method	Characteristic	Calcite	Aragonite
Intensity Ratio peak area (XRD)	Morphology Description	I(104)/I(116) 6.17±0.05	-
Intensity Ratio peak area (XRD)	Morphology Description	I(104)/I(012) 9.09±0.19	-
Intensity Ratio peak area (XRD)	Morphology Description	I(104)/I(202) 6.21±0.49	-
Intensity Ratio peak area (XRD)	Morphology Description	I(104)/I(113) 5.28±0.16	-
Intensity Ratio peak area (XRD)	Morphology Description	I(104)/I(018) 6.68±0.16	-
Intensity Ratio peak area (XRD)	Morphology Description	I(104)/I(122) 13.38±0.20	-
Intensity Ratio peak height (XRD)	Morphology Description	I(104)/I(116) 6.20±0.12	-
Intensity Ratio peak height (XRD)	Morphology Description	I(104)/I(012) 9.19±0.37	-
Intensity Ratio peak height (XRD)	Morphology Description	I(104)/I(202) 6.27±0.30	-
Intensity Ratio peak height (XRD)	Morphology Description	I(104)/I(113) 5.33±0.11	-
Intensity Ratio peak height (XRD)	Morphology Description	I(104)/I(018) 6.60±0.30	-
Intensity Ratio peak height (XRD)	Morphology Description	I(104)/I(122) 13.52±0.18	-

Sample Name Pre carb-600 Abbreviation Pre600

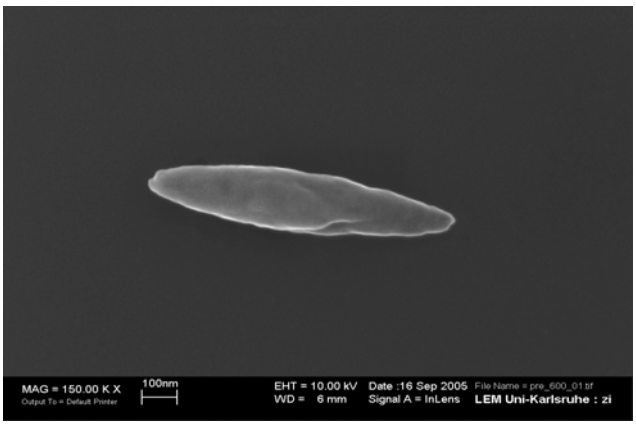

Figure 9.1. The SEM image (Pre600)

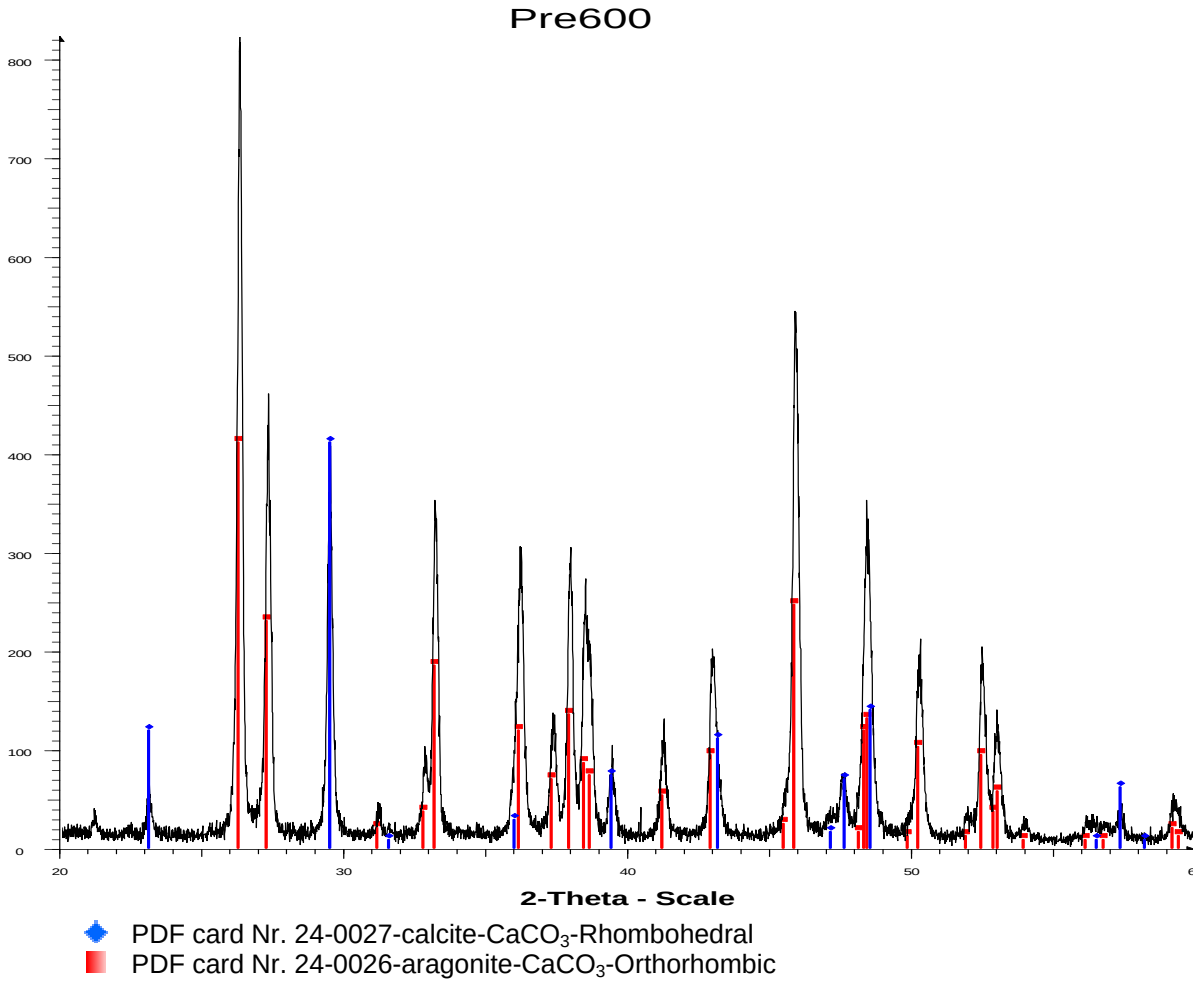

Figure 9.2. The diffractogram (Pre600)

Table-9.1. The peak list (Pre600)

Angle 2-Theta °	d value Angstrom	Intensity Count	Intensity %	$FWHM_{obs}$
23.063	3.85325	32	6.5	0.257
26.218	3.39635	51	10.3	0.239
27.214	3.27418	76	15.3	0.240
29.459	3.02959	496	100	0.223
31.134	2.87036	118	23.8	0.189
32.748	2.73249	75	15.1	0.214
33.152	2.70007	42	8.5	0.293
35.973	2.49452	296	59.7	0.336
36.132	2.48393	357	72	0.325
37.29	2.40941	24	4.8	0.229
37.905	2.37174	68	13.7	0.210
38.635	2.3286	139	28	0.328
41.203	2.1892	247	49.8	0.263
42.911	2.10591	187	37.7	0.238
45.867	1.97683	122	24.6	0.236
47.157	1.92572	43	8.7	0.329
47.651	1.90689	220	44.4	0.243
48.336	1.88149	114	23	0.325
49.876	1.82694	81	16.3	0.311
51.928	1.75945	22	4.4	0.140
52.48	1.74224	11	2.2	0.246
52.913	1.729	23	4.6	0.316
56.553	1.62604	195	39.3	0.224
56.798	1.61961	26	5.2	0.312

Table-9.2. Concentration, crystallite size and strain (Pre600)

Method	Characteristic	Calcite	Aragonite
Rietveld method (XRD)	Concentration%	15.6±0.98	84.4±1.30
Rietveld method (XRD)	Crystallite size $<L>_{vol}$ (nm)	114	91
Williamson-Hall (XRD)	Crystallite size <L>vol (nm)	127.6±11.6	87.1±6.5
Williamson-Hall (XRD)	Strain value	0.501±0.047	0.275±0.02

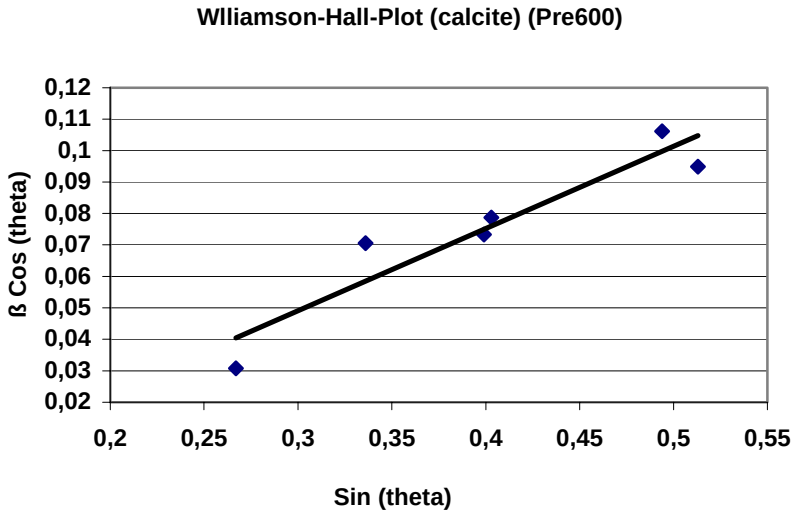

Figure 9.3a. The Williamson-Hall plot (calcite) (Pre600)
(Y= 0.501X+0.0121,R^2=0.8846)

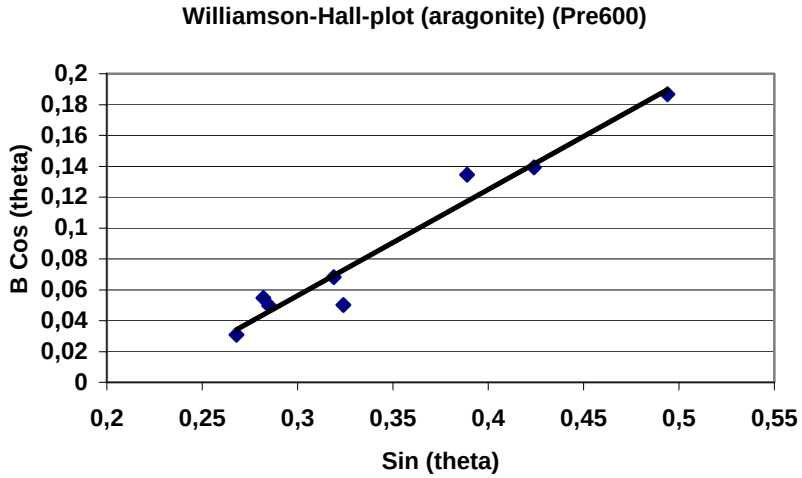

Figure 9.3b. The Williamson-Hall plot (aragonite) (Pre600)
(Y=0.275X+ 0.0177, R^2=0.9568)

Table-9.3. Morphology description based on intensity ratio data (pre600)

Method	Characteristic	Calcite	Aragonite
Intensity Ratio peak area (XRD)	Morphology Description	I(104)/I(116) 1.31±0.21	I(040)/I(111) 0.92±0.02
Intensity Ratio peak area (XRD)	Morphology Description	I(104)/I(012) 5.66±0.25	I(040)/I(202) 1.51±0.06
Intensity Ratio peak area (XRD)	Morphology Description	I(104)/I(202) 1.73±0.08	I(040)/I(022) 2.15±0.09
Intensity Ratio peak area (XRD)	Morphology Description	I(104)/I(113) 3.60±0.17	I(040)/I(113) 2.05±0.04
Intensity Ratio peak area (XRD)	Morphology Description	I(104)/I(018) 4.64±0.17	I(040)/I(102) 1.91±0.03
Intensity Ratio peak area (XRD)	Morphology Description	I(104)/I(122) 8.85±0.20	-
Intensity Ratio peak height (XRD)	Morphology Description	I(104)/I(116) 1.14±0.05	I(040)/I(111) 0.66±0.01
Intensity Ratio peak height (XRD)	Morphology Description	I(104)/I(012) 5.58±0.19	I(040)/I(202) 1.14±0.04
Intensity Ratio peak height (XRD)	Morphology Description	I(104)/I(202) 1.68±0.09	I(040)/I(022) 2.16±0.13
Intensity Ratio peak height (XRD)	Morphology Description	I(104)/I(113) 3.34±0.08	I(040)/I(113) 1.61±0.03
Intensity Ratio peak height (XRD)	Morphology Description	I(104)/I(018) 4.87±0.14	I(040)/I(102) 1.89±0.06
Intensity Ratio peak height (XRD)	Morphology Description	I(104)/I(122) 8.68±0.20	-

Sample Name	Sphärolitisches PCC,Versuchsmuster FB2-30
Abbreviation	Fb230

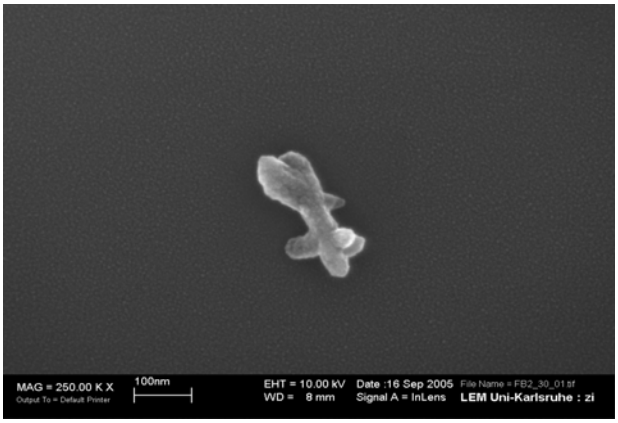

Figure 10.1. The SEM image (Fb230)

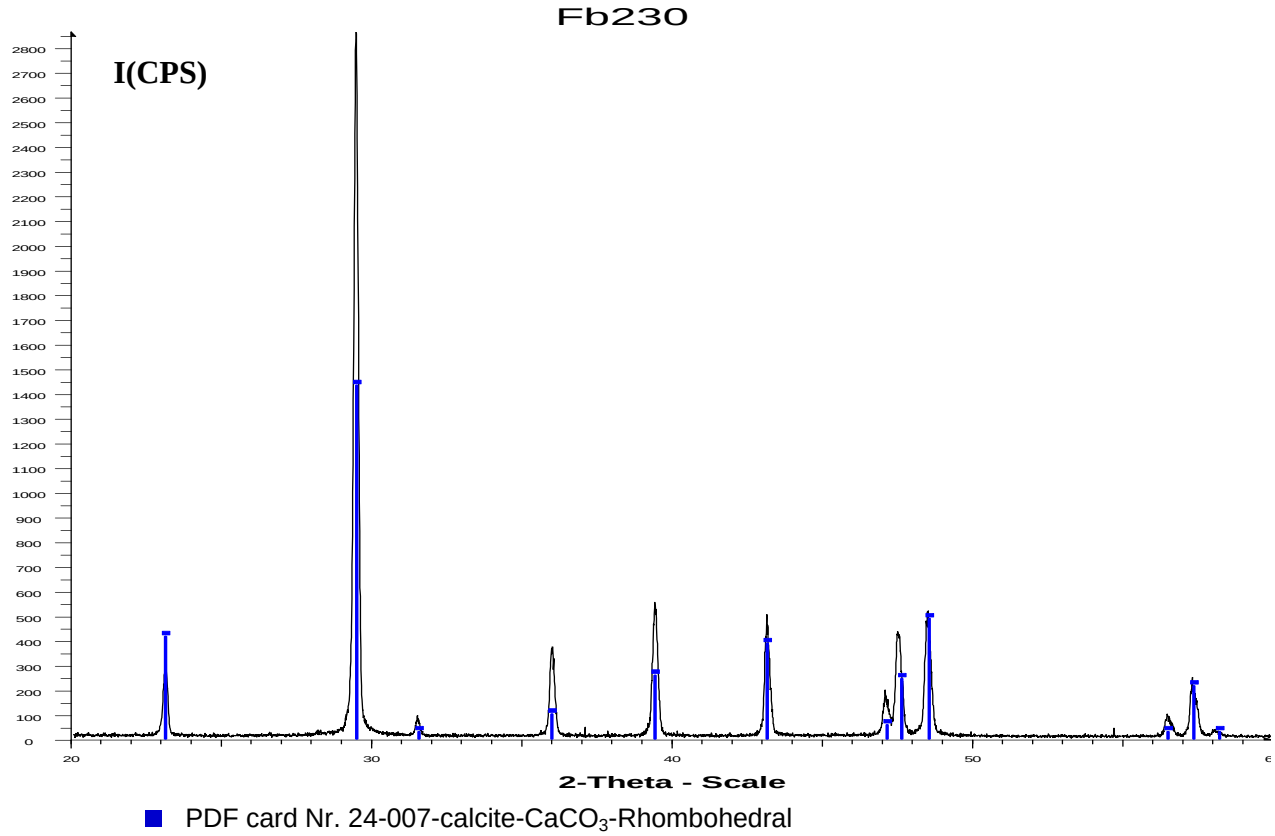

Figure 10.2. The diffractogram (Fb230)

Table-10.1. The peak list (Fb230)

Angle 2-Theta °	d value Angstrom	Intensity Count	Intensity % %	$FWHM_{obs}$
23.063	3.85325	321	11.5	0.210
29.459	3.02959	2781	100	0.291
31.537	2.8346	76	2.7	0.225
35.973	2.49452	344	12.4	0.231
39.412	2.28444	534	19.2	0.225
43.166	2.09407	422	15.2	0.236
47.651	1.90689	274	9.9	0.230
48.572	1.87289	433	15.6	0.248
56.553	1.62604	90	3.2	0.240
57.411	1.60376	210	7.6	0.237
58.273	1.58208	24	0.9	0.194

Table- 10.2. Concentration, crystallite size, strain and crystal size (Fb230)

Method	Characteristic	Calcite	Aragonite
Rietveld method (XRD)	Concentration%	100±1.11	-
Rietveld method (XRD)	Crystallite size $<L>_{vol}$ (nm)	47	-
Williamson-Hall (XRD)	Crystallite size $<L>_{vol}$ (nm)	46.7±6.6	-
Williamson-Hall (XRD)	Strain value	0.147±0.018	-
(SEM)	Crystal size (nm)	60±7	-

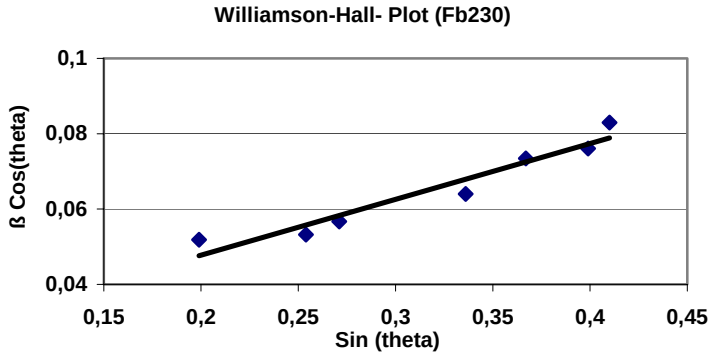

Figure 10.3. The Wiliamson-Hall plot (Fb230)
(Y=0.147X+0.033, R^2=0.9317)

Table- 10.3.Morphology description based on intensity ratio data (Fb230)

Method	Characteristic	Calcite	Aragonite
Intensity Ratio peak area (XRD)	Morphology Description	I(104)/I(116) 5.41±0.26	-
Intensity Ratio peak area (XRD)	Morphology Description	I(104)/I(012) 9.19±0.20	-
Intensity Ratio peak area (XRD)	Morphology Description	I(104)/I(202) 5.67±0.16	-
Intensity Ratio peak area (XRD)	Morphology Description	I(104)/I(113) 4.61±0.09	-
Intensity Ratio peak area (XRD)	Morphology Description	I(104)/I(018) 5.70±0.26	-
Intensity Ratio peak area (XRD)	Morphology Description	I(104)/I(122) 13.66±0.12	-
Intensity Ratio peak height (XRD)	Morphology Description	I(104)/I(116) 5.56± 0.26	-
Intensity Ratio peak height (XRD)	Morphology Description	I(104)/I(012) 9.15±0.27	-
Intensity Ratio peak height (XRD)	Morphology Description	I(104)/I(202) 5.80±0 .10	-
Intensity Ratio peak height (XRD)	Morphology Description	I(104)/I(113) 5.06±0.36	-
Intensity Ratio peak height (XRD)	Morphology Description	I(104)/I(018) 6.27±0.32	-
Intensity Ratio peak height (XRD)	Morphology Description	I(104)/I(122) 13.38±0.29	-

Sample Name	PCC F-S 210
Abbreviation	PFS210

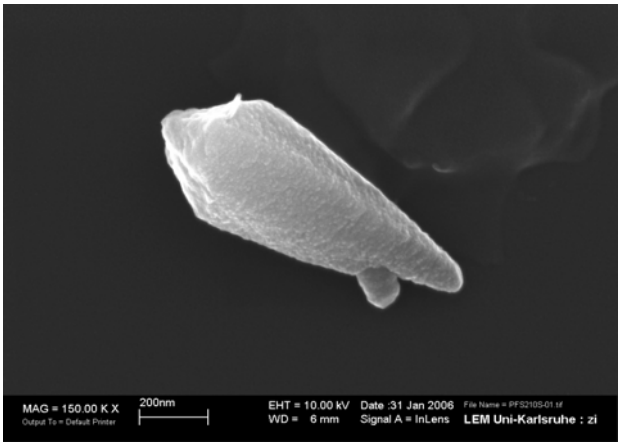

Figure 11.1. The SEM image (PFS210)

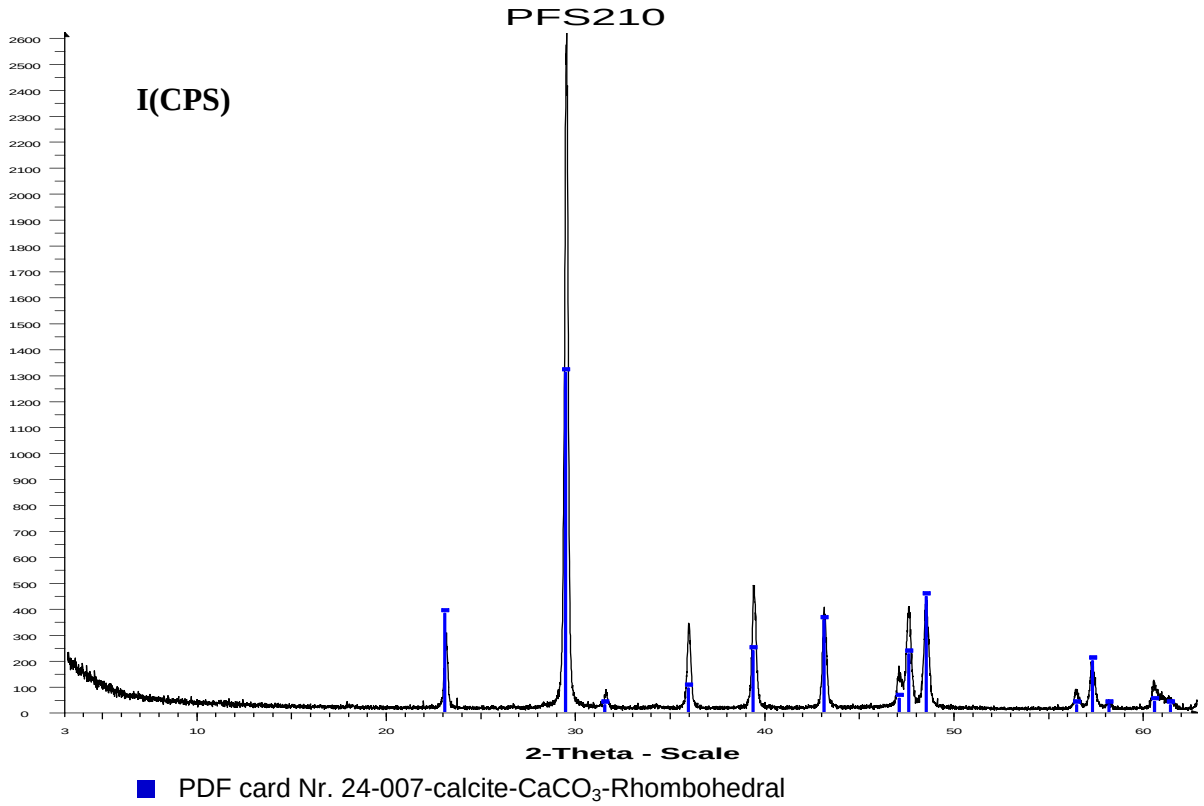

Figure 11.2. The diffractogram (PFS210)

Table-11.1. The peak list (PFS210)

Angle 2-Theta °	d value Angstrom	Intensity Count	Intensity %	$FWHM_{obs}$
23.063	3.85325	185	9.3	0.269
29.459	3.02959	1990	100	0.246
31.537	2.8346	65	3.3	0.248
35.973	2.49452	273	13.7	0.271
39.412	2.28444	392	19.7	0.302
43.166	2.09407	360	18.1	0.294
47.157	1.92572	176	8.8	0.361
47.651	1.90689	384	19.3	0.300
48.572	1.87289	378	19	0.345
56.553	1.62604	66	3.3	0.319
57.411	1.60376	181	9.1	0.362
58.273	1.58208	46	2.3	0.292
60.68	1.52494	94	4.7	0.393

Table- 11.2. Concentration, crystallite size, strain and crystal size (PFS 210)

Method	Characteristic	Calcite	Aragonite
Rietveld method (XRD)	Concentration%	100±1.1	-
Rietveld method (XRD)	Crystallite size $<L>_{vol}$ (nm)	85	-
Williamson-Hall (XRD)	Crystallite size $<L>_{vol}$ (nm)	73±10.2	-
Williamson-Hall (XRD)	Strain value	0.450±0.075	-
(SEM)	Crystal size (nm)	265±44	-

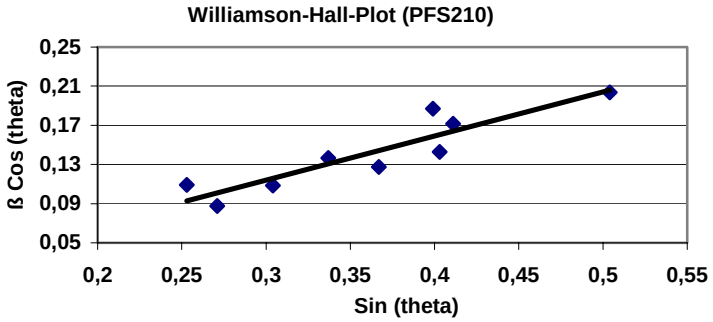

Figure 11.3. The Williamson-Hall plot (PFS210)
($Y=0.450X - 0.0211$, $R^2= 0.8358$)

Table-11.3. Morphology description based on intensity ratio data (PFS210)

Method	Characteristic	Calcite	Aragonite
Intensity Ratio peak area (XRD)	Morphology Description	I(104)/I(116) 6.58±0.06	
Intensity Ratio peak area (XRD)	Morphology Description	I(104)/I(012) 8.92±0.09	
Intensity Ratio peak area (XRD)	Morphology Description	I(104)/I(202) 6.26±0.03	
Intensity Ratio peak area (XRD)	Morphology Description	I(104)/I(113) 5.40±0.07	
Intensity Ratio peak area (XRD)	Morphology Description	I(104)/I(018) 6.04±0.12	
Intensity Ratio peak area (XRD)	Morphology Description	I(104)/I(122) 14.69±0.17	
Intensity Ratio peak height (XRD)	Morphology Description	I(104)/I(116) 6.33±0.17	
Intensity Ratio peak height (XRD)	Morphology Description	I(104)/I(012) 8.43±0.16	
Intensity Ratio peak height (XRD)	Morphology Description	I(104)/I(202) 6.34±0.28	
Intensity Ratio peak height (XRD)	Morphology Description	I(104)/I(113) 5.23±0.14	
Intensity Ratio peak height (XRD)	Morphology Description	I(104)/I(018) 6.22±0.16	
Intensity Ratio peak height (XRD)	Morphology Description	I(104)/I(122) 14.48±0.20	

Sample Name PCC R-PCC Abbreviation PRP

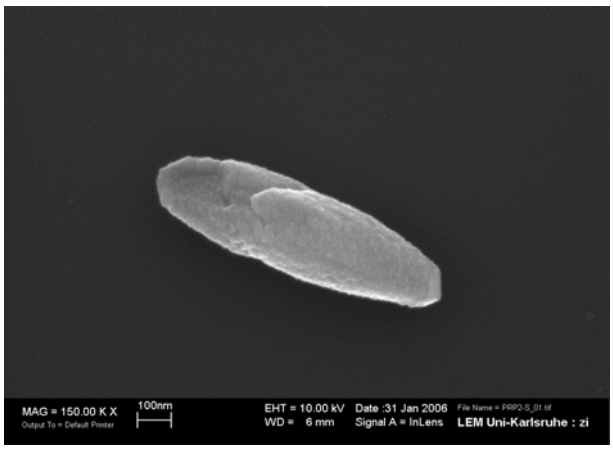

Figure 12.1. The SEM image (PRP)

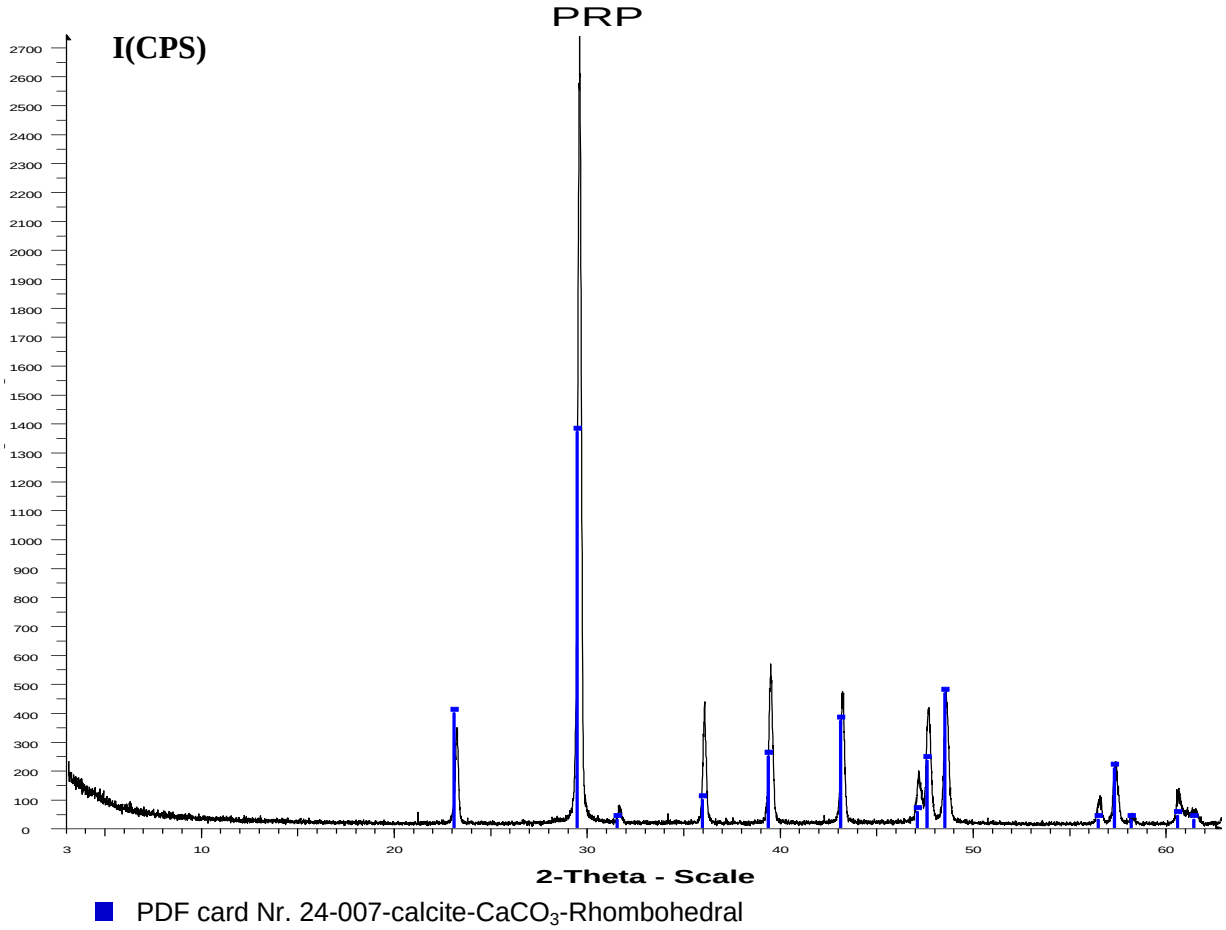

Figure 12.1. The diffractogram (PRP)

Table-12.1. The peak list (PRP)

Angle 2-Theta °	d value Angstrom	Intensity Count	Intensity %	$FWHM_{obs}$
23.063	3.85325	89	11.3	0.240
29.459	3.02959	791	100	0.219
31.537	2.8346	27	3.4	0.284
35.973	2.49452	143	18.1	0.261
39.412	2.28444	194	24.5	0.262
43.166	2.09407	231	29.2	0.265
47.157	1.92572	131	16.6	0.270
47.651	1.90689	284	35.9	0.280
48.572	1.87289	308	38.9	0.312
56.553	1.62604	80	10.1	0.279
57.411	1.60376	194	24.5	0.311
58.273	1.58208	29	3.7	0.257
60.68	1.52494	105	13.3	0.248
61.531	1.50588	58	7.3	0.256

Table-12.2. Concentration, crystallite size, strain and crystal size (PRP)

Method	Characteristic	Calcite	Aragonite
Rietveld method (XRD)	Concentration%	100±1.1	-
Rietveld method (XRD)	Crystallite size $<L>_{vol}$ (nm)	120	-
Williamson-Hall (XRD)	Crystallite size <L>vol (nm)	118 ±8.4	-
Williamson-Hall (XRD)	Strain value	0.043±0.007	-
(SEM)	Crystal size (nm)	265±58	-

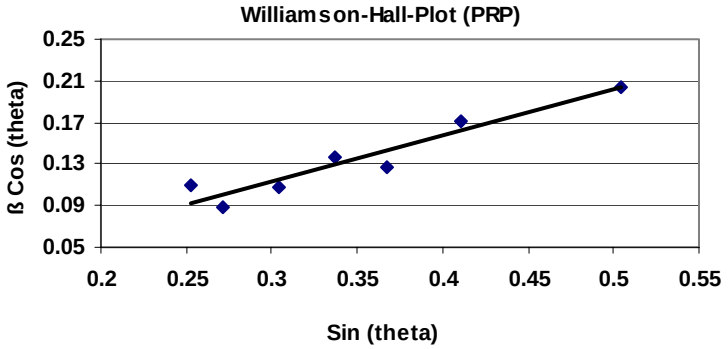

Figure 12-2. The Williamson-Hall plot (PRP)
(Y=0.0432X+0.0131, R^2=0.9116)

Table- 12.3. Morphology description based on intensity ratio data (PRP)

Method	Characteristic	Calcite	Aragonite
Intensity Ratio peak area (XRD)	Morphology Description	I(104)/I(116) 5.70±0.19	-
Intensity Ratio peak area (XRD)	Morphology Description	I(104)/I(012) 7.70±0.33	-
Intensity Ratio peak area (XRD)	Morphology Description	I(104)/I(202) 5.65±0.19	-
Intensity Ratio peak area (XRD)	Morphology Description	I(104)/I(113) 5.06±0.04	-
Intensity Ratio peak area (XRD)	Morphology Description	I(104)/I(018) 6.51±0.17	-
Intensity Ratio peak area (XRD)	Morphology Description	I(104)/I(122) 12.50±0.23	-
Intensity Ratio peak area (XRD)	Morphology Description	I(104)/I(116) 5.70±0.19	-
Intensity Ratio peak area (XRD)	Morphology Description	I(104)/I(012) 7.70±0.33	-
Intensity Ratio peak area (XRD)	Morphology Description	I(104)/I(202) 5.65±0.19	-
Intensity Ratio peak area (XRD)	Morphology Description	I(104)/I(113) 5.06±0.04	-
Intensity Ratio peak area (XRD)	Morphology Description	I(104)/I(018) 6.51±0.17	-
Intensity Ratio peak area (XRD)	Morphology Description	I(104)/I(122) 12.50±0.23	-

Sample Name	GCC-Carbilux
Abbreviation	GCCX

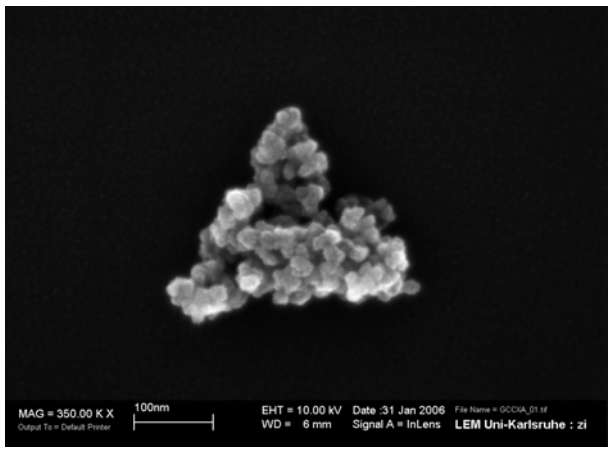

Figure 13.1. The SEM image (GCCX)

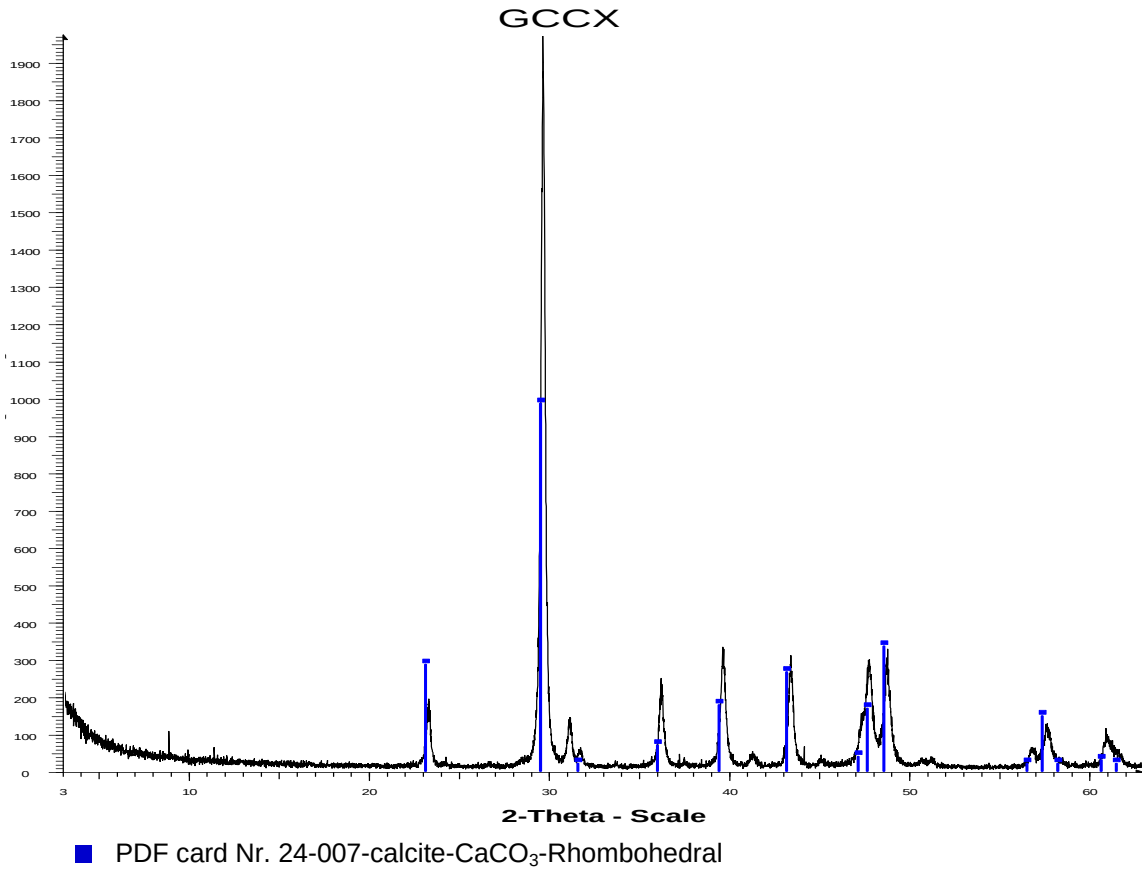

Figure 13.2. The diffractogram (GCCX)

Table-13.1. The peak list (GCCX)

Angle 2-Theta °	d value Angstrom	Intensity Count	Intensity % %	$FWHM_{obs}$
23.063	3.85325	68	9.1	0.374
29.459	3.02959	746	100	0.560
35.973	2.49452	55	7.4	0.443
39.412	2.28444	97	13	0.435
43.166	2.09407	67	9	0.436
47.157	1.92572	59	7.9	0.630
47.651	1.90689	221	29.6	0.630
48.572	1.87289	155	20.8	0.458
56.553	1.62604	30	4	0.422
57.411	1.60376	47	6.3	0.397
58.273	1.58208	27	3.6	0.155

Table-13.2. Concentration, crystallite size, strain and crystal size (GCCX)

Method	Characteristic	Calcite	Aragonite
Rietveld method (XRD)	Concentration%	100±1.1	-
Rietveld method (XRD)	Crystallite size$<L>_{vol}$ nm	21	-
Williamson-Hall (XRD)	Crystallite size $<L>_{vol}$ (nm)	11.2±2.3	-
Williamson-Hall (XRD)	Strain value	0.347±0.041	-
(SEM)	Crystal size (nm)	28±11	-

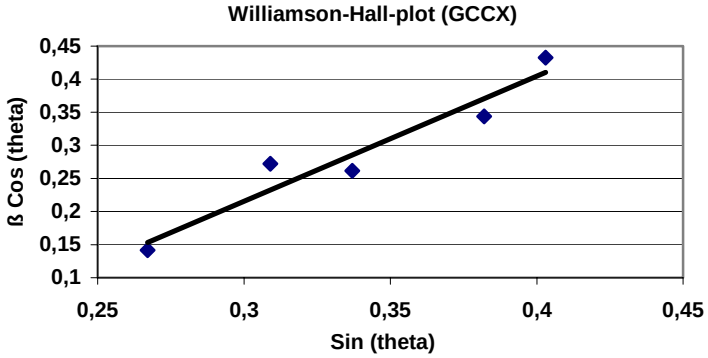

Figure 13.3. The Williamson-Hall plot (GCCX) (Y=0.347X – 0.137, R^2=0.92)

Table-13.3. Morphology description based on intensity ratio data (GCCX)

Method	Characteristic	Calcite	Aragonite
Intensity Ratio peak area (XRD)	Morphology Description	I(104)/I(116) 5.9±0.1	-
Intensity Ratio peak area (XRD)	Morphology Description	I(104)/I(012) 10.3±0.2	-
Intensity Ratio peak area (XRD)	Morphology Description	I(104)/I(202) 6.7±0.3	-
Intensity Ratio peak area (XRD)	Morphology Description	I(104)/I(113) 6.8±0.1	-
Intensity Ratio peak area (XRD)	Morphology Description	I(104)/I(018) 11.8±0.2	-
Intensity Ratio peak area (XRD)	Morphology Description	I(104)/I(122) 15.3±0.2	-
Intensity Ratio peak height (XRD)	Morphology Description	I(104)/I(116) 6.50±0.30	-
Intensity Ratio peak height (XRD)	Morphology Description	I(104)/I(012) 10.40±0.50	-
Intensity Ratio peak height (XRD)	Morphology Description	I(104)/I(202) 6.70±0.20	-
Intensity Ratio peak height (XRD)	Morphology Description	I(104)/I(113) 6.60±0.20	-
Intensity Ratio peak height (XRD)	Morphology Description	I(104)/I(018) 11.10±0.30	-
Intensity Ratio peak height (XRD)	Morphology Description	I(104)/I(122) 15.50±0.60	-

Sample Name	GCC-Hydrocarb 90
Abbreviation	GCC90

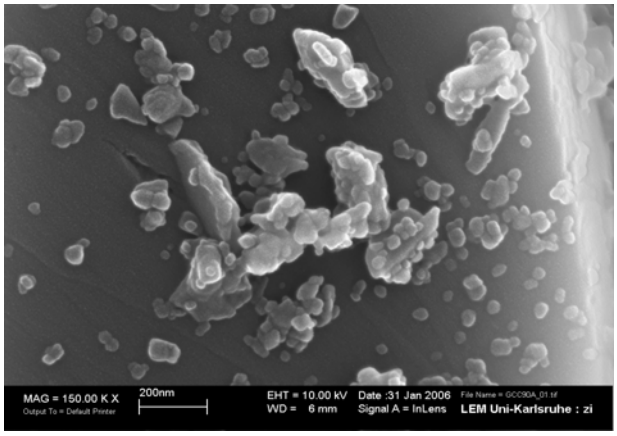

Figure 14.1. The SEM image (GCC90)

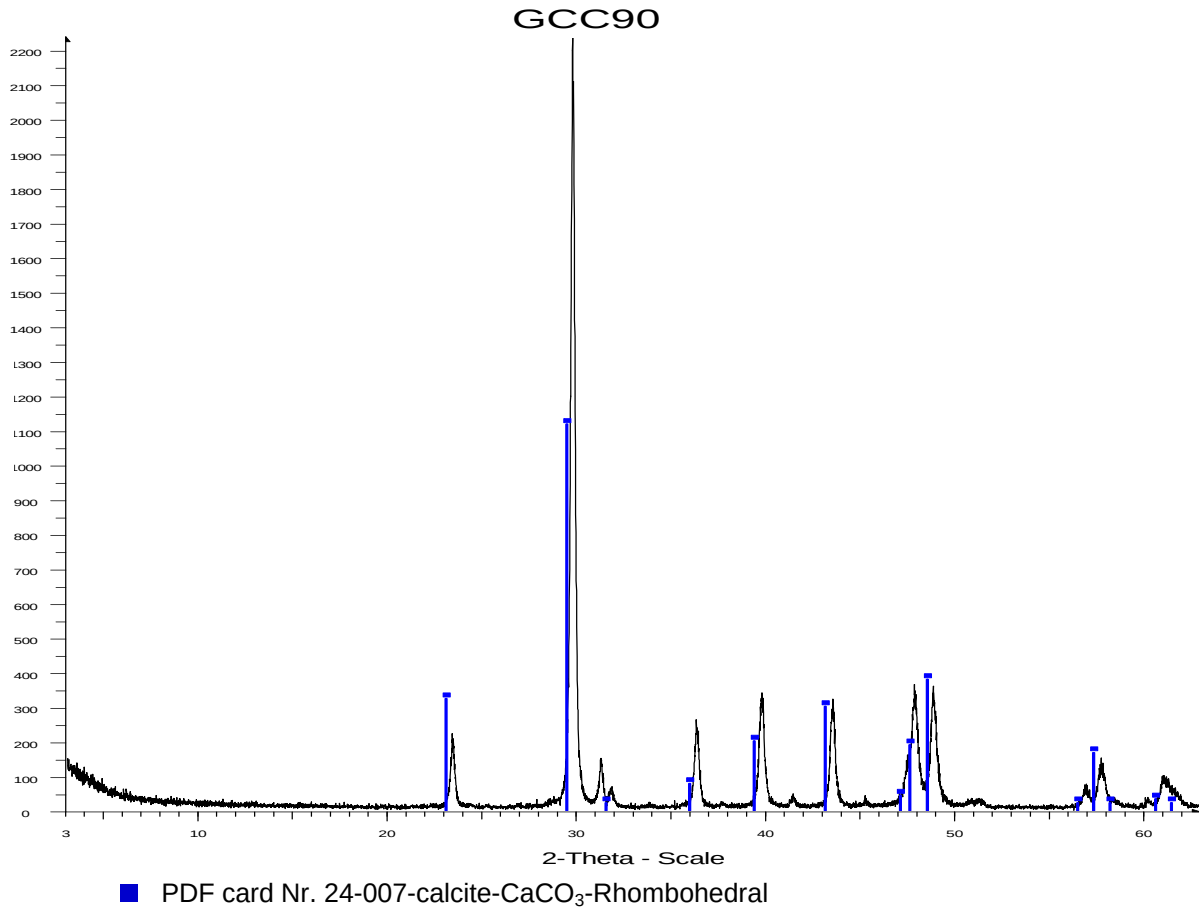

Figure 14.2. The diffractogram (GCC90)

Table -14.1. The peak list (GCC90)

Angle 2-Theta °	d value Angstrom	Intensity Count	Intensity %	$FWHM_{obs}$
23.063	3.85325	68	9.1	0.311
29.459	3.02959	746	100	0.395
35.973	2.49452	55	7.4	0.443
39.412	2.28444	97	13	0.371
43.166	2.09407	67	9	0.386
47.157	1.92572	59	7.9	0.476
48.572	1.87289	155	20.8	0.458
56.553	1.62604	30	4	0.422
57.411	1.60376	47	6.3	0.397
58.273	1.58208	27	3.6	0.155
60.68	1.52494	36	4.8	0.716

Table-14.2. Concentration, crystallite size, strain and crystal size (GCC90)

Method	Characteristic	Calcite	Aragonite
Rietveld method (XRD)	Concentration%	100±1.1	-
Rietveld method (XRD)	Crystallite size $<L>_{vol}$ (nm)	26	-
Williamson-Hall (XRD)	Crystallite size $<L>_{vol}$ (nm)	20.2±3.7	-
Williamson-Hall (XRD)	Strain value	0.388±0.074	-
(SEM)	Crystal size (nm)	30±14	-

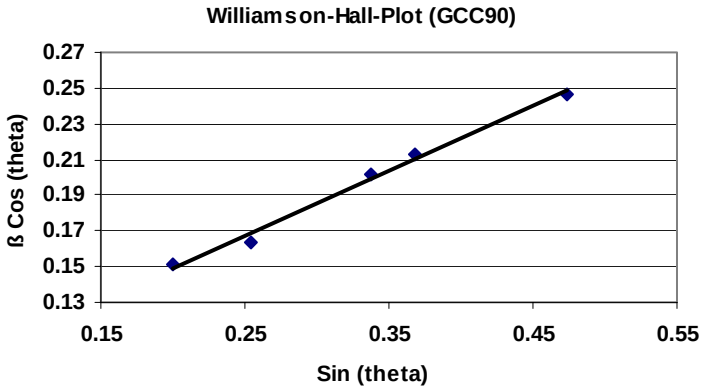

Figure 14.3. The Williamson-Hall plot (GCC90)

Table-14.3. Morphology description based on intensity ratio data (GCC90)

Method	Characteristic	Calcite	Aragonite
Intensity Ratio peak area (XRD)	Morphology Description	I(104)/I(116) 6.1±0.6	-
Intensity Ratio peak area (XRD)	Morphology Description	I(104)/I(012) 11.3±0.2	-
Intensity Ratio peak area (XRD)	Morphology Description	I(104)/I(202) 5.6±0.4	-
Intensity Ratio peak area (XRD)	Morphology Description	I(104)/I(113) 4.8±0.5	-
Intensity Ratio peak area (XRD)	Morphology Description	I(104)/I(018) 15.4±0.7	-
Intensity Ratio peak area (XRD)	Morphology Description	I(104)/I(122) 16.5±0.3	-
Intensity Ratio peak height (XRD)	Morphology Description	I(104)/I(116) 6.7±0.4	-
Intensity Ratio peak height (XRD)	Morphology Description	I(104)/I(012) 11.5±0.5	-
Intensity Ratio peak height (XRD)	Morphology Description	I(104)/I(202) 5.5±0.2	-
Intensity Ratio peak height (XRD)	Morphology Description	I(104)/I(113) 4.8±0.3	-
Intensity Ratio peak height (XRD)	Morphology Description	I(104)/I(018) 14.8±0.4	-
Intensity Ratio peak height (XRD)	Morphology Description	I(104)/I(122) 16.3±0.7	-

Sample Name PCC-F-R120 Abbreviation PRF120

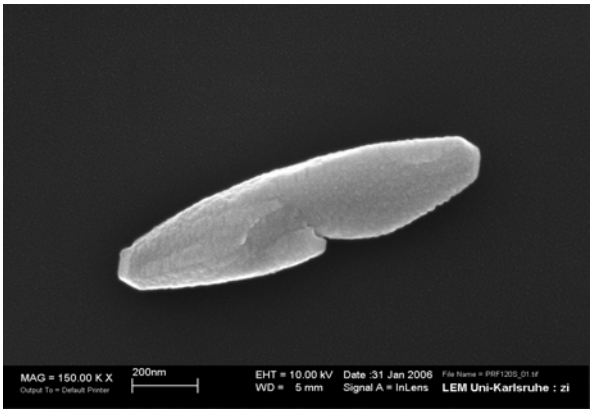

Figure 15.1. The SEM image (PRF120)

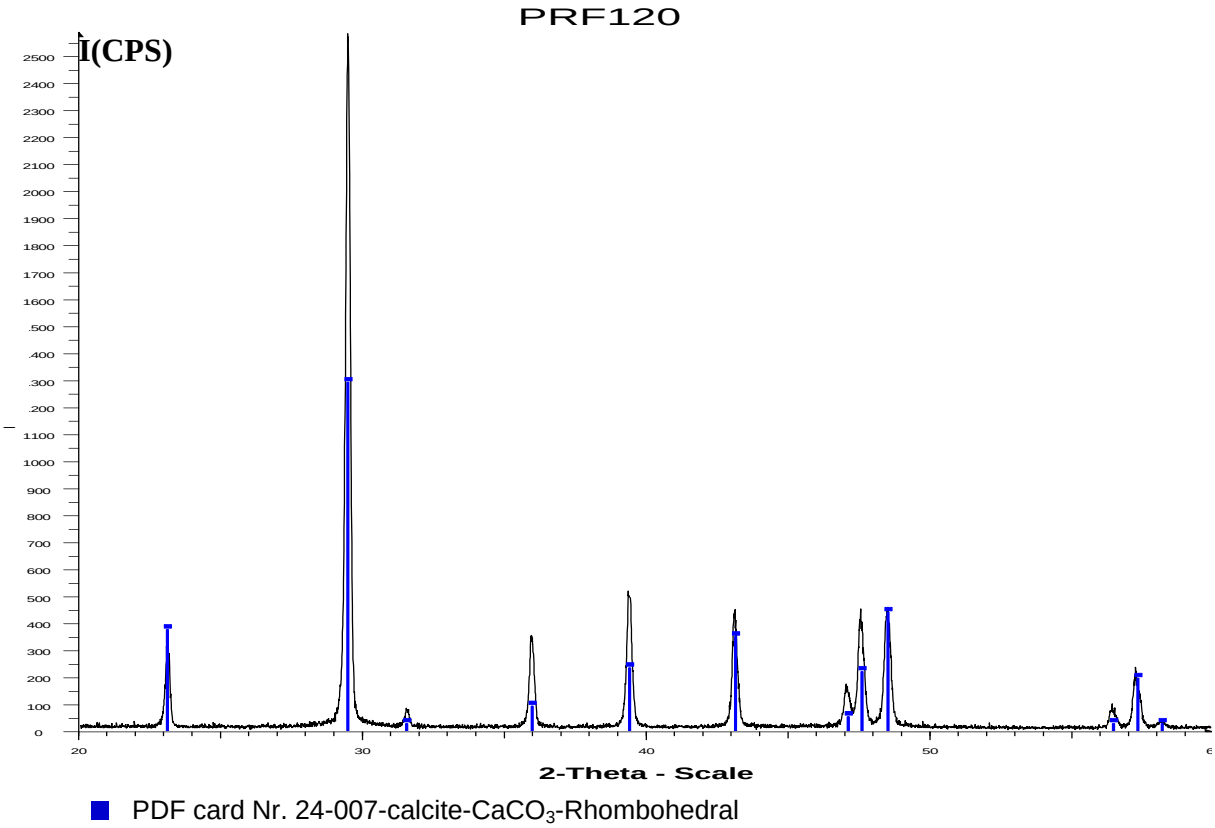

Figure 15.1. The diffractogram (PRF120)

Table-15.1. The peak list (PRF120)

Angle 2-Theta °	d value Angstrom	Intensity Count	Intensity %	$FWHM_{obs}$
23.063	3.85325	267	10.3	0.227
29.459	3.02959	2589	100	0.198
31.537	2.8346	78	3	0.203
35.973	2.49452	349	13.5	0.247
39.412	2.28444	503	19.4	0.245
43.166	2.09407	380	14.7	0.334
47.157	1.92572	141	5.4	0.319
48.572	1.87289	457	17.7	0.304
56.553	1.62604	75	2.9	0.318
57.411	1.60376	180	7	0.289
58.273	1.58208	36	1.4	0.288

Table-15.2. Concentration, crystallite size, strain and crystal size (PRF120)

Method	Characteristic	Calcite	Aragonite
Rietveld method (XRD)	Concentration%	100±1.1	-
Rietveld method (XRD)	Crystallite size $<L>_{vol}$ (nm)	175	-
Williamson-Hall (XRD)	Crystallite size $<L>_{vol}$ (nm)	177.2±9.9	-
Williamson-Hall (XRD)	Strain value	0.088±0.011	-
Williamson-Hall (XRD)	Crystal size (nm)	290±34	-

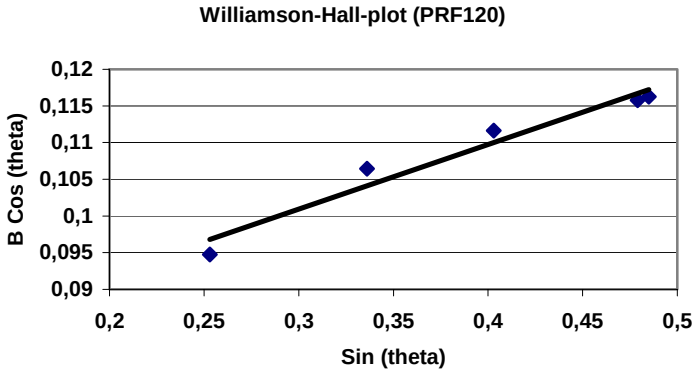

Figure 15.3. The Williamson-hall plot (PRF120)
(Y=0.088X + 0.0087, R2=0.9552)

Table-15.3. Morphology description based on intensity ratio data (PRF120)

Method	Characteristic	Calcite	Aragonite
Intensity Ratio peak area (XRD)	Morphology Description	I(104)/I(116) 5.59±0.32	-
Intensity Ratio peak area (XRD)	Morphology Description	I(104)/I(012) 7.80±0.07	-
Intensity Ratio peak area (XRD)	Morphology Description	I(104)/I(202) 5.60±0.26	-
Intensity Ratio peak area (XRD)	Morphology Description	I(104)/I(113) 4.82±0.32	-
Intensity Ratio peak area (XRD)	Morphology Description	I(104)/I(018) 5.66±0.26	-
Intensity Ratio peak area (XRD)	Morphology Description	I(104)/I(122) 10.40±0.08	-
Intensity Ratio peak height (XRD)	Morphology Description	I(104)/I(116) 5.67±0.14	-
Intensity Ratio peak height (XRD)	Morphology Description	I(104)/I(012) 7.56±0.12	-
Intensity Ratio peak height (XRD)	Morphology Description	I(104)/I(202) 5.58±0.18	-
Intensity Ratio peak height (XRD)	Morphology Description	I(104)/I(113) 4.89±0.25	-
Intensity Ratio peak height (XRD)	Morphology Description	I(104)/I(018) 5.72±0.26	-
Intensity Ratio peak height (XRD)	Morphology Description	I(104)/I(122) 10.61±0.28	-

Sample Name PCC-S-PCC Abbreviation PS

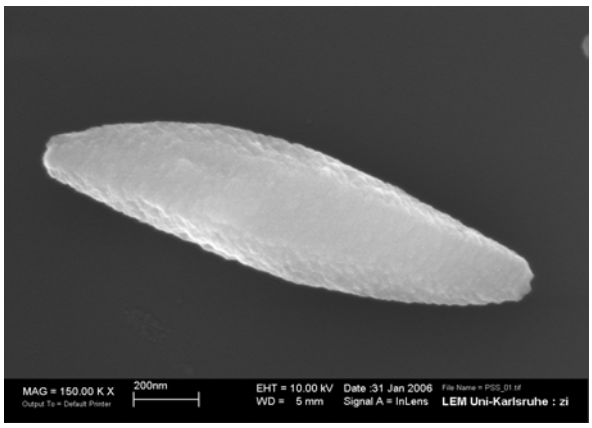

Figure 16.1. The SEM image (PS)

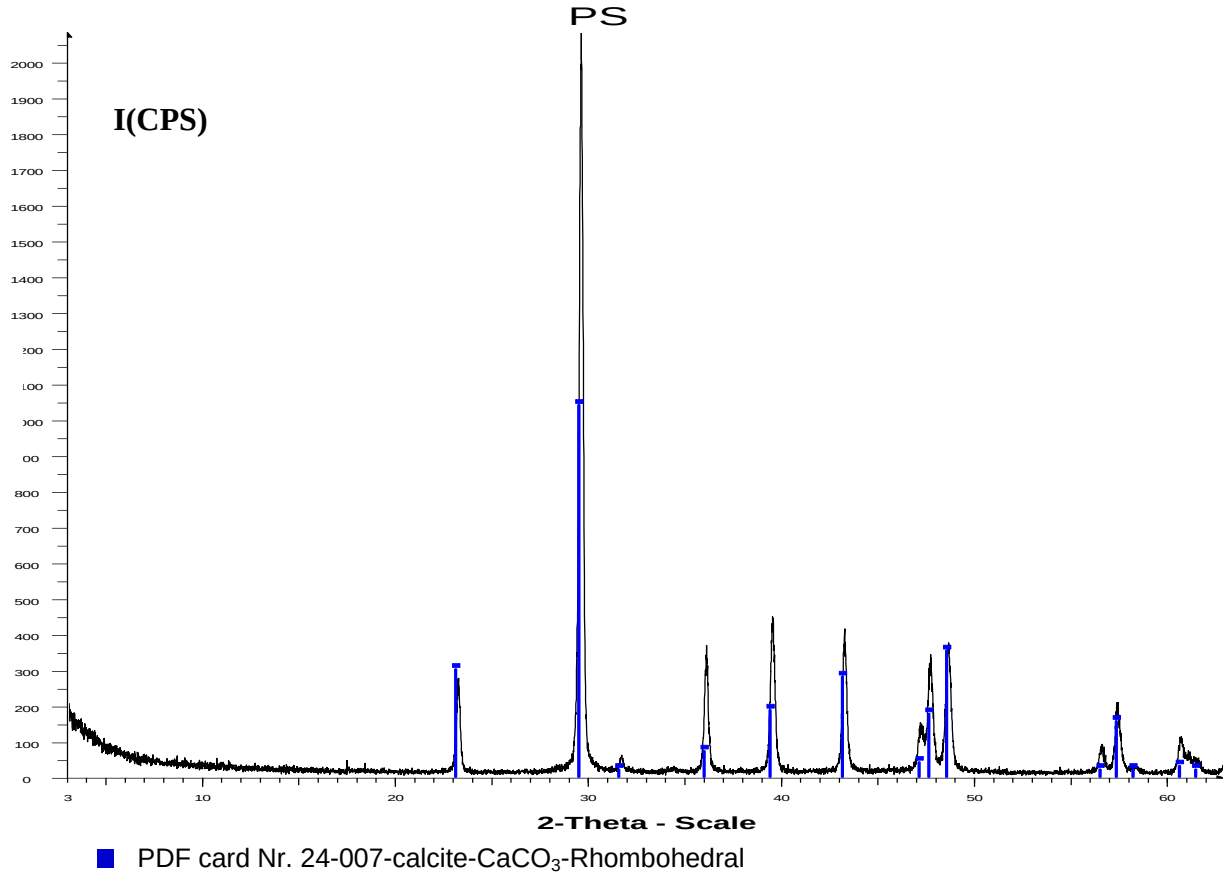

Figure 16.2. The diffractogram (PS)

Table-16.1. The peak list (PS)

Angle 2-Theta °	d value Angstrom	Intensity Count	Intensity %	$FWHM_{obs}$
23.063	3.85325	94	12.7	0.267
29.459	3.02959	740	100	0.283
31.537	2.8346	33	4.5	0.248
35.973	2.49452	132	17.8	0.290
39.412	2.28444	176	23.8	0.234
43.166	2.09407	242	32.7	0.337
47.157	1.92572	110	14.9	0.289
48.572	1.87289	275	37.2	0.325
56.553	1.62604	60	8.1	0.335
57.411	1.60376	183	24.7	0.320
58.273	1.58208	21	2.8	0.257
60.68	1.52494	88	11.9	0.429
61.531	1.50588	42	5.7	0.184

Table-16.2. Concentration, crystallite size, strain and crystal size (PS)

Method	Characteristic	Calcite	Aragonite
Rietveld method (XRD)	Concentration%	100±1.1	-
Rietveld method (XRD)	Crystallite size $<L>_{vol}$ (nm)	60	-
Williamson-Hall (XRD)	Crystallite size $<L>_{vol}$ (nm)	58.3±5.6	-
Williamson-Hall (XRD)	Strain value	0.212±0.033	-
(SEM)	Crystal size (nm)	340±42	-

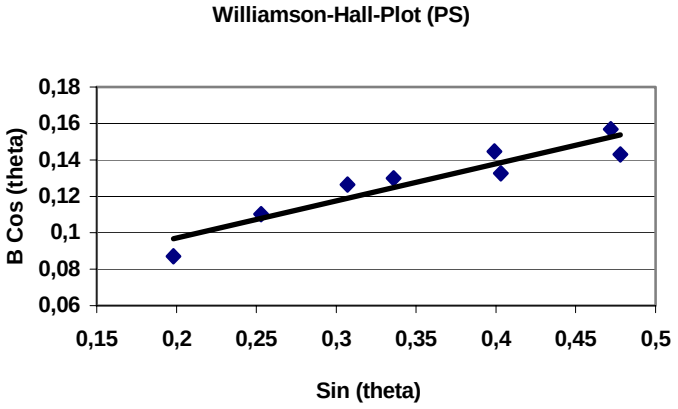

Figure 16.2. The Williamson-Hall plot (PS)
(Y= 0.212X+ 0.026, R^2=0.881)

Table- 16.3.Morphology description based on intensity ratio data (PS)

Method	Characteristic	Calcite	Aragonite
Intensity Ratio peak area (XRD)	Morphology Description	I(104)/I(116) 5.60±0.37	-
Intensity Ratio peak area (XRD)	Morphology Description	I(104)/I(012) 7.66±0.15	-
Intensity Ratio peak area (XRD)	Morphology Description	I(104)/I(202) 5.63±0.43	-
Intensity Ratio peak area (XRD)	Morphology Description	I(104)/I(113) 4.98±0.09	-
Intensity Ratio peak area (XRD)	Morphology Description	I(104)/I(018) 6.48±0.29	-
Intensity Ratio peak area (XRD)	Morphology Description	I(104)/I(122) 12.87±1.40	-
Intensity Ratio peak height (XRD)	Morphology Description	I(104)/I(116) 5.68±0.18	-
Intensity Ratio peak height (XRD)	Morphology Description	I(104)/I(012) 7.74±0.47	-
Intensity Ratio peak height (XRD)	Morphology Description	I(104)/I(202) 5.74±0.49	-
Intensity Ratio peak height (XRD)	Morphology Description	I(104)/I(113) 4.90±0.25	-
Intensity Ratio peak height (XRD)	Morphology Description	I(104)/I(018) 6.32±0.39	-
Intensity Ratio peak height (XRD)	Morphology Description	I(104)/I(122) 12.80±1.49	-

Sample Name	PCC-Slurry Ulrabulk1
Abbreviation	PSU1

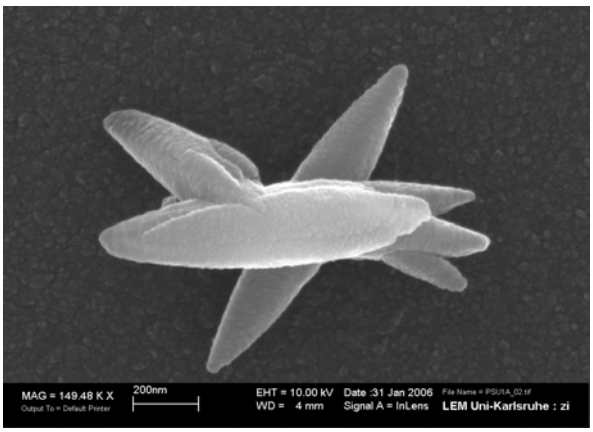

Figure 17.1. The SEM image (PSU1)

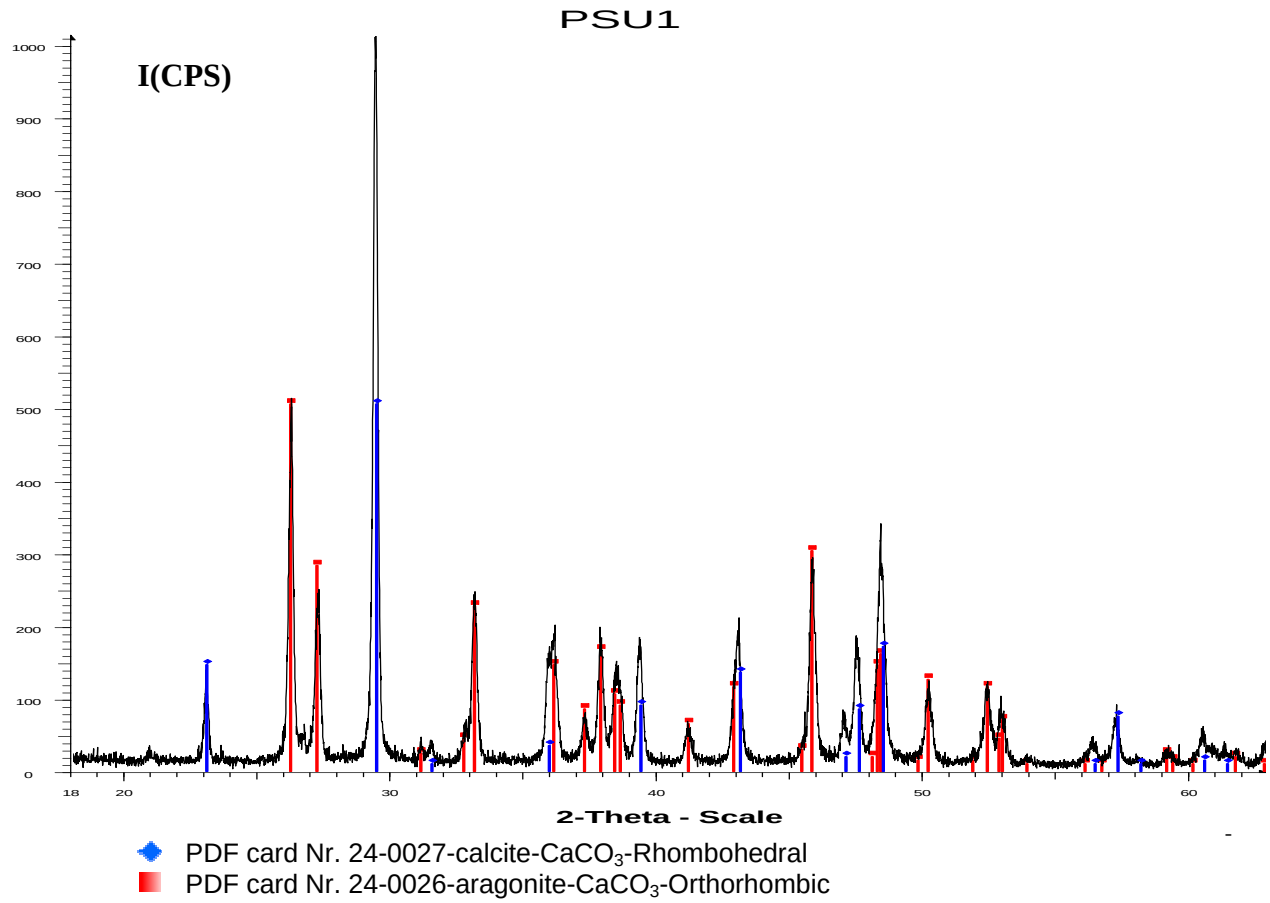

Figure 17.2. The diffractogram (PSU1)

Table- 17.1. The peak list (PSU1)

Angle 2-Theta °	d value Angstrom	Intensity Count	Intensity %	$FWHM_{obs}$
23.063	3.85325	132	13.8	0.281
26.218	3.39635	412	43.1	0.271
27.214	3.27418	225	23.5	0.283
29.459	3.02959	956	100	0.215
31.134	2.87036	33	3.5	0.174
33.152	2.70007	229	24	0.325
36.132	2.48393	172	18	0.481
37.29	2.40941	71	7.4	0.229
37.905	2.37174	178	18.6	0.238
38.429	2.34057	110	11.5	0.296
39.412	2.28444	154	16.1	0.283
41.203	2.1892	69	7.2	0.279
43.166	2.09407	146	15.3	0.412
45.867	1.97683	292	30.5	0.335
47.651	1.90689	132	13.8	0.292
48.336	1.88149	174	18.2	0.345
50.256	1.81399	99	10.4	0.356
51.928	1.75945	22	2.3	0.316
52.913	1.729	57	6	0.251
56.553	1.62604	37	3.9	0.333
56.798	1.61961	20	2.1	0.287

Table- 17.2. Concentration, crystallite size and strain (PSU1)

Method	Characteristic	Calcite	Aragonite
Rietveld method (XRD)	Concentration%	13.4±0.68	86.6±1.30
Rietveld method (XRD)	Crystallite size $<L>_{vol}$ (nm)	129	82
Williamson-Hall (XRD)	Crystallite size <L>vol (nm)	113.4±10.9	83.2±6.7
Williamson-Hall (XRD)	Strain value	0.312±0.033	0.316±0.02

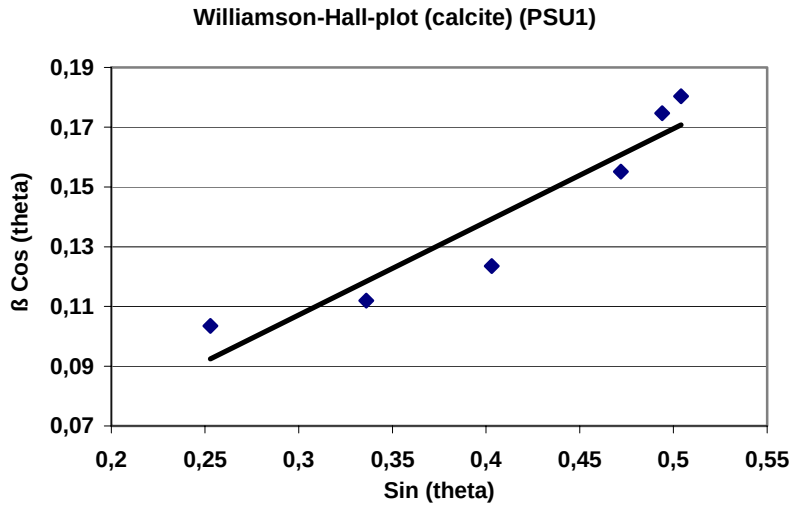

Figure 17.3. The Williamson-Hall plot (calcite) (PSU1)
(Y= 0.312X + 0.0316, R^2=0.8926)

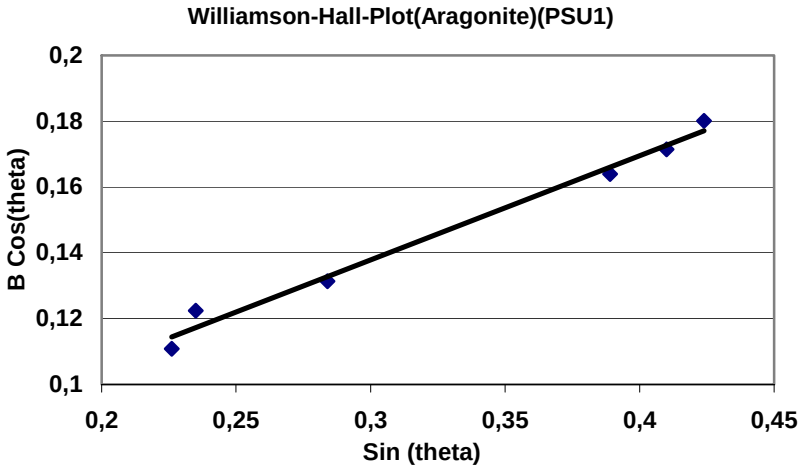

Figure 17.4. The Williamson-Hall plot (aragonite) (PSU1)
(Y= 0.316X + 0.0185, R^2=0.9864)

Table -17.3. Morphology description based on intensity ratio (PSU1)

Method	Characteristic	Calcite	Aragonite
Intensity Ratio peak area (XRD)	Morphology Description	I(104)/I(116) 3.19±0.04	I(040)/I(111) 0.72±0.03
Intensity Ratio peak area (XRD)	Morphology Description	I(104)/I(012) 7.75±0.11	I(040)/I(202) 1.313±0.048
Intensity Ratio peak area (XRD)	Morphology Description	I(104)/I(202) 5.48±0.13	I(040)/I(022) 1.92±0.08
Intensity Ratio peak area (XRD)	Morphology Description	I(104)/I(113) 5.81±0.39	I(040)/I(113) 1.41±0.08
Intensity Ratio peak area (XRD)	Morphology Description	I(104)/I(018) 6.49±0.23	I(040)/I(102) 1.69±0.04
Intensity Ratio peak area (XRD)	Morphology Description	I(104)/I(122) 14.60±0.27	-
Intensity Ratio peak height (XRD)	Morphology Description	I(104)/I(116) 3.34±0.26	I(040)/I(111) 0.55±0.02
Intensity Ratio peak height (XRD)	Morphology Description	I(104)/I(012) 8.25±0.41	I(040)/I(202) 1.13±0.05
Intensity Ratio peak height (XRD)	Morphology Description	I(104)/I(202) 5.74±0.48	I(040)/I(022) 2.03±0.06
Intensity Ratio peak height (XRD)	Morphology Description	I(104)/I(113) 5.33±0.36	I(040)/I(113) 1.13±0.04
Intensity Ratio peak height (XRD)	Morphology Description	I(104)/I(018) 6.47±0.19	I(040)/I(102) 1.56±0.11
Intensity Ratio peak height (XRD)	Morphology Description	I(104)/I(122) 14.68±0.29	-

Sample Name PCC-Slurry Ulrabulk2 Abbreviation PSU2

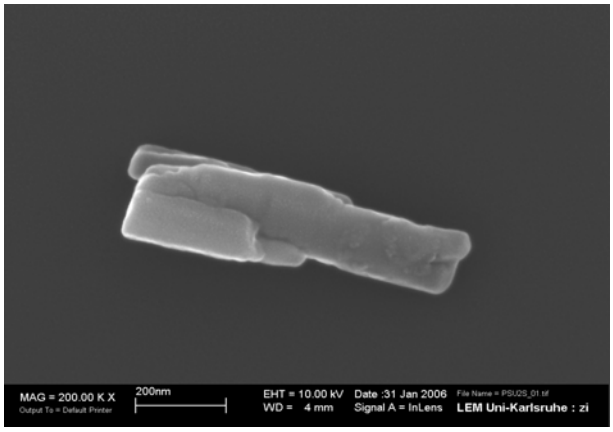

Figure 18.1. The SEM image (PSU2)

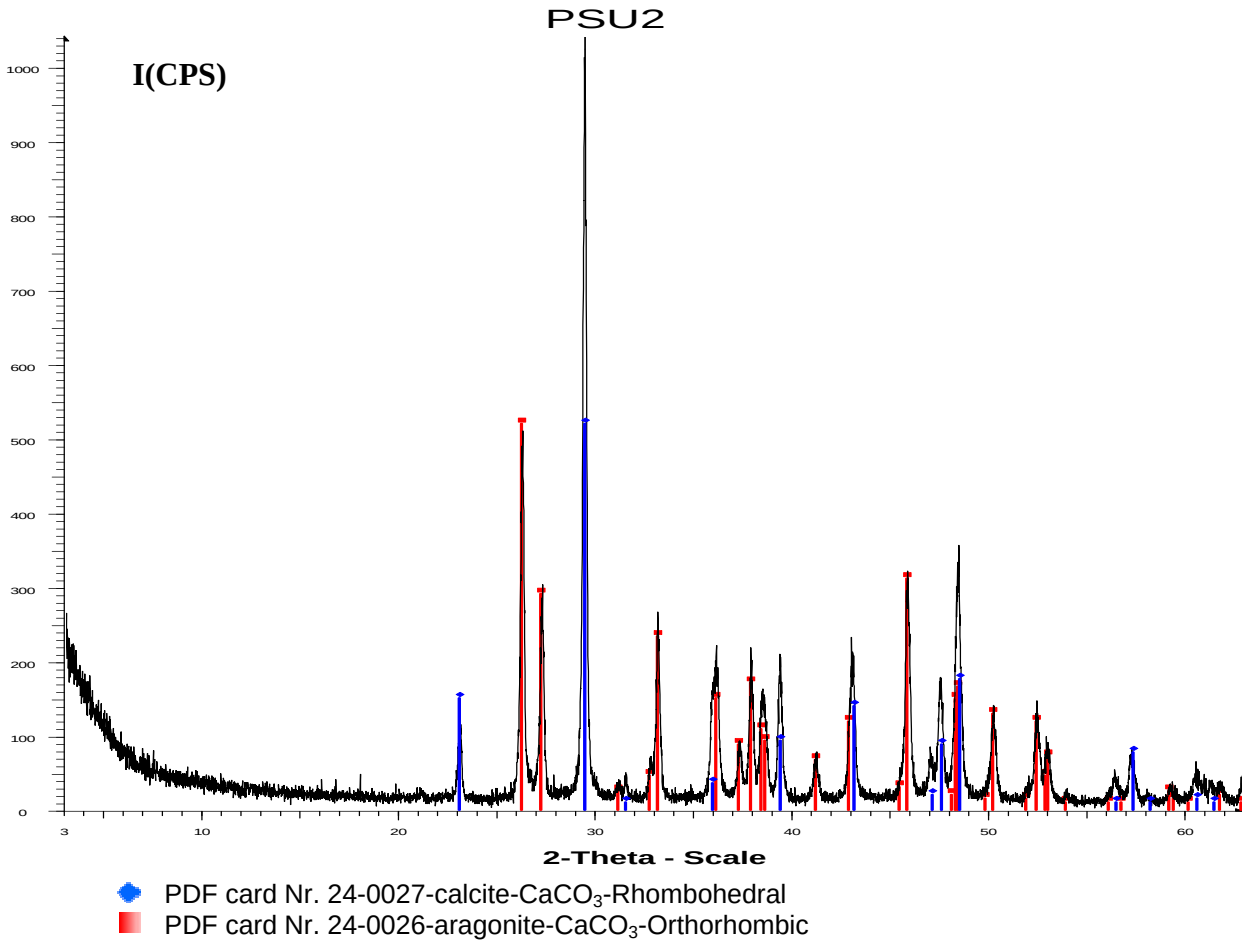

Figure 18.2. The diffractogram (PSU2)

Table- 18.1. The diffractogram (PSU2)

Angle 2-Theta °	d value Angstrom	Intensity Count	Intensity %	$FWHM_{obs}$
23.063	3.85325	108	10.6	0.254
26.218	3.39635	402	39.6	0.283
27.214	3.27418	219	21.6	0.253
29.459	3.02959	1015	100	0.224
31.134	2.87036	31	3.1	0.176
33.152	2.70007	188	18.5	0.326
35.973	2.49452	155	15.3	0.492
37.29	2.40941	60	5.9	0.248
37.905	2.37174	160	15.8	0.238
38.429	2.34057	117	11.5	0.378
39.299	2.2892	52	5.1	0.265
42.911	2.10591	106	5.1	0.356
45.867	1.97683	296	10.4	0.310
47.157	1.92572	68	29.2	0.291
48.572	1.87289	288	6.7	0.357
50.256	1.81399	114	28.4	0.412
52.48	1.74224	115	11.2	0.288
53.057	1.72463	88	11.3	0.236
56.162	1.63644	19	8.7	0.389
57.411	1.60376	65	1.9	0.242

Table- 18.2. Concentration, crystallite size and strain (PSU2)

Method	Characteristic	Calcite	Aragonite
Rietveld method (XRD)	Concentration%	20.0±0.91	80.0±1.40
Rietveld method (XRD)	Crystallite size $<L>_{vol}$ (nm)	113	79
Williamson-Hall (XRD)	Crystallite size $<L>_{vol}$ (nm)	110±9.6	76.1±5.3
Williamson-Hall (XRD)	Strain value	0.249±0.035	0.331±0.049

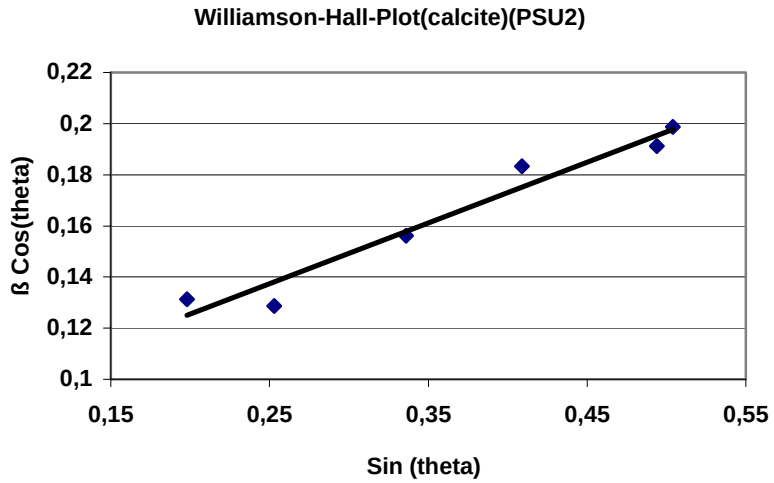

Figure 18.3. The Williamson-Hall plot (calcite)(PSU2)
(Y= 0.249X + 0.014,R^2 = 0.8933)

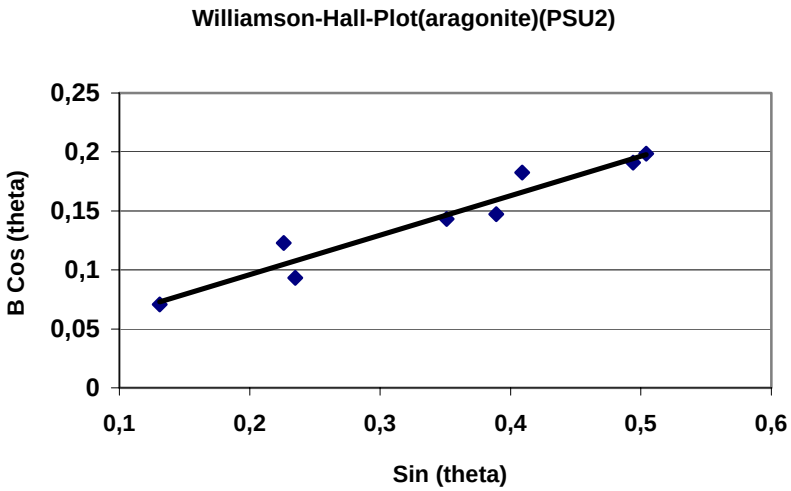

Figure 18-4. The Williamson-Hall plot (aragonite)(PSU2)
(Y= 0.331X + 0.020,R^2 = 0.8530)

Table-18.3. Morphology description based on intensity ratio (PSU2)

Method	Characteristic	Calcite	Aragonite
Intensity Ratio peak area (XRD)	Morphology Description	I(104)/I(116) 3.37±0.21	I(040)/I(111) 0.78±0.05
Intensity Ratio peak area (XRD)	Morphology Description	I(104)/I(012) 8.57±0.38	I(040)/I(202) 1.32±0.04
Intensity Ratio peak area (XRD)	Morphology Description	I(104)/I(202) 5.30±0.09	I(040)/I(022) 1.94±0.10
Intensity Ratio peak area (XRD)	Morphology Description	I(104)/I(113) 5.45±0.09	I(040)/I(113) 1.46±0.11
Intensity Ratio peak area (XRD)	Morphology Description	I(104)/I(018) 5.51±0.15	I(040)/I(102) 1.23±0.17
Intensity Ratio peak area (XRD)	Morphology Description	I(104)/I(122) 13.52±0.18	-
Intensity Ratio peak area (XRD)	Morphology Description	I(104)/I(116) 3.14±0.12	I(040)/I(111) 0.59±0.05
Intensity Ratio peak area (XRD)	Morphology Description	I(104)/I(012) 8.25±0.43	I(040)/I(202) 1.08±0.06
Intensity Ratio peak area (XRD)	Morphology Description	I(104)/I(202) 5.32±0.37	I(040)/I(022) 1.91±0.04
Intensity Ratio peak area (XRD)	Morphology Description	I(104)/I(113) 5.43±0.45	I(040)/I(113) 1.12±0.08
Intensity Ratio peak area (XRD)	Morphology Description	I(104)/I(018) 5.42±0.18	I(040)/I(102) 1.43±0.02
Intensity Ratio peak area (XRD)	Morphology Description	I(104)/I(122) 13.06±0.41	-

Sample Name PCC-Slurry Ulrabulk3 Abbreviation PSU3

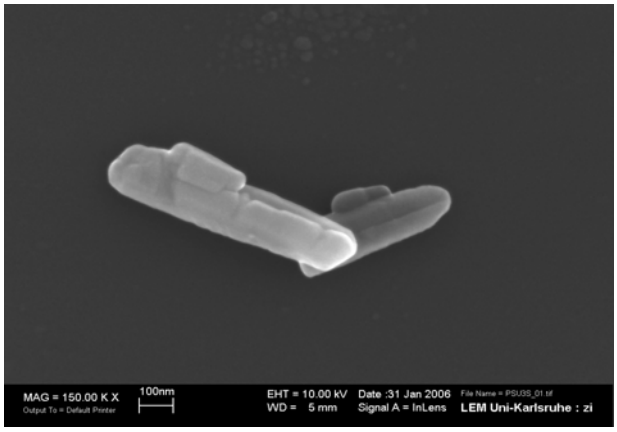

Figure 19.1. The SEM image (PSU3)

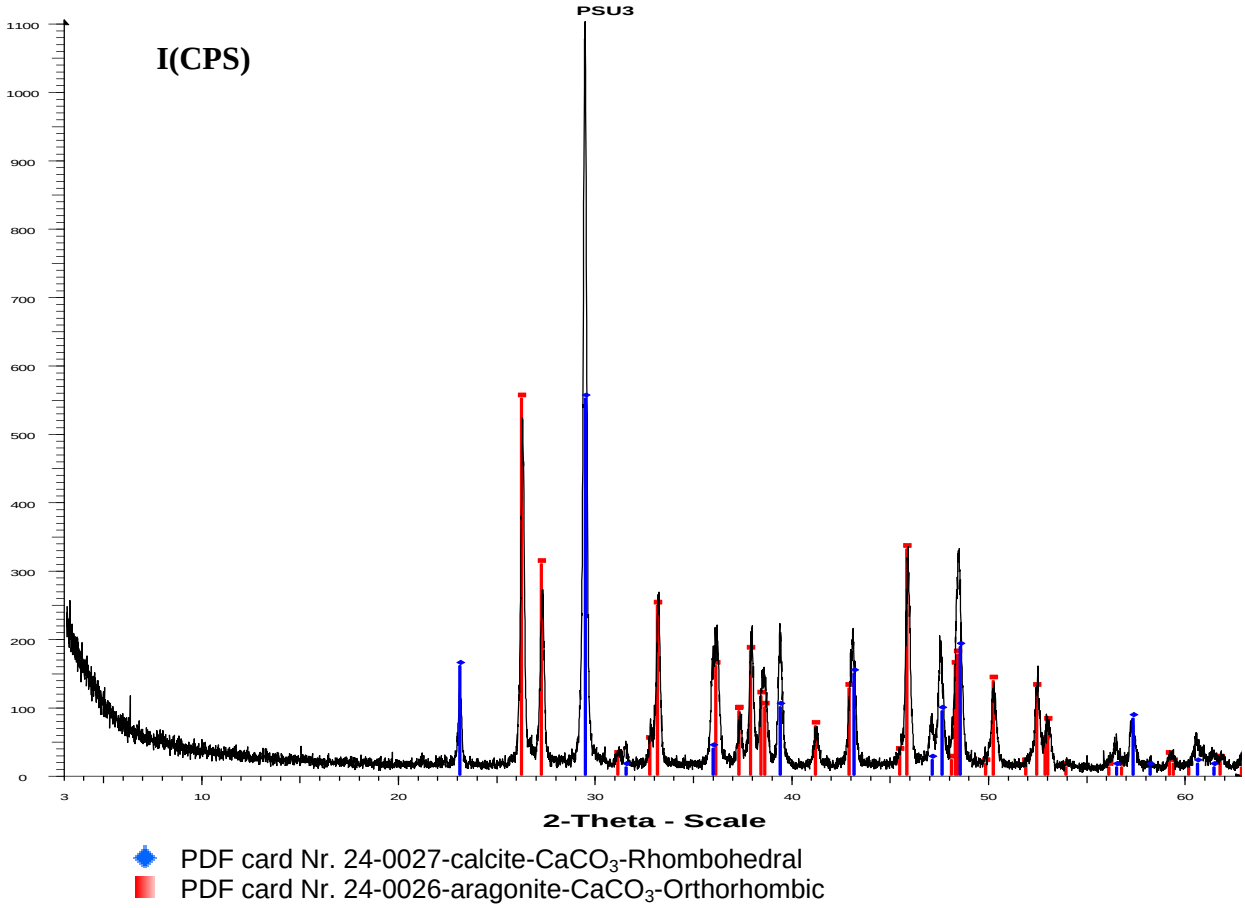

Figure 19.2. The diffractogram (PSU3)

Table- 19.1. The peak list (PSU3)

Angle 2-Theta °	d value Angstrom	Intensity Count	Intensity %	$FWHM_{obs}$
23.063	3.85325	129	11.9	0.224
26.218	3.39635	375	34.7	0.249
27.214	3.27418	200	18.5	0.253
29.459	3.02959	1081	100	0.206
31.134	2.87036	32	3	0.224
31.537	2.8346	38	3.5	0.192
32.748	2.73249	48	4.4	0.318
35.973	2.49452	164	15.2	0.478
37.29	2.40941	81	7.5	0.255
37.905	2.37174	164	15.2	0.234
38.429	2.34057	117	10.8	0.361
39.412	2.28444	164	15.2	0.248
41.203	2.1892	70	6.5	0.292
43.166	2.09407	187	17.3	0.384
45.867	1.97683	272	25.2	0.345
47.157	1.92572	90	8.3	0.268
48.147	1.88843	60	5.6	0.344
50.256	1.81399	117	10.8	0.369
51.928	1.75945	24	2.2	0.256
52.48	1.74224	119	11	0.311
53.975	1.69747	13	1.2	0.295
56.162	1.63644	28	2.6	0.393
56.798	1.61961	25	2.3	0.275

Table- 19.2. Concentration, crystallite size and strain (PSU3)

Method	Characteristic	Calcite	Aragonite
Rietveld method (XRD)	Concentration%	12.3±0.78	87.7±1.30
Rietveld method (XRD)	Crystallite size $<L>_{vol}$ (nm)	148	74
Williamson-Hall (XRD)	Crystallite size $<L>_{vol}$ (nm)	163.5±11.1	68.7±4.9
Williamson-Hall (XRD)	Strain value	0.427±0.085	0.397±0.047

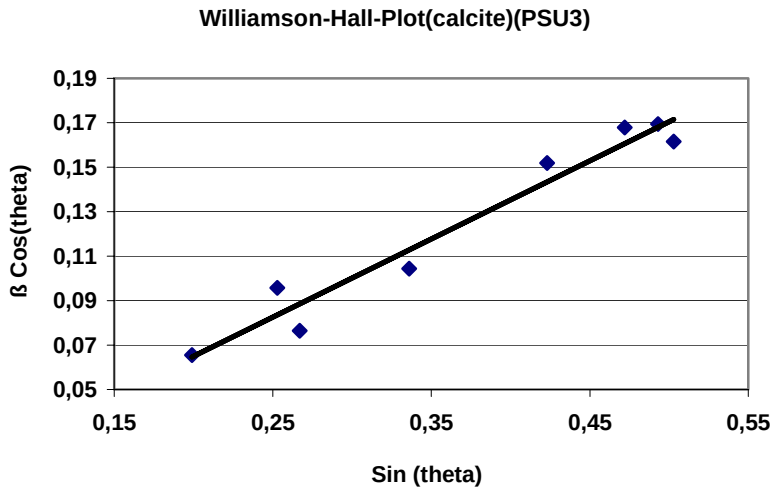

Figure 19.3. The Williamson-Hall plot (calcite)(PSU3)
(Y= 0.427X + 0.009,R^2 = 0.9084)

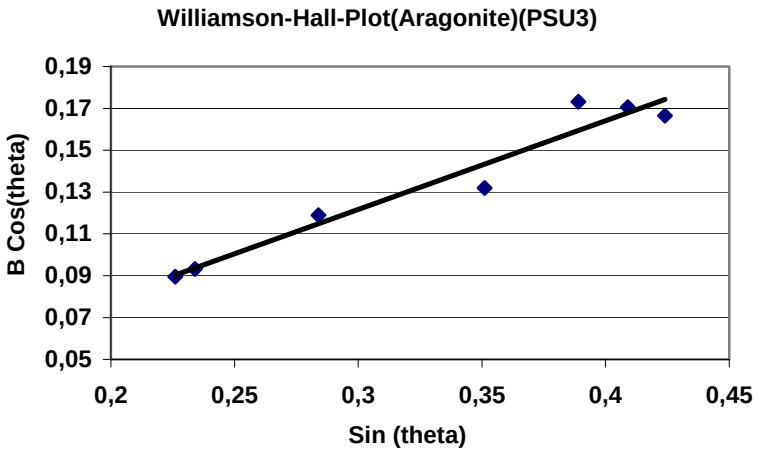

Figure 19.4. The Williamson-Hall plot (aragonite)(PSU3)
(Y= 0.397X + 0.0224,R^2 = 0.9084)

Table-19.3. Morphology description based on intensity ratio data (PSU3)

Method	Characteristic	Calcite	Aragonite
Intensity Ratio peak area (XRD)	Morphology Description	I(104)/I(116) 3.26±0.13	I(040)/I(111) 0.76±0.03
Intensity Ratio peak area (XRD)	Morphology Description	I(104)/I(012) 8.27±0.25	I(040)/I(202) 1.27±0.06
Intensity Ratio peak area (XRD)	Morphology Description	I(104)/I(202) 5.26±0.39	I(040)/I(022) 2.29±0.17
Intensity Ratio peak area (XRD)	Morphology Description	I(104)/I(113) 5.33±0.18	I(040)/I(113) 1.34±0.05
Intensity Ratio peak area (XRD)	Morphology Description	I(104)/I(018) 5.66±0.13	I(040)/I(102) 1.25±0.04
Intensity Ratio peak area (XRD)	Morphology Description	I(104)/I(122) 13.42±0.21	-
Intensity Ratio peak area (XRD)	Morphology Description	I(104)/I(116) 3.40±0.17	I(040)/I(111) 0.60±0.10
Intensity Ratio peak area (XRD)	Morphology Description	I(104)/I(012) 8.29±0.24	I(040)/I(202) 1.14±0.06
Intensity Ratio peak area (XRD)	Morphology Description	I(104)/I(202) 5.34±0.37	I(040)/I(022) 2.19±0.03
Intensity Ratio peak area (XRD)	Morphology Description	I(104)/I(113) 5.32±0.25	I(040)/I(113) 1.18±0.05
Intensity Ratio peak area (XRD)	Morphology Description	I(104)/I(018) 5.82±0.11	I(040)/I(102) 1.57±0.13
Intensity Ratio peak area (XRD)	Morphology Description	I(104)/I(122) 13.40±0.16	-

Sample Name PCC-Slurry Ulrabulk4 Abbreviation PSU4

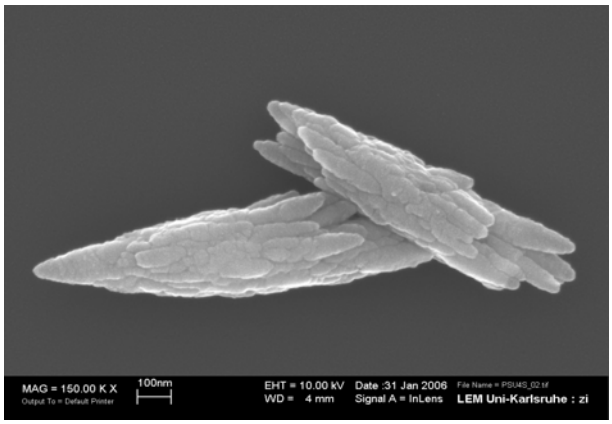

Figure 20.1. The SEM image (PSU4)

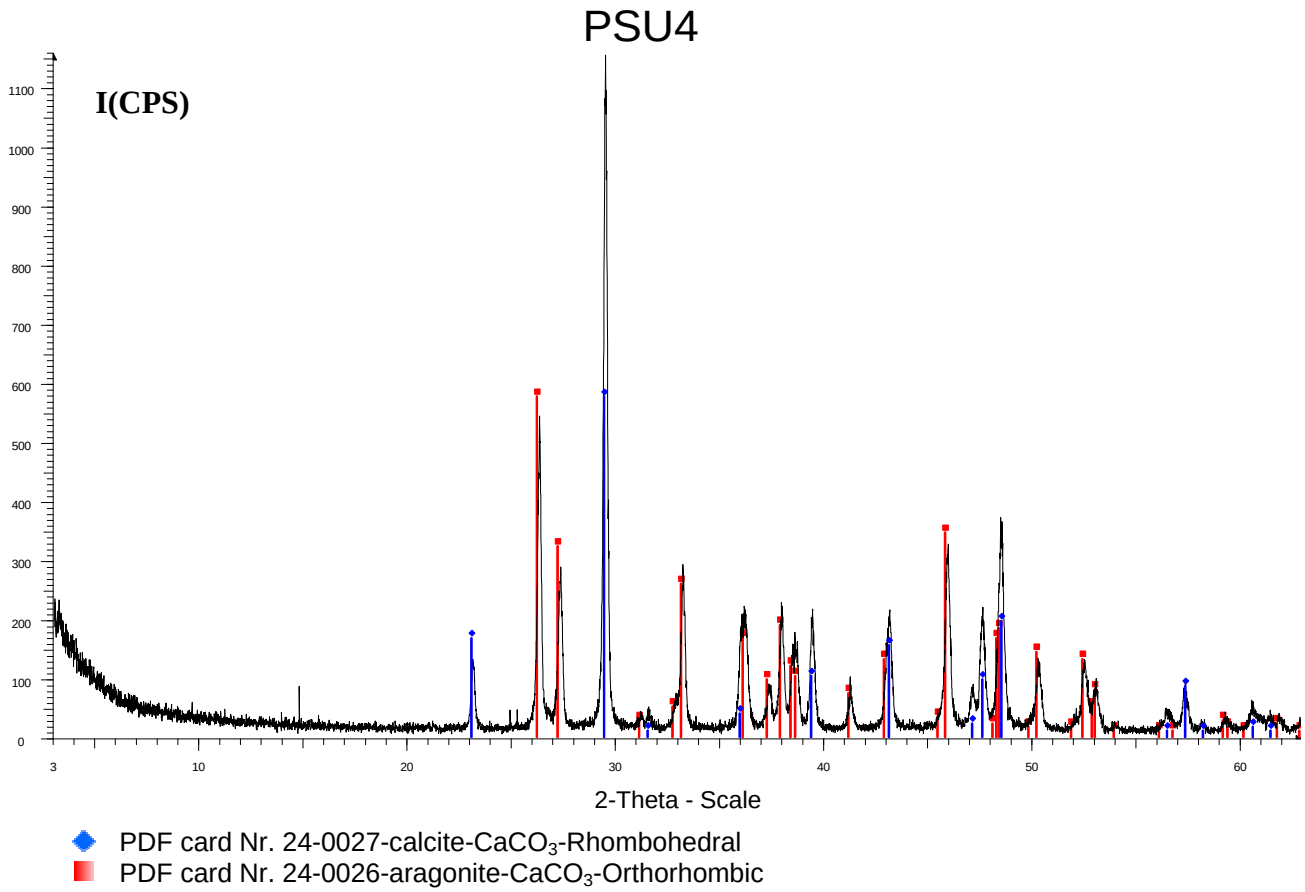

Figure 20-2. The diffractogram (PSU4)

Table- 20.1. The peak list (PSU4)

Angle 2-Theta °	d value Angstrom	Intensity Count	Intensity %	$FWHM_{obs}$
23.063	3.85325	129	11.9	0.268
26.218	3.39635	375	34.7	0.231
27.214	3.27418	200	18.5	0.245
29.459	3.02959	1081	100	0.226
31.134	2.87036	32	3	0.140
31.537	2.8346	38	3.5	0.234
32.748	2.70249	48	4.4	0.345
35.973	2.49452	164	15.2	0.481
37.29	2.40941	81	7.5	0.250
37.905	2.37174	164	15.2	0.238
38.429	2.34057	117	10.8	0.366
39.412	2.28444	164	15.2	0.276
41.203	2.1892	70	6.5	0.403
43.166	2.09407	187	17.3	0.381
45.867	1.97683	272	25.2	0.313
47.157	1.92572	90	8.3	0.287
48.147	1.88843	60	5.6	0.332
50.256	1.81399	117	10.8	0.356
51.928	1.75945	24	2.2	0.424
52.48	1.74224	119	11	0.325
53.975	1.69747	13	1.2	0.263
56.162	1.63644	28	2.6	0.368
56.798	1.61961	25	2.3	0.338

Table- 20.2. Concentration, crystallite size and strain (PSU4)

Method	Characteristic	Calcite	Aragonite
Rietveld method (XRD)	Concentration%	16.9±0.78	83.1±1.30
Rietveld method (XRD)	Crystallite size $<L>_{vol}$ (nm)	109	82
Williamson-Hall (XRD)	Crystallite size $<L>_{vol}$ (nm)	97.7±7.7	84.5±6.3
Williamson-Hall (XRD)	Strain value	0.343±0.045	0.590±0.120

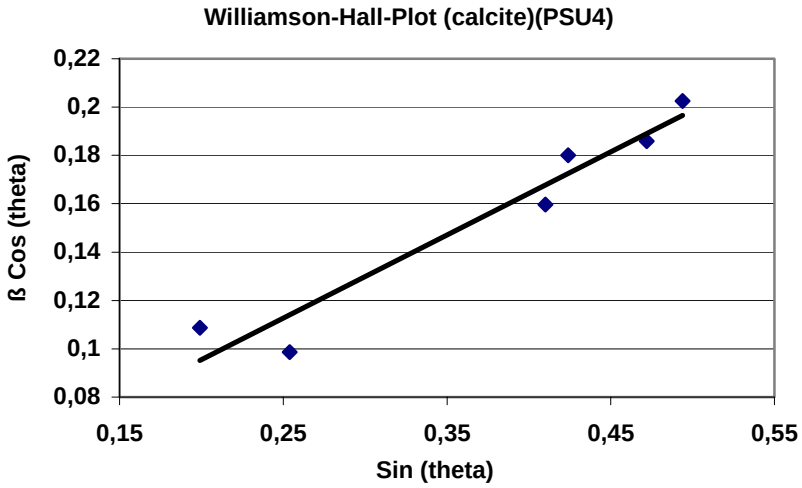

Figure 20.3. The Williamson-Hall plot (calcite)(PSU4)
(Y= 0.3435X + 0.016,R^2 = 0.9359)

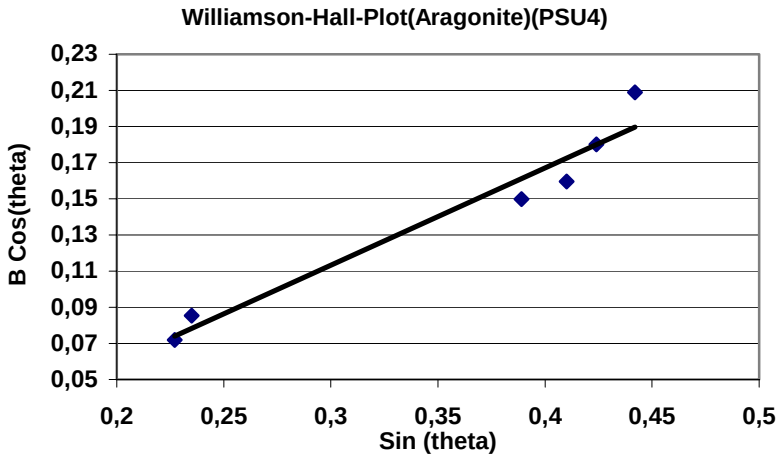

Figure 20.4. The Williamson-Hall plot (aragonite)(PSU4)
(Y= 0.590X + 0.018,R^2 = 0.8555)

Table- 20.3.Morphology description based on intensity ratio data (PSU4)

Method	Characteristic	Calcite	Aragonite
Intensity Ratio peak area (XRD)	Morphology Description	I(104)/I(116) 3.33±0.12	I(040)/I(111) 0.73±0.02
Intensity Ratio peak area (XRD)	Morphology Description	I(104)/I(012) 8.26±0.09	I(040)/I(202) 1.28±0.05
Intensity Ratio peak area (XRD)	Morphology Description	I(104)/I(202) 5.24±0.33	I(040)/I(022) 1.83±0.09
Intensity Ratio peak area (XRD)	Morphology Description	I(104)/I(113) 5.46±0.23	I(040)/I(113) 1.30±0.11
Intensity Ratio peak area (XRD)	Morphology Description	I(104)/I(018) 5.49±0.33	I(040)/I(102) 1.25±0.09
Intensity Ratio peak area (XRD)	Morphology Description	I(104)/I(122) 14.25±0.43	-
Intensity Ratio peak area (XRD)	Morphology Description	I(104)/I(116) 3.35±0.07	I(040)/I(111) 0.59±0.02
Intensity Ratio peak area (XRD)	Morphology Description	I(104)/I(012) 8.25±0.41	I(040)/I(202) 1.08±0.05
Intensity Ratio peak area (XRD)	Morphology Description	I(104)/I(202) 5.34±0.32	I(040)/I(022) 1.85±0.13
Intensity Ratio peak area (XRD)	Morphology Description	I(104)/I(113) 5.30±0.11	I(040)/I(113) 1.05±0.053
Intensity Ratio peak area (XRD)	Morphology Description	I(104)/I(018) 5.41±0.53	I(040)/I(102) 1.51±0.03
Intensity Ratio peak area (XRD)	Morphology Description	I(104)/I(122) 13.31±1.42	-

Sample Name PCC-CalciLS Abbreviation PCLS

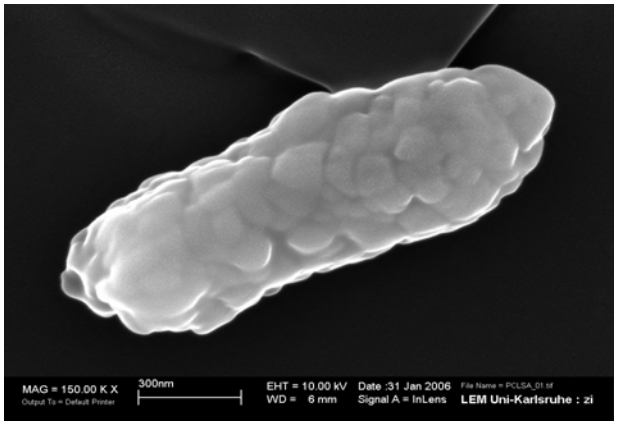

Figure 21.1. The SEM image (PCLS)

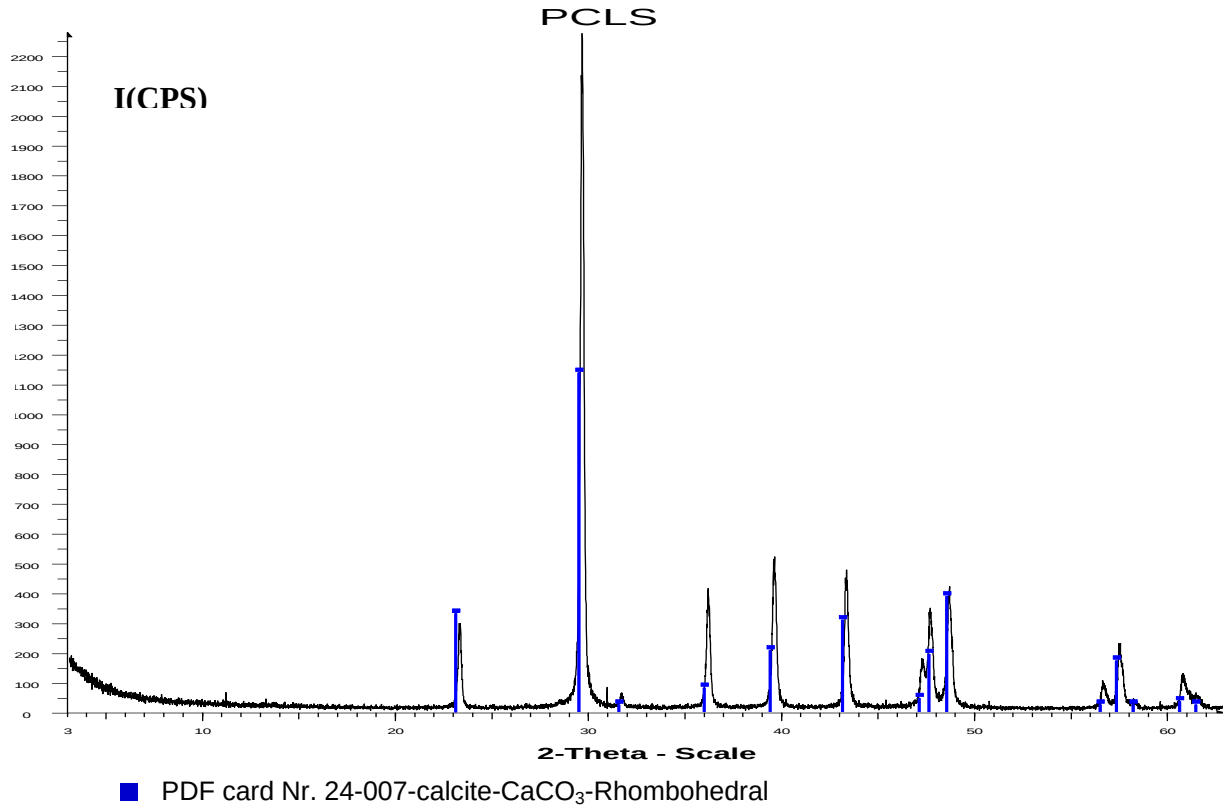

Figure 21.2. The diffractogram (PCLS)

Table- 21.1. The peak list (PCLS) ($FWHM_{Instrumental}$=0.157°)

Angle 2-Theta °	d value Angstrom	Intensity Count	Intensity %	$FWHM_{obs}$
23.063	3.85325	52	12.2	0.254
29.459	3.02959	427	100	0.236
31.537	2.8346	24	5.6	0.288
35.973	2.49452	55	12.9	0.293
39.412	2.28444	78	18.3	0.265
43.166	2.09407	80	18.7	0.345
47.157	1.92572	61	14.3	0.275
47.651	1.90689	223	52.2	0.294
48.572	1.87289	152	35.6	0.308
56.553	1.62604	29	6.8	0.346
57.411	1.60376	72	16.9	0.326
60.68	1.52494	41	9.6	0.501
61.531	1.50588	45	10.5	0.312

Table -21.2. Concentration, crystallite size, strain and crystal size (PCLS)

Method	Characteristic	Calcite	Aragonite
Rietveld method (XRD)	Concentration%	100±1.11	-
Rietveld method (XRD)	Crystallite size $<L>_{vol}$ (nm)	101	.
Williamson-Hall (XRD)	Crystallite size <L>vol (nm)	106.2±1.4	-
Williamson-Hall (XRD)	Strain value	0.111±0.004	-
(SEM)	Crystal size (nm)	100±8	-

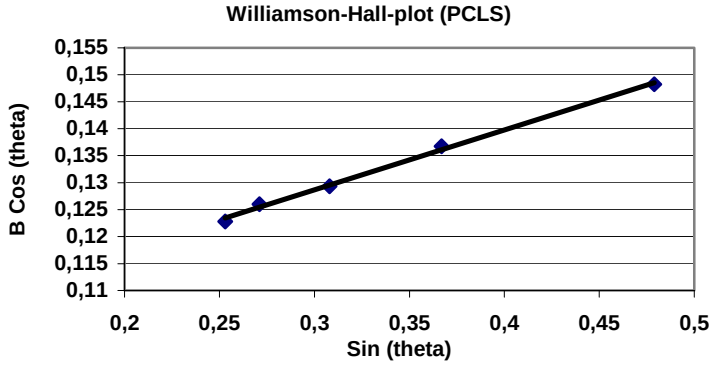

Figure 21.3. The Williamson-Hall plot (calcite)(PCLS)
(Y= 0.1108X + 0.014,R^2 = 0.9909)

Table- 21.3. morphology description based on intensity ratio data (PCLS)

Method	Characteristic	Calcite	Aragonite
Intensity Ratio peak area (XRD)	Morphology Description	I(104)/I(116) 5.66±0.09	-
Intensity Ratio peak area (XRD)	Morphology Description	I(104)/I(012) 7.94±0.05	-
Intensity Ratio peak area (XRD)	Morphology Description	I(104)/I(202) 4.90±0.04	-
Intensity Ratio peak area (XRD)	Morphology Description	I(104)/I(113) 4.848±0.29	-
Intensity Ratio peak area (XRD)	Morphology Description	I(104)/I(018) 6.69±0.18	-
Intensity Ratio peak area (XRD)	Morphology Description	I(104)/I(122) 10.49±0.31	-
Intensity Ratio peak height (XRD)	Morphology Description	I(104)/I(116) 5.50±0.17	-
Intensity Ratio peak height (XRD)	Morphology Description	I(104)/I(012) 7.59±0.12	-
Intensity Ratio peak height (XRD)	Morphology Description	I(104)/I(202) 4.83±0.14	-
Intensity Ratio peak height (XRD)	Morphology Description	I(104)/I(113) 4.31±0.21	-
Intensity Ratio peak height (XRD)	Morphology Description	I(104)/I(018) 6.53±0.32	-
Intensity Ratio peak height (XRD)	Morphology Description	I(104)/I(122) 10.19±0.54	-

Sample Name PCC-CalciSG Abbreviation PCCSG

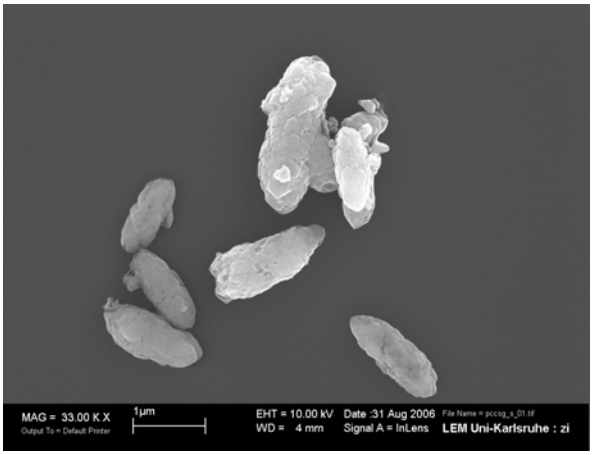

Figure 22.1. The SEM image (PCCSG)

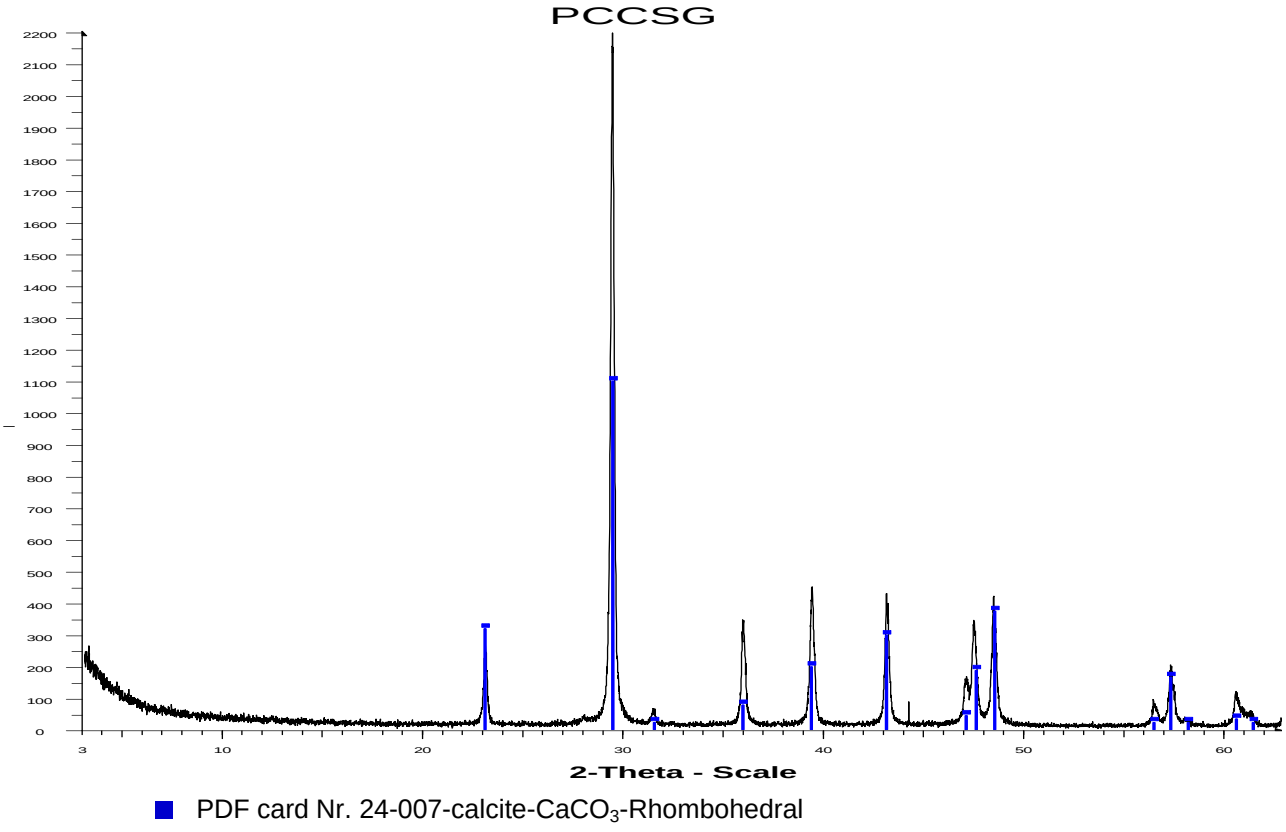

Figure 22.2. The diffractogram (PCCSG)

Table –22.1. The peak list (PCCSG) ($FWHM_{Instrumental}$=0.157°)

Angle 2-Theta °	d value Angstrom	Intensity Count	Intensity %	$FWHM_{obs}$
23.063	3.85325	226	10.5	0.302
29.459	3.02959	2161	100	0.210
31.537	2.8346	46	2.1	0.293
35.973	2.49452	277	12.8	0.300
39.412	2.28444	366	16.9	0.307
43.166	2.09407	372	17.2	0.293
47.157	1.92572	158	7.3	0.313
47.651	1.90689	242	11.2	0.314
48.572	1.87289	387	17.9	0.328
56.553	1.62604	89	4.1	0.310
57.411	1.60376	204	9.4	0.332

Table-22.2. Concentration, crystallite size, strain and crystal size (PCCSG)

Method	Characteristic	Calcite	Aragonite
Rietveld method (XRD)	Concentration%	100±1.11	-
Rietveld method (XRD)	Crystallite size $<L>_{vol}$ (nm)	143	.
Williamson-Hall (XRD)	Crystallite size <L>vol (nm)	136.2±7.9	-
Williamson-Hall (XRD)	Strain value	0.123±0.095	-
(SEM)	Crystal size (nm)	519±37	-

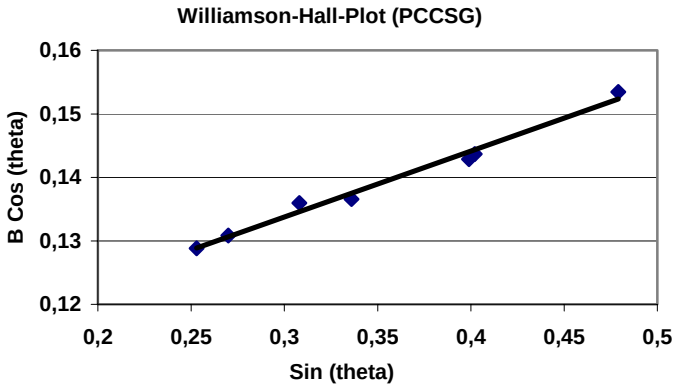

Figure 22.3. The Williamson-Hall plot (calcite)(PCCSG) (Y= 0.1038X + 0.011,R^2 = 0.9863)

Table –22.3. Morphology description based on intensity ratio data (PCCSG)

Method	Characteristic	Calcite	Aragonite
Intensity Ratio peak area (XRD)	Morphology Description	I(104)/I(116) 5.55±0.06	-
Intensity Ratio peak area (XRD)	Morphology Description	I(104)/I(012) 9.33±0.22	-
Intensity Ratio peak area (XRD)	Morphology Description	I(104)/I(202) 5.52±0.12	-
Intensity Ratio peak area (XRD)	Morphology Description	I(104)/I(113) 4.89±0.26	-
Intensity Ratio peak area (XRD)	Morphology Description	I(104)/I(018) 6.83±0.12	-
Intensity Ratio peak area (XRD)	Morphology Description	I(104)/I(122) 10.59±0.27	-
Intensity Ratio peak height (XRD)	Morphology Description	I(104)/I(116) 5.34±0.17	-
Intensity Ratio peak height (XRD)	Morphology Description	I(104)/I(012) 8.40±0.39	-
Intensity Ratio peak height (XRD)	Morphology Description	I(104)/I(202) 5.35±0.19	-
Intensity Ratio peak height (XRD)	Morphology Description	I(104)/I(113) 4.71±0.21	-
Intensity Ratio peak height (XRD)	Morphology Description	I(104)/I(018) 6.46±0.19	-
Intensity Ratio peak height (XRD)	Morphology Description	I(104)/I(122) 10.75±0.23	-